QUANTUM MECHANICAL CALCULATIONS OF REACTIVE SCATTERING CROSS-SECTIONS IN BIMOLECULAR ENCOUNTERS

A THESIS

Presented to

The Faculty of the Graduate Division

by

James Carl Pirkle, Jr.

In Partial Fulfillment

of the Requirements for the Degree

Doctor of Philosophy in the School of Chemical Engineering

Georgia Institute of Technology

April, 1967

QUANTUM MECHANICAL CALCULATIONS OF REACTIVE SCATTERING CROSS-SECTIONS IN BIMOLECULAR ENCOUNTERS

A THESIS

Presented to

The Faculty of the Graduate Division

by

James Carl Pirkle, Jr.

In Partial Fulfillment

of the Requirements for the Degree

Doctor of Philosophy in the School of Chemical Engineering

Georgia Institute of Technology

April, 1967

ACKNOWLEDGMENTS

The author wishes to express his gratitude to Professor Henry A. McGee, Jr. for his encouragement and guidance during the course of this work. He also would like to thank Dr. J. Ross of the Massachusetts Institute of Technology and Dr. J. C. Polanyi of the University of Toronto for some helpful suggestions. Both men also supplied several preprints which the author found beneficial.

The author gratefully acknowledges financial support from the General Electric Foundation during the years 1963 to 1965. This research was also assisted by funds from the National Aeronautics and Space Administration.

For the many hours of dedicated instruction he received during his enrollment in the Graduate School of Chemical Engineering, the author especially desires to thank Professors W. M. Newton, H. C. Ward, and W. T. Ziegler.

Finally, the author wishes to acknowledge the devotion and encouragement shown by his wife, Helen Smith Pirkle, while the research for this work was being performed.

TABLE OF CONTENTS

TABLE OF CONTENTS (Continued)

LIST OF TABLES

LIST OF TABLES (Continued)

LIST OF FIGURES

SUMMARY

Quantum mechanical calculations are carried out for the reaction cross-sections of $H + Br_2 \rightarrow HBr + Br$. A technique is used which is an improvement over the distorted wave Born approximation in that an account is made of the distortion of the HBr bond by the outgoing Br atom. This approach, called the perturbed Morse oscillator method, is generalized for all bimolecular, exothermic reactions $A + BC \rightarrow AB + C$ for which the potential energy surface can be described as:

(1) A Morse-like bonding interaction between A and B which gradually approaches the normal AB bond as C departs.

(2) A mostly repulsive interaction between AB and C which gradually vanishes as C departs.

The perturbed Morse oscillator method was applied to the specific case of $H + Br_2 \rightarrow HBr + Br$, a potential energy surface for which was calculated by the diatomics-in-molecules method of Ellison. This particular potential energy surface possessed the features (1) and (2) listed above.

For a wide variety of initial conditions, reaction cross-sections were obtained which were highest for the higher possible vibrational states of HBr. Since Ellison's potential energy surface was one which released most of the energy of reaction upon the approach of H to Br_2, it was dubbed an "attractive" potential energy surface. The high vibrational excitation of the product molecule indicated by the quantum mechanical calculations of this investigation lends support to the

classical mechanical calculation of Polanyi, who likewise observed a high degree of product vibration for an "attractive" potential energy surface.

To make additional comparisons with the classical mechanical results of Polanyi, a physically plausible Morse-like potential energy surface was constructed which released a major portion of the energy of reaction upon the departure of the product Br atom from HBr. This type surface was referred to as a "repulsive" potential energy surface and also possessed the features (1) and (2) mentioned previously. Repeating the quantum mechanical calculations for this surface, reaction cross-sections were obtained which attained their highest values for the lowest four vibrational states of HBr. This result compared favorably with that of the classical mechanical result of Polanyi for a "repulsive" potential energy surface.

Since the infrared chemiluminescence studies of the $H + Br_2 \rightarrow HBr + Br$ reaction indicate that most of the HBr molecules are formed in the lower vibrational states, it was concluded that the "repulsive" potential energy surface more nearly represented the actual interaction of $H + Br_2 \rightarrow HBr + Br$. Thus, calculations of the rate constants of the above reaction were performed using the reaction cross-sections obtained for the "repulsive" potential energy surface. Due to the substantial amounts of computer time involved, it was feasible to calculate the reaction cross-sections corresponding to only a few initial conditions. The resulting paucity of cross-sections necessitated the simplification of the modern collision theory of rate constants for bimolecular reactions. Rather than summing over all the statistically weighted initial

states at a given temperature, only the initial condition corresponding to a Maxwell-Boltzmann averaged initial energy at that temperature was considered. Even this simplified calculation, however, gave rate constants in excellent agreement with experiment; that is, at $1000^{\circ}K$ a total rate constant of 1.81×10^{14} cc/mole-sec was obtained as compared to the experimental range of 1.04×10^{14} - 6.30×10^{14} cc/mole-sec reported by different investigators. Detailed rate constants (rate constants referring to the rate of formation of HBr in specific vibrational states) obtained from these calculations were in excellent qualitative agreement with the experimental results of Polanyi. That is, at $500^{\circ}K$ the detailed rate constants of the fourth, fifth, and sixth excited vibrational states of HBr relative to the detailed rate constant for the third excited vibrational state were found by Polanyi to be 0.64, 0.19, and 0.05, respectively. In the present study, the corresponding values determined by the simplified collision theory were 0.38, 0.12, and 0.07.

CHAPTER I

INTRODUCTION

Statement of the Problem

Theoretical treatments of gas phase chemical reactions can be conveniently classified into two parts. The first involves the study of the details of intermolecular or intramolecular energy transfer, particle exchange, particle emission, or particle capture. Secondly, a study must be made of the manner in which a usually broad spectrum of the above microscopic processes are reflected in the macroscopic or bulk behavior of gas phase reactions. In other words, the former task is concerned with the calculation of the probability of particular events, whereas the latter effort is concerned with formalizing mathematical relationships between these detailed probabilities and observable reaction phenomena.

This study will be involved with the application of the nonequilibrium collision theory of reaction rates (1-2) to the estimation of rate constants for simple reactions. In the nonequilibrium collision theory, the molecular collisions are individually studied with regard to initial conditions, particle exchange, and energy exchange, the results being defined in terms of cross-sections*. Then, the kinetic theory of gases (3) is used to average over all the effects of the individual

---

* A definition and discussion of the term "cross-section" as it applies to collisions is given in Appendix A.

collisions resulting in reaction to obtain the rate constants.

Scope of the General Discussion

In general, the present investigation will be confined to chemical reactions that:

(1) Are bimolecular, occurring in a homogeneous gas phase under practially ideal gas conditions.

(2) Are highly exothermic, releasing more than 20 kilocalories per mole of one reactant.

(3) Are bimolecular exchange reactions involving only three atoms

$$A + BC \rightarrow AB + C \quad . \qquad (1\text{-}1)$$

The corresponding reasons for these restrictions are:

(1) Only bimolecular collisions are important at ideal gas conditions, termolecular and higher order collisions occurring only rarely. Also, the average time between bimolecular collisions in an ideal gas is long compared to the average collision time (4). Thus, each bimolecular collision can be analyzed individually, the influence of the other molecules being negligible. Afterwards, the conventional kinetic theory of gases can be used to obtain the reaction rate by averaging the effects of all possible types of reaction collisions. This approach is used in the nonequilibrium collision theory of Hirschfelder, Ross, and others (1-2).

(2) Recent molecular beam and infrared chemiluminescence experiments have yielded data on how the energy of highly exothermic reactions of this type is distributed among the products (5-8). Attempts have been made to use the results of these experiments to elucidate the nature

of the potential energy function governing the nuclear motion.

Assuming an expression, possessing reasonable mathematical form and containing adjustable parameters, for the potential energy function, the various nuclear motions occurring during a bimolecular collision are tracked by classical mechanics. The potential energy parameters are adjusted until agreement between theory and experiment is reached. So far, no detailed analyses of the nuclear motion occurring in highly exothermic, reactive collisions have been carried out quantum mechanically.

(3) One of the simplest possible chemical reactions is the exchange reaction

$$A + BC \rightarrow AB + C \quad . \tag{1-2}$$

A third body, atom C in this case, is required to carry away sufficient energy to make AB stable, so the simplest reaction must involve at least three atoms. On the other hand, mathematical difficulties make it expedient to limit theoretical studies of the nuclear motion to a three-body problem. It is well known, of course, that analytical solutions are not available for the general problem of three-body motion and hence numerical methods are necessary to study reactions of the above type. In addition, many complex reactions involve one or more steps like Equation (1-2), so these simple processes are well worth studying.

The Specific Task

The nonequilibrium collision theory of reaction rates (1) will be applied to the reaction

$$H + Br_2 \rightarrow HBr + Br \quad . \tag{1-3}$$

This reaction has an exothermicity of 41 kilocalories and is an important process in the overall combustion reaction

$$H_2 + Br_2 \rightarrow 2\ HBr \quad . \tag{1-4}$$

Recently, a semiempirical calculation of the potential energy surface for the linear system H--Br--Br was performed by Ellison (9) using his "diatomics-in-molecules" method. In addition, an infrared chemiluminescence study of this reaction has just been performed by Polanyi (10), and the distribution of energy among the products analyzed. The approach to be used in the present study is to modify Ellison's basic potential energy surface with appropriate terms and include adjustable parameters. Then preliminary theoretical studies of the nuclear motion will be performed, the resulting energy distribution among the products examined, and the potential energy parameters adjusted until reasonable agreement with the infrared chemiluminescence experiments of Polanyi is obtained.

After the adjustment of the potential energy function, the theoretical treatment of the collision dynamics will continue until the cross-sections required in the nonequilibrium collision theory of reaction rates are obtained. From these cross-sections the specific rate constants will be calculated and compared with experimental estimates of the rate constant for the reaction, i.e., Equation (1-3).

Background

Elementary, exothermic, gas phase reactions having low activation energies have been the center of much scientific and engineering interest

in recent years. The engineering interest derives primarily from the importance of these rapid, energy releasing processes in combustion reactions of the sort

$$H_2 + Br_2 \rightarrow 2\ HBr \quad , \tag{1-5}$$

which is thought (11) to proceed via the mechanism

(1) $M + Br_2 \rightarrow 2\ Br + M$

(2) $Br + H_2 \rightarrow HBr + H$

(3) $H + Br_2 \rightarrow HBr + Br$

(4) $H + HBr \rightarrow H_2 + Br$

(5) $M + Br + Br \rightarrow Br_2 + M$.

Here, the symbol M denotes any of the molecular species listed above.

Using the steady-state treatment gives rise to (11)

$$\frac{d[HBr]}{dt} = \frac{2\,k_2\,(k_1/k_5)^{1/2}\,[H_2]\,[Br_2]^{1/2}}{1 + \dfrac{k_4[HBr]}{k_3[Br_2]}} \tag{1-6}$$

The most rapid, most exothermic step above contributing to the forward progress of the total combustion reaction, Equation (1-5), is the reaction given by Equation (1-3), i.e., the test system to be used in this investigation.

Need for Rate Constants of Simple Reactions

In flame propagation studies, it is usually desirable to know the rate constants for each of the elementary processes contributing to the

overall combustion reaction (12-14). The rate constants for the slower elementary reactions can sometimes be determined by direct experimentation, but some elementary reactions occur so rapidly that the measurement of their rate constants cannot be accomplished by direct means. Very often rate constants for very fast reactions must be approximated by an analysis of the overall reaction rate. Usually this analysis requires the use of a very complicated deductive process in conjunction with the steady-state treatment (11).

It is apparent, therefore, that a suitable theory for predicting the rate constants of very fast, simple reactions would find immediate application in the study of combustion processes. Unfortunately, the simple collision and absolute reaction rate theories, the more traditional theories of chemical kinetics, are usually inappropriate for these reactions. Unless the activation energy of the reaction is sufficiently large, for instance, the more energetic reactant molecules will be depleted faster than they can be replenished by nonreactive collisional processes (15-16). In this case, the Maxwell-Boltzmann distribution of energy states among the reactants is distorted, thus invalidating the equilibrium hypothesis inherent in the theory of absolute reaction rates. With regard to the simple collision theory, some reactions involve such complicated intermolecular interactions that steric factors and collision diameters are difficult to estimate correctly. Thus, there is a definite need to examine the possibility of estimating rate constants of rapid, elementary processes by using a theory which not only avoids the equilibrium hypothesis but also allows for more detailed study of the intermolecular interactions.

Nonequilibrium Collision Theory

Such a theory is the nonequilibrium collision theory established by Hirschfelder and Eliason (1) and Ross and Mazur (2). Conceptually, this theory bears a resemblance to the nonequilibrium theory for transport properties of polyatomic molecules devised by Wang-Chang and Uhlenbeck (17). In the latter theory, a molecule of definite chemical type A and having a definite internal state i is said to constitute a "species" A(t). The transport processes in a gas of polyatomic molecules were studied in light of the transitions from "species" A(t) to "species" A(t′) occurring as a result of bimolecular collisions. For chemical processes, therefore, it is only necessary to extend the examination to transitions of the type A(t) to B(j).

Relation Between the Rate Constant and the Reaction Cross-Section

Consider the isolated reaction between A(t) and B(j) to form C(k) and D(l)

$$A(t) + B(j) \rightleftarrows C(k) + D(l) \quad . \tag{1-7}$$

The nonequilibrium collision theory gives the detailed rate constant in the forward reaction as

$$K(k,l;t,j) = \int\cdots\int (p/\mu)\,\sigma_f^i(k,l;t,j,p;\Omega)\,F_t(\vec{p}_A)\,F_j(\vec{p}_B)\,d\Omega\,d^3\vec{p}_A\,d^3\vec{p}_B \tag{1-8}$$

where p is the initial relative momentum, μ is the reduced mass of A and B, σ_f^i is the differential cross-section for transition from the initial state i to the final state f via chemical reaction, Ω is the solid angle

of scattering, and $F_t(\vec{p}_A)$ is the momentum distribution function of A(t), normalized according to

$$\int F_t(\vec{p}_A)\, d^3\vec{p}_A = 1 \qquad (1\text{-}9)$$

The momentum distribution function of B(j), i.e., $F_j(\vec{p}_B)$ is also normalized according to Equation (1-9).

The relation between the total and differential cross-sections for chemical reaction is

$$\sigma(k,l;t,j,p) = \int_{\Phi=0}^{2\pi}\int_{\Theta=0}^{\pi} \sigma_f^{\,i}(k,l;t,j,p;\Omega)\sin\Theta\, d\Theta\, d\Phi \qquad (1\text{-}10)$$

The total reaction cross-section $\sigma(k,l;t,j,p)$ has the units of area and represents the effective target area presented by a molecule B(j) to an oncoming molecule A(t), approaching with relative momentum p, in order for the collision outcome to be C(k) and D(l).

The total reaction rate constant K_t is given by averaging Equation (1-8) over all possible internal states of the reactants and then summing over all possible internal states of the products. The resulting expression for K_t is

$$K_t = \sum_{k,l}\sum_{t,j}\iint (p/\mu)\,\sigma(k,l;t,j,p)\,F_t(\vec{p}_A)F_j(\vec{p}_B)\, d^3\vec{p}_A\, d^3\vec{p}_B \qquad (1\text{-}11)$$

Determination of the Reaction Cross-Sections

Before the reaction rate K_t can be evaluated, an expression for the total reaction cross-section must be obtained. In recent years attempts have been made to measure $\sigma(k,l;t,j,p)$ by molecular beam experiments (5,7,18,19). At present, however, molecular beam technology is not sufficiently developed to be of much use for a majority of reactions. It seems that the problem of detecting the product molecules after collision has limited most molecular beam investigations to reactions involving alkali atoms.

Several attempts to calculate reaction cross-sections theoretically have been made recently, and the results were compared with data from molecular beam scattering experiments. Thus far, all of these theoretical treatments have assumed that the electronic energy can be separated from the nuclear energy in bimolecular encounters (the Born-Oppenheimer separation) and that the electrons remain in one state (the "adiabatic" assumption). Therefore, the theoretical investigation of molecular collisions is reduced to the following problem in kinematics.

Let N represent the number of nuclei comprising the two colliding molecules. Then the motion of the two nuclei is governed by the potential-energy hypersurface dependent only on the $\frac{1}{2}N(N-1)$ internuclear distances. For linear systems the potential energy function depends only on (N-1) variables.

In order to obtain the potential-energy hypersurface, the Schroedinger equation corresponding to the electronic motion must be solved. Unfortunately, an exact solution of the electronic Schroedinger equation is presently impossible for systems involving more than one

electron, and hence, semiempirical methods (9,20,21) are necessary if one wishes to calculate the potential energy hypersurface for complicated systems. Further mention will be made of these methods in Chapter II. The discussion that follows will assume that the required potential-energy hypersurfaces have already been obtained.

The classical mechanical method of solving the above kinematical problem involves the numerical integration of Hamilton's canonical equations of motion for the interacting nuclei. If, for a large number of test cases, one picks a naturally occurring set of initial conditions for the collision of two reactive molecules, and integrates the equations of motion to obtain the complete trajectories of all the nuclei involved, then by simply counting the number of test trajectories that lead to reaction and noting the solid angle into which the products are scattered, one can obtain the differential reaction cross-section. If the potential-energy hypersurface is precisely known, then the calculation of the individual nuclear trajectories is as exact as classical mechanics can be. Because of the many thousands of calculations (test trajectories) required in order to average over all of the various initial conditions, the use of classical mechanics in making kinematical studies of the sort above require an excessively large amount of computer time, even for the high-speed computers of today. For instance, the most complete classical mechanical study to date (22) required about ten seconds per trajectory. Thus, 100,000 trajectories would require about 270 hours of computer time. In contrast, the statistical nature of quantum mechanics allows for the averaging over many of these initial conditions (impact parameter, molecular orientation, and vibrational phase) with but a single calculation.

Furthermore, classical mechanics may not be valid for studying the motion of light nuclei at thermal energies under the influence of valence type forces (23). Thus, a quantum mechanical treatment of the reactive collision problem might be not only less time consuming than a classical treatment but also more theoretically correct.

On the other hand, an exact solution of the Schroedinger equation corresponding to the nuclear motion is practically impossible, and recourse must be made to some approximation scheme. Fortunately, an approximate method suitable to the problem of reactive collisions between molecules has already been formulated (24-25). This method is known as the perturbed stationary state approximation or molecular wave function method and will be employed in the present study. In classical mechanics, suitable approximate methods have not been developed, and the calculation of reaction cross-sections must be made on an all or nothing basis.

CHAPTER II

REVIEW OF PREVIOUS CONTRIBUTIONS

This chapter will be concerned primarily with past attempts at calculating the reaction cross-sections necessary in the nonequilibrium collision theory of reaction rates. As such, the emphasis will be on the more promising methods of obtaining the potential-energy hypersurfaces and the more recent kinematical studies. No discussion will be made of the simple collision and absolute rate theories since they have been extensively presented in the standard textbooks (4,21,26) for the last quarter of a century. Also, in order to save space, no discussion of the derivation of Equation (1-8) will be given. Reference to the papers by Ross (1) and Hirschfelder (2) can be made by those interested in the development of the nonequilibrium collision theory of reaction rates.

Born-Oppenheimer Separation

Most theoretical treatments of reactions of the type

$$A + BC \rightarrow AB + C \quad , \tag{2-1}$$

have involved the Born-Oppenheimer separation (27), i.e., the separation of the electronic and nuclear motions. When this methodology is used, the nuclear motion is assumed to be "adiabatic," i.e., the motions of electrons and nuclei are independent and the potential energy of the system varies continuously during nuclear motion, so that this motion is

not accompanied by electronic transition. A concise discussion of the Born-Oppenheimer separation has been presented by Kondratiev (28) so only the important points are presented here.

The Electronic States

The Schroedinger equation governing the electronic motion in the reacting system is given by (28)

$$\left[-\frac{\hbar^2}{2m_e}\sum_{\alpha=1}^{N}\nabla_{r_\alpha}^2 + U\left(\{\vec{R}_\beta\},\{\vec{r}_\alpha\}\right)\right]\varphi_k\left(\{\vec{R}_\beta\},\{\vec{r}_\alpha\}\right) = \epsilon_k\left(\{\vec{R}_\beta\}\right)\varphi_k\left(\{\vec{R}_\beta\},\{\vec{r}_\alpha\}\right) \tag{2-2}$$

where $\{\vec{R}_\beta\}$ and $\{\vec{r}_\alpha\}$ represent the set of position vectors for the nuclei and electrons, respectively, m_e is the electron mass, N is the total number of electrons, and $\nabla_{r_\alpha}^2$ is the Laplacian operator with respect to $\vec{r}_\alpha$. As indicated, the electronic eigenfunctions φ_k and eigenvalues ϵ_k depend on the coordinates of the nuclei, while the total potential energy function U depends on the coordinates of the electrons and the nuclei.

During the course of a chemical reaction, the electronic state is assumed to remain constant; thus, the nuclear motion is assumed to be governed by a single electronic potential energy function ϵ_k. At ordinary temperatures, the ground electronic state of the reacting system should prevail (28). For example, at 1000°K only 0.1 percent of the reactive collisions $H + Br_2 \rightarrow HBr + Br$ involve species in excited electronic states.

The Motion of the Nuclei

Another result of the Born-Oppenheimer separation is that the

motion of the nuclei is described by a Schroedinger equation involving only the nuclear coordinates (28), or

$$\left[-\frac{\hbar^2}{2}\sum_{\beta=1}^{Q}\frac{1}{M_\beta}\nabla^2_{R_\beta} + \epsilon_k\left(\{\vec{R}_\beta\}\right)\right]\Psi_k = E\,\Psi_k\left(\{\vec{R}_\beta\}\right) \qquad (2\text{-}3)$$

where E is the total energy, Q is the number of nuclei, M denotes the mass of the βth nucleus, and k represents the electronic states, usually taken as the ground state. Since only one electronic state is considered during the collision the subscript can be suppressed when denoting the nuclear wave function Ψ_k and the potential energy function ϵ_k.

Potential-Energy Functions

As mentioned earlier, the initial stage of the nonequilibrium collision theory of reaction rates involves solving the problem of the dependence of the potential energy of the colliding molecules on the coordinates of all their component atoms. For the case of reactions of a diatomic molecule, BC, with an atom A, it is necessary to know the energy of the system A + B + C for any relative position of the three atoms. In general, this problem must be solved not only for the ground state but also for the excited electronic states. If the total number of atoms in the system is N, the potential-energy of their interaction will depend on $M = \frac{1}{2}N(N-1)$ coordinates of the atoms (in the case of a linear system N-1 coordinates). The problem, therefore, consists of finding a mathematical expression for the potential-energy hypersurface

$$\epsilon = \epsilon\left(|\vec{R}_1 - \vec{R}_2|, \cdots, |\vec{R}_{N-1} - \vec{R}_N|\right) \qquad (2\text{-}4)$$

To derive an exact expression for Equation (2-4), for the case of A + BC → AB + C, one must solve Equation (2-2). Unfortunately, overwhelming mathematical complications usually prevent the determination of an exact solution to Equation (2-2), and recourse must be made to one of the approximate methods outlined below.

Ab Initio Calculations

Ab initio calculations have proven quite unsatisfactory for the study of reaction rates. The treatments have usually involved using the variational method in conjunction with trial wave functions embroidered with all sorts of adjustable parameters (29-32). Some well known examples of these methods are the valence-bond method (33), the linear combination of atomic orbitals-molecular orbital method (31), and the molecular orbital method with configuration interaction (34).

How unsatisfactory for reaction rate calculations ab initio methods are was clearly pointed out in a recent calculation by Boys and Shavitt (35) for the potential energy surface of the simple reaction H + H_2 → H_2 + H. Carrying out an extensive linear combination of atomic orbitals-molecular orbital calculation, they obtained an activation energy (36) of 15.4 kcal/mole, whereas the experimental activation energy is about 8.8 kcal/mole (37).

Semiempirical Methods

The semiempirical methods of calculating potential-energy surfaces combine the electronic energy expressions obtained from valence bond theory with appropriate spectroscopic data. Generally held in higher

regard than ab initio methods, semiempirical techniques have been widely used in the absolute reaction rate theory of Eyring (21).

Eyring-Polanyi-Sato Method. The most widely used semiempirical method in the early stages of the absolute reaction rate theory was the technique devised by Eyring and Polanyi (38). The London equation, derived from simple valence-bond theory, was used in conjunction with the Morse parameters for all the diatomic molecules obtainable from the total reaction system. Thus, if one desired the potential energy surface of the reaction A + BC → AC + B, the appropriate London equation would be

$$E = Q_{AB} + Q_{AC} + Q_{BC} - \left|\left\{\tfrac{1}{2}\left[(\epsilon_{AB}-\epsilon_{AC})^2+(\epsilon_{AB}-\epsilon_{BC})^2+(\epsilon_{AC}-\epsilon_{BC})^2\right]\right\}^{1/2}\right| \qquad (2\text{-}5)$$

where ϵ_{KL} and Q_{KL} are the exchange and coulombic energies, respectively, of the molecule KL. Now, if Q_{KL} is assumed to be a constant fraction ρ_{KL} of the total binding energy of the diatomic, KL, then the Morse function (39)

$$E_{KL} = D'_{KL}\left[\exp(-2a_{KL}(r_{KL}-r^{o}_{KL}))-2\exp(-a_{KL}(r_{KL}-r^{o}_{KL}))\right] \qquad (2\text{-}6)$$

where D'_{KL}, a_{KL}, and r^{o}_{KL} are the spectroscopically determined Morse parameters, can be used to obtain ϵ_{KL} and Q_{KL} as functions of r_{KL}. Since

$$E_{KL} = Q_{KL} + \epsilon_{KL} \qquad (2\text{-}7)$$

then

$$\epsilon_{KL} = (1 - \rho_{KL})\, D'_{KL} \left[\exp(-2a_{KL}(r_{KL} - r^{\circ}_{KL})) - 2\exp(-a_{KL}(r_{KL} - r^{\circ}_{KL})) \right] \tag{2-8}$$

$$Q_{KL} = \rho_{KL}\, D'_{KL} \left[\exp(-2a_{KL}(r_{KL} - r^{\circ}_{KL})) - 2\exp(-a_{KL}(r_{KL} - r^{\circ}_{KL})) \right] \tag{2-9}$$

According to Eyring (38), the activation energies obtained by this procedure are relatively insensitive to the ρ_{KL}'s over a large range of values.

In the middle 1950's, Sato (40) devised a technique to avoid the assumption of constant coulombic fraction in the Eyring-Polanyi method. Using the information available on the shape of the antibonding $^3\Sigma$ curve for H_2, he discovered that the antibonding energy-state $^3E(r)$ could be expressed approximately as

$$^3E(r) = \frac{D}{2} \left\{ \exp[-2a(r - r^{\circ})] + 2\exp[-a(r - r^{\circ})] \right\} \tag{2-10}$$

for the hydrogen molecule. By assuming that this relation holds for diatomic molecules KL in general, and by using the London expression (38)

$$^3E_{KL} = Q_{KL} - \epsilon_{KL} \tag{2-11}$$

for the antibonding energy-state, Sato solved Equations (2-6), (2-10), (2-7), and (2-11) for Q_{KL} and ϵ_{KL} at each interatomic distance; thus,

he avoided the assumption of constant Coulombic fraction.

In addition, Sato included an adjustable parameter k in the London equation for the ground-state triatomic energy surface:

$$E = \frac{1}{k}\left[Q_{AB} + Q_{AC} + Q_{BC} - \left|\left\{\frac{1}{2}\left[(\epsilon_{AB}-\epsilon_{AC})^2 + (\epsilon_{AB}-\epsilon_{BC})^2 + (\epsilon_{AC}-\epsilon_{BC})^2\right]\right\}^{1/2}\right|\right] \qquad (2\text{-}12)$$

Originally, Sato proposed setting k equal to $1 + S^2$, where S is the Heitler-London overlap integral (38), assumed equal for the three diatomic fragments.

When applied to the system $H + H_2$, however, Sato's treatment requires that $S^2 = 0.148$, whereas the correct value of S^2 at the activated state configuration is about three times larger (37). Furthermore, the use of a constant S is erroneous since S changes appreciably with interatomic distance. The net result is that Sato's method gives an activated energy barrier that is much too thin; that is, the contribution of tunneling to reaction is in substantial contrast with experimental findings (37).

Diatomics in Molecules Theory. In 1963, Ellison (41) proposed a scheme in which the electronic structure of a polyatomic molecule is expressed in terms of electronic structures for all possible diatomic and monatomic fragments composing it. Although bearing a strong resemblance

to the Eyring-Polanyi-Sato method, Ellison's theory contains no exchange integrals, no coulomb integrals, and no calibration parameters.

A derivation of this new theory will now be demonstrated for the case of the reaction A + BC → AB + C, where the reaction configuration is assumed to be linear.

Consider valence-bond structure wave functions Ψ_I and Ψ_{II} corresponding to A-BC and AB-C, respectively. If the symbols D_r represent determinantal wave functions (antisymmetrical products of atomic spin orbitals), then each of the functions Ψ_I and Ψ_{II} can be written as

$$\Psi_n = \sum_r b_{nr} D_r \qquad (2\text{-}13)$$

Here, the b_{nr} coefficients are chosen so that (1) Ψ_n is antisymmetric with respect to the interchange of spin factors of orbitals forming an electron pair, (2) Ψ_n is the proper eigenfunction of S^2 (square of total spin momentum) and S_z (component of S upon z-axis), and (3) Ψ_n is normalized for infinite separation of the atoms.

Suppose that the polyatomic molecule ABC can be represented by a resonance of the two valence-bond canonical structures Ψ_I and Ψ_{II} as

$$\Psi = \sum_n a_n \Psi_n \qquad (2\text{-}14)$$

Determination of the optimum coefficients a_n for which the molecular electronic energy W is minimized results from the solution of the secular determinant

$$\begin{vmatrix} H_{I,I} - S_{I,I} W & H_{I,II} - S_{I,II} W \\ H_{II,I} - S_{II,I} & H_{II,II} - S_{II,II} W \end{vmatrix} = 0 \qquad (2\text{-}15)$$

in which

$$S_{nm} = \int \Psi_n^* \Psi_m \, d\tau \qquad (2\text{-}16)$$

$$H_{nm} = \int \Psi_n^* H \Psi_m \, d\tau \qquad (2\text{-}17)$$

Here, H is the total electronic Hamiltonian of the polyatomic molecule, and the integration is over all of real space, $d\tau$ being a small element of real space.

Each valence-bond structure can be written as

$$\Psi_m = A \Psi_m \qquad (2\text{-}18)$$

where A is the total antisymmetrization operator and Ψ_m, referred to as the primitive function of the mth structure, is a linear combination of simple products of atomic spin orbitals. Now, a typical energy matrix element can be expressed as

$$H_{nm} = \int \Psi_n^* A H \Psi_m \, d\tau \tag{2-19}$$

since the operators H and A commute.

Next, consider that the total electronic Hamiltonian operator for the polyatomic molecule ABC can be written as

$$H = H_A + H_B + H_C + V_{AB} + V_{AC} + V_{BC} \tag{2-20}$$

Each H_P contains all kinetic energy operators and all intraatomic potential-energy terms in H which depend exclusively upon the coordinates of electrons assigned originally to atom P and not upon the coordinates of any nuclei other than nucleus P; V_{PQ} contains all interatomic interaction potential-energy terms in H depending upon electron coordinates common to atom P and Q only. This method of partitioning H is called the atoms-in-molecules method by Ellison.

The Hamiltonian H_{PQ} for a diatomic molecule, written in its atoms-in-molecules form, is

$$H_{PQ} = H_P + H_Q + V_{PQ} \tag{2-21}$$

Solving this expression for V_{PQ} and substituting into Equation (2-20), one obtains

$$H = H_{AB} + H_{AC} + H_{BC} - H_A - H_B - H_C \tag{2-22}$$

This form of H is referred to as the diatomics-in-molecules (DIM) Hamiltonian; it contains explicitly no "interaction" operators but only Hamiltonians for the constituent diatomic molecules and atoms.

Substituting of Equation (2-22) into Equation (2-19) yields

$$H_{nm} = H_{nm}^{AB} + H_{nm}^{BC} + H_{nm}^{AC} - H_{nm}^{A} - H_{nm}^{B} - H_{nm}^{C} \qquad (2\text{-}23)$$

where

$$H_{nm}^{PQ} = \int \Psi_n^* A H_{PQ} \Psi_m \, d\tau \qquad (2\text{-}24)$$

$$H_{nm}^{P} = \int \Psi_n^* A H_{P} \Psi_m \, d\tau \qquad (2\text{-}25)$$

At this point, Ellison states that the matrices $\langle H^{PQ} \rangle$ and $\langle H^{P} \rangle$ are not separately Hermitian, and indeed are not completely independent. This is due to a relationship which exists between $\langle H^{PQ} \rangle$ and $\langle H^{P} \rangle$. Since $\langle H \rangle$ is Hermitian, $\langle H \rangle = \langle H \rangle^{+}$, and thus

$$\left[\langle H^{AB}\rangle - \langle H^{AB}\rangle^{+}\right] + \left[\langle H^{AC}\rangle - \langle H^{AC}\rangle^{+}\right] + \left[\langle H^{BC}\rangle - \langle H^{BC}\rangle^{+}\right] \qquad (2\text{-}26)$$

$$- \left[\langle H^{A}\rangle - \langle H^{A}\rangle^{+}\right] - \left[\langle H^{B}\rangle - \langle H^{B}\rangle^{+}\right] - \left[\langle H^{C}\rangle - \langle H^{C}\rangle^{+}\right] = 0$$

When Equation (2-23) is rewritten in the form

$$H_{nm} = \bar{H}^{AB}_{nm} + \bar{H}^{AC}_{nm} + \bar{H}^{BC}_{nm} - \bar{H}^{A}_{nm} - \bar{H}^{B}_{nm} - \bar{H}^{C}_{nm} \tag{2-27}$$

where

$$\bar{H}^{PQ}_{nm} = \frac{1}{2}\left(H^{PQ}_{nm} + H^{PQ}_{mn}\right) \tag{2-28}$$

$$\bar{H}^{P}_{nm} = \frac{1}{2}\left(H^{P}_{nm} + H^{P}_{mn}\right) \tag{2-29}$$

there is no necessary relationship between the elements of what may be called the diatomic valence state energy matrices $\langle H^{PQ} \rangle$ and atomic valence state matrices $\langle H^{P} \rangle$. Both new matrices are Hermitian, and both are defined uniquely in any representation which may be constructed linearly from our set of canonical valence-bond structures Ψ_n (42).

Equation (2-27) is the fundamental equation in the method of diatomics in molecules. The total matrix element H_{nm} has been partitioned into parts corresponding to independent contributions from each diatomic and monatomic fragment. The theory is still exact, no approximations having been made as yet. Only the use of a limited set of canonical structures in Equations (2-13) and (2-14) can contribute to errors in this first portion of the theory; this restriction is common to nearly all theories of electronic structure.

Consider now a partitioning of the total antisymmetrization

operator A:

$$A = A_{PQ}^{(PQ)} \; A_{PQ} \; A_{(PQ)} \tag{2-30}$$

Here, the function of the operators $A_{(PQ)}$ is to antisymmetrize that set of electrons which are not originally assigned to the diatomic fragment PQ, whereas A_{PQ} antisymmetrizes that set of electrons which are originally assigned to PQ. The operator, $A_{PQ}^{(PQ)}$ is the partial or "supplementary" antisymmetrizer which completes the identity. The original assignment of the electrons into the two sets is specified by the assignment of electrons within the primitive function Ψ_m in Equation (2-24). Substitution of Equation (2-30) into Equation (2-24) yields

$$H_{nm}^{PQ} = \int \bar{\Psi}_n^* \; A_{PQ}^{(PQ)} \; H_{PQ} \; A_{PQ} \; A_{(PQ)} \; \Psi_m \; d\tau \tag{2-31}$$

since H_{PQ} commutes with both $A_{(PQ)}$ and A_{PQ}.

Since the primitive function Ψ_m is a linear combination of simple products of atomic spin orbitals, then

$$\Psi_m = \sum_r b_{mr} \; d_r \tag{2-32}$$

where

$$D_r = A \; d_r \tag{2-33}$$

Each sample product d_r may be written as

$$d_r = d_r^{PQ}\, d_r^{(PQ)} \tag{2-34}$$

Here, d_r^{PQ} contains all atomic spin orbitals associated with the diatomic fragment PQ only, whereas $d_r^{(PQ)}$ contains all other atomic spin orbitals. Thus, the right hand of the integrand in Equation (2-31) can be expressed as

$$A_{PQ}\, A_{(PQ)}\, \Psi_m = \sum_r b_{mr}\, D_r^{PQ}\, D_r^{(PQ)} \tag{2-35}$$

since

$$A_{PQ}\, A_{(PQ)}\, d_r^{PQ}\, d_r^{(PQ)} = D_r^{PQ}\, D_r^{(PQ)} \tag{2-36}$$

The latter two factors are determinantal functions totally antisymmetric with respect to those electrons in the set belonging to and not belonging to the diatomic fragment PQ, respectively.

Now, if the valence-bond approximations to the ground and excited states of the diatomic molecule PQ are available, then

$$\Psi_s^{PQ} = \sum_r c_{sr}\, D_r^{PQ} \tag{2-37}$$

The inverse of Equation (2-37) should be a good approximation of the

determinantal function in terms of the eigenfunction

$$D_r^{PQ} = \sum_s (c^{-1})_{rs} \Psi_s^{PQ} \tag{2-38}$$

Substitution of Equation (2-38) into Equation (2-35) and operation from the left upon the results by H_{PQ} yields

$$H_{PQ} A_{PQ} A_{(PQ)} \Psi_m = \sum_r \sum_s b_{mr} (c^{-1})_{rs} E_s^{PQ} \Psi_s^{PQ} D_r^{(PQ)} \tag{2-39}$$

$$= \sum_s E_s^{PQ} \Psi_s^{PQ} \sum_r b_{mr} (c^{-1})_{rs} D_r^{(PQ)} \tag{2-40}$$

Using Equation (2-37), Equation (2-40) is now transformed back to the determinantal wave function basis:

$$H_{PQ} A_{PQ} A_{(PQ)} \Psi_m = \sum_s E_s^{PQ} \sum_t \sum_r c_{st} b_{mr} (c^{-1})_{rs} D_{t,r} \tag{2-41}$$

since

$$A_{PQ}^{(PQ)} D_t^{PQ} D_r^{(PQ)} = D_{t,r} \tag{2-42}$$

Accumulating the double sum over t and r into a single sum over the independent determinants, D_u, Equation (2-41) can be written as

$$A_{PQ}^{(PQ)} H_{PQ} A_{PQ} A_{(PQ)} \Psi_m = \sum_s E_s^{PQ} \sum_u \varphi_{su} D_u \qquad (2\text{-}43)$$

Beginning with a canonical set of structures, Ψ_n, for the polyatomic molecule, Equation (2-13) can be inverted to obtain equations for each D_u in terms of canonical structure wave functions:

$$D_u = \sum_v (b^{-1})_{uv} \Psi_v \qquad (2\text{-}44)$$

Substituting Equation (2-44) into Equation (2-43) and combining the double sum over u and v into a single sum over w, gives

$$A_{PQ}^{(PQ)} H_{PQ} A_{PQ} A_{(PQ)} \Psi_m = \sum_s E_s^{PQ} \sum_w h_{sw} \Psi_w \qquad (2\text{-}45)$$

Introducing Equation (2-45) into Equation (2-31) yields

$$H_{nm}^{PQ} = \sum_s E_s^{PQ} \sum_w h_{sw} S_{nw} \qquad (2\text{-}46)$$

where the integrals S_{nw} are the overlap integrals between valence-bond structures as defined in Equation (2-16). The E_s^{PQ} are the experimental energies for the ground and excited electronic states of the diatomic molecule PQ.

The same procedure can be carried out to obtain the energy integrals H_{nm}^{P}, appearing in Equation (2-29), as

$$H^{P}_{nm} = \sum_{s} E^{P}_{s} \sum_{w} \gamma_{sw} S_{nw} \qquad (2\text{-}47)$$

in which the E^{P}_{s} are experimental energies for electronic states of the atom P.

It is obvious that Equations (2-27, (2-28), (2-29), (2-46), and (2-47) are fundamental in the method of diatomics-in-molecules. From these five relationships, the total energy matrix H_{nm} may be evaluated in terms of overlap integrals S_{nw} and experimental energies of diatomic and monatomic fragments which comprise the given polyatomic.

In actuality, Equation (2-37) will be available only in approximation. According to Ellison, however, use of the inverse of Equation (2-37)into Equation(2-39) followed by direct introduction of Equation (2-37) into Equation (2-40) suggests a partial cancellation of concomitant errors, and thus a possibly effective way to bridge the gap between polyatomic structure and one- and two-atom structures using valence-bond theory.

In Chapter V a potential energy surface for the linear system H--Br--Br will be derived using the diatomics in molecules method.

Classical Mechanical Calculations of Reaction Cross-Sections

The classical mechanical method of investigating reaction cross-sections is by numerical integration of Hamilton's canonical equations of motion for the colliding system. If one picks a random set of initial conditions for the collision of potentially reactive molecules, and numerically integrates the equations of motion to obtain the complete

trajectories of the particles involved, then by simply counting the number of trajectories that lead to reaction and noting the solid angle into which the products are scattered, one can obtain the reaction cross-section. If all interactions are previously known, then the calculation of individual trajectories is as exact as classical mechanics can be.

Wall, Hiller, and Mazur (43-44) used this approach to calculate reaction probabilities for the system $H_2 + H \rightarrow H + H_2$. This calculation clearly points out the complexities of this approach. For the system of three hydrogen atoms there are eighteen independent dynamical variables, six of which can be eliminated by requiring the center of mass of the system to be at rest. The total number of equations can be reduced further by taking into account the fact that the total energy and the three total angular momenta must be conserved. Wall and his colleagues deliberately retained twelve equations so that they could check the accuracy of their numerical integration. They assumed a London-Eyring-Polanyi (38) form for the potential-energy and integrated Hamilton's equations with the aid of a computer. This integration assumed that q_i and p_i, the position and momentum variables, respectively, corresponding to the ith degree of freedom, remained constant, at some average value, over time intervals Δt (2×10^{-16} seconds in their calculations; this is much less than the period of vibration of a hydrogen molecule, and it was found that both the total energy and angular momentum were accurately conserved for this value of Δt).

In the first work of Wall, Hiller, and Mazur, $H + H_2$ were held collinear and the initial conditions were varied systematically. In the second paper the atoms were no longer constrained to move in a straight

line, but were restricted to a single plane. The starting conditions (rotational, vibrational, and translational energies) were chosen by a weighted random method (Monte Carlo method). The first paper showed the reaction probability to be a complicated banded function of the energy of the reactants. Unfortunately, in the second calculation very little reaction took place (6 out of 700 approaches led to reaction) so that the results did not achieve a statistical significance.

Wall and Porter (45) returned to the original pattern of calculation (collinear reaction, systematic variation of reactant energies) with an altered $H + H_2$ potential-energy function. The new function (46), more empirical than the London-Polanyi-Eyring function, had a smooth potential barrier without a "basin" which characterizes their earlier surface. Removal of the "basin" had the effect of eliminating the marked oscillation in reaction probability, characteristic of the earlier surface.

Studying the same reaction and performing more extensive calculations, Karplus, Porter, and Sharma (47) found the rate constant at 1000°K to be 11×10^{11} cm^3 $mole^{-1}$ sec^{-1}, as compared to an experimental range of 11 to 22×10^{11} cm^3 $mole^{-1}$ sec^{-1}. They used a semiempirical potential-energy function (48) that is probably the best available at present for the $H + H_2$ interaction. An IBM 7094 computer was used to integrate the equations of motion. The initial rotational and vibrational energies of the reactant molecules were set, along with the value of the initial relative energy of approach, and a Monte Carlo scheme was used to average over the molecular orientation, vibrational phase, and the impact parameter. The reaction cross-section was found to be essentially the same for the first six rotational states of the reactant molecule, i.e., for

about 95 percent of the reactant molecules. This is a significant discovery since it eliminates the need for varying the initial rotational energy and hence the number of required calculations is reduced to only one-sixth of the number originally expected. The generality of this phenomenon with regard to reactions other than $H + H_2 \rightarrow H_2 + H$, will be discussed later.

Noteworthy work in classical mechanical treatments of bimolecular exchange reactions by Bunker (49-51) has treated the general case for reactions of type $A + BC \rightarrow AB + C$ by varying the reactant masses, the type of interaction potential, and the exothermicity. The motion was restricted to a plane. On the basis of 10,000 calculated trajectories, the following general conclusions were reached:

(1) The energy of reaction is converted predominantly into internal excitation of the product.

(2) A normal reaction is one in which AB is most likely to recoil backward along the approach line of A.

(3) The final rotation of AB absorbs as large a fraction of the initial orbital angular momentum as is allowed by conservation of energy.

Bunker also made calculations for the three-dimensional case. The treatment of Bunker and Karplus differed mainly in the averaging over initial conditions. Karplus, as stated above, set the initial values of the rotational and vibrational energies of the reactant molecule and the value of the initial energy of approach. He then averaged over the impact parameter and vibrational phase and orientation of the reactant molecule by a Monte Carlo method. Bunker, however, averaged over all the initial conditions by Monte Carlo techniques. The advantage of Karplus'

approach is that the reaction cross-section can be plotted as a function of the vibrational and rotational energies of the reactant molecule and the relative energy of approach. This reaction cross-section can then be fed into Equation (1-11) and the rate constant obtained by numerical integration. Any distribution function can be used, either the Maxwell-Boltzmann distribution or some perturbed distribution function. Bunker's method, however, requires that the distribution function be incorporated into the Monte Carlo segment of the calculation. As a result, a new set of calculations must be made if the distribution function is changed. Nevertheless, Bunker's approach has the advantage of requiring fewer trajectory calculations for the determination of a single reaction rate constant.

Collision Complex

In analyzing the details of collision, Karplus and his colleagues found no evidence of their potential energy hypersurface (48) of a H-H-H complex. The collision time was approximately 3×10^{-4} seconds, which is roughly the time required for an atom to make a single traversal of the field-of-force of the molecule. Reaction was found to be favored when the three atoms had a more linear configuration upon collision. These observations were in essential agreement with those of Wall, et al., (43-44) and with the crossed molecular beam experiments of the $D + H_2 \rightarrow DH + H$ reaction, by Datz and Taylor (52).

Comparison of Two-Dimensional and Three-Dimensional Calculations

A classical analysis of the reactive collisions of K and CH_3I ($K + CH_3I \rightarrow KI + CH_3$) was performed by Karplus and Raff (53-54) to aid in the elucidation of crossed molecular beam studies of this system by

Herschbach and his co-workers (55-56). The methods of calculation were similar to those used in the study of the $H + H_2 \rightarrow H_2 + H$ reaction (47). In the first paper (53), a comparison was made between the results calculated from a formulation that restricts the motion to a plane and one that treats the complete three-dimensional motion. The partitioning of the exothermicity of the reaction (22 kilocalories per mole) among the products and the total reaction cross-section were found to be similar in the two- and three-dimensional treatments. Other reaction attributes, however, were found to require a three-dimensional calculation for an accurate evaluation. These were the form of the differential reaction cross-section and the final-state angular-momentum distribution.

Elucidation of the Potential Energy Hypersurface

The potential-energy function used by Karplus and Raff (53) was one used by Bunker (49) in his two-dimensional treatment of the same reaction. Although the product-energy distribution was in reasonable agreement with the experimental estimate (55) (approximately 90 percent of the energy of reaction appears as rotational-vibrational energy of KI), the result obtained for the total reaction cross-section was in serious disagreement with the experimental data (400 $Å^2$ as compared with experimental value of 7 $Å^2$). By an examination of the dependence of the total reaction cross-section on the form of the interaction potential, it was found that the over-estimate of the long-range attraction between the K atom and the CH_3I molecule was the probable source of error and that introduction of an appropriate three-body attenuation term into Bunker's potential-energy function led to more reasonable results.

Later (54), Karplus and Raff calculated the differential cross-

section for the $K + CH_3I \rightarrow KI+CH_3$ reaction for four types of potential-energy hypersurfaces: (A) the modified Bunker surface used in their first paper (53); (B) a potential-energy function identical to A, except for a difference in the term designed to attenuate the K-I attraction when the CH_3 radical is near; (C) a potential-energy function similar to A, except for a different $K-CH_3$ repulsion term; (D) a special function designed to maintain some CH_3I attraction upon the approach of K, so that some semblance of a collision complex will result. They found that potential functions A and B gave results in reasonable agreement with experimental data on the differential cross-section (56). Potential function C gave a differential cross-section too peaked in the backward direction, while surface D gave results in complete disagreement with the three others and with experiment by yielding an essentially uniform center-of-mass differential reaction cross-section.

Although these comparisons between theory and experiment provided some information concerning the form of the potential energy hypersurface, Karplus and Raff felt more refined measurements and more general calculations are required before a definite analysis can be completed.

Classical mechanical calculations have also been used to elucidate the potential energy surface for certain exothermic reactions involving hydrogen and the halogens. The evidence from infrared chemiluminescence studies (6,10,57,58) indicates that the reactions $H + X_2 \rightarrow HX + X$ (H = H or D, and X = Cl or Br) channel the heat of reaction preferentially into relative translation and possibly rotation of the products, rather than into vibration. This behavior sharply contrasts with that of the reactions $X + M_2 \rightarrow MX + M$ (58) and $M + RX \rightarrow MX + R$ (56) (M is an alkali metal, R is

an alkyl radical, and X is a halogen atom) for which a major part of the heat of reaction goes into internal excitation (vibration and perhaps rotation) of the products. Evans and Polanyi (59) linked the behavior of the latter reactions to a type of potential-energy surface for linear reaction, which can be called a purely "attractive" surface (10). On an attractive surface the heat of reaction is liberated (potential → kinetic energy) along the coordinate corresponding to the approach of atom A to within a normal bonding distance of BC. By contrast, one can conceive of a purely "repulsive" surface, according to which the entire heat of reaction is liberated along the coordinate which corresponds to increasing separation of the products, AB + C. Of course, the most probable path across the potential-energy surface is not a strictly rectilinear one, in which r_{AB} decreases with r_{BC} constant, and then r_{BC} increases with r_{AB} constant. The "attractive" versus "repulsive" criterion is used simply as a means of characterizing the potential-energy surface.

The behavior of the H + X_2 reaction was accounted for in terms of a repulsive surface (6,8,10,57,60) by Nemeth, Polanyi, and their colleagues. The potential-energy surface used in their work was based on an empirical extension of the London-Eyring-Polanyi-Sato surface, and the atoms were constrained to move in a plane. In order to save computer time, initial conditions were varied systematically. Since the product energy distribution was very insensitive to the initial conditions (this is apparently a characteristic of the repulsive, but not of the attractive surface (60)) statistical averaging was not essential.

A gradually repulsive surface which is a modified London-Eyring-Polanyi-Sato potential-energy surface (60) gave on the average approxi-

mately three percent of the heat of the H + Cl_2 reaction as vibration for planar motion, roughly in agreement with experiment (57). Furthermore, the surface did not possess an unreasonably prolonged HCl-Cl interaction in comparison with experimental data on the HCl-Argon repulsion (61).

Not all the potential-energy surfaces which imply a purely "repulsive" interaction between the product molecules lead to a channeling of the heat of reaction into relative translation. It has recently been pointed out (60,62) that a repulsive surface which has a sufficiently steep outrun will lead to a substantial degree of vibrational excitation.

Quantum Mechanical Calculations of Reaction Cross-Sections

In comparison to the many classical mechanical treatments of bimolecular exchange reactions, relatively few reactions of this type have been studied quantum mechanically. As mentioned earlier, the calculation of reaction cross-sections by classical mechanics is quite time consuming, since the various molecular orientations and impact parameters (nonenergetic initial conditions) require the investigations of a large number of collisions. On the other hand, quantum mechanics offers an alternative method of averaging directly over the nonenergetic initial conditions. A new problem is encountered, however, in the form of the highly complicated Schroedinger equation governing the nuclear motion.

Earlier Treatments

One of the earliest quantum mechanical studies was made by Golden (63) who regarded both reactants and products (including electronic degrees of freedom) as different states of the same quantum mechanical system corresponding to different regions of configuration space. He then

approximated the transition probability between these states by the first order time-dependent perturbation theory of Dirac (64). Using the Born-Oppenheimer separation (27) to uncouple the electronic and nuclear motions, Golden obtained an explicit expression for the reaction rate in terms of the reactant and product state functions and a "perturbing" interaction between them. He also showed that the two above approximations enable the deduction of:

(1) the adiabatic hypothesis;

(2) the dependence of the reaction rate upon the concentration of the reactants;

(3) the condition for a vanishing reaction rate, which is equivalent to the statistical mechanical condition for equilibrium; and

(4) the dependence of the chemical reaction rate upon the temperature.

Golden and Peiser (65) applied the above theory to the reaction $H_2 + Br \rightarrow HBr + H$ at temperatures around 500°K. For the complete interaction potential of the reacting system, they used a simplified London-Eyring-Polanyi type surface. The "perturbed" interaction appearing in the expression for the transition probability is the complete potential minus the H_2 intramolecular interaction.

Now, the reactant and product state functions essentially vanish except for configurations in which the Br - H (A - B) and H - H (B - C) distances are in the neighborhood of their equilibrium values. Thus, it was necessary only to consider the behavior of the "perturbing" potential corresponding to this "equilibrium" configuration, so the "perturbing" potential was replaced by its expansion around the equilibrium distances.

Then, since the H - Br (A - B) and H - H (B - C) distances were essentially the equilibrium values, the interaction between the outer atoms Br and H (A and C) depended essentially upon the angle ABC. To simplify calculations, Golden and Peiser crudely approximated the coulombic and exchange integrals Q_{AC} and J_{AC}, by constant values Q^*_{AC} and J^*_{AC}. Since the London-Eyring-Polanyi potential usually relies on the increase in J_{AC}, upon the approach of A to BC, to produce the activation barrier, this was a significant modification. Since the reaction $H_2 + Br \rightarrow HBr + H$ is highly endothermic, however, the overall activation barrier was not seriously affected.

The reaction rate for $H_2 + Br \rightarrow HBr + H$ did not appear to be sensitive to the choice of J^*_{AC} and Q^*_{AC}. The rate was far more sensitive, however, to the choice of the fraction of coulombic binding, χ. Corresponding to $\chi = 0$, the calculated rate was 10^{-4} cc mole^{-1} sec^{-1} and then decreased monotonically with increasing χ until, at $\chi = 0.3$, it was 10^{-6} cc mole^{-1} sec^{-1}. Because of the extreme sensitivity of the perturbation treatment to the choice of χ, Golden and Peiser never decided on a reaction rate.

Several other results were derived, however, which were not sensitive to the assumed fraction of coulombic binding. It was found that the variation of the absolute rate with temperature, as calculated at 500°K, agrees well with the observed variation. Surprisingly, approximately 95 percent of the rate of reaction appeared to come from those hydrogen molecules in the first excited vibrational state. Furthermore, the distribution of the initially formed hydrogen bromide molecules were found to be representable by a pseudo-Boltzmann distribution function with a "rotational temperature" approximately one-half the initial temperature.

Reactions of the same type as above ($X + H_2 \rightarrow HX + H$, where X is Br or Cl) were studied by Bauer and Wu (66). For mathematical simplification, the reactive collisions between H_2 and X were treated as adiabatic and collinear. Furthermore, since the activation energy E_a is empirically of the order vibrational rather than rotational quanta, the authors assumed that reaction involved an interchange of translational and vibrational energy.

Beginning with the above assumptions, Bauer and Wu calculated the rate of formation $k^{\#}$ of short-lived activated states $H_2X^{\#}$ and then multiplied $k^{\#}$ by the probability κ of passing from the activated state into the product state. The resulting product was said to equal the rate constant k for the overall reaction. Assuming about equal probabilities of the system in the state $H_2X^{\#}$ going back to the initial state or forward to the final state, κ was set equal to one-half. A comparison of $k = \frac{1}{2}k^{\#}$ was then made with simple collision theory, or

$$k = P Z \exp(-E_a/RT) \qquad (2\text{-}48)$$

where Z is the statistical collision number and P is the steric factor (67). The predicted steric factor resulting from the comparison was about 8×10^{-3} for both reactions (X = Cl, Br); this figure is disappointly low.

Bauer and Wu also calculated the lifetime of the activated complex to be about 5×10^{-12} seconds. As this corresponds to the time required for 10-100 vibrations, this result is in total disagreement with classical

kinematics, which predicts a collision lifetime of the order of a single vibration.

By using a high-speed computer, Mazur and Rubin (68) attempted to calculate the average quantum mechanical probability of the reaction $A + BC \rightarrow AB + C$ for collinear collisions at a temperature T when BC is initially in its ground or first excited vibrational state. The average refers to the average over the distribution of the relative moments of collisions between A and BC at temperature T. These authors used a procedure, involving the numerical solution of the time-dependent Schroedinger equation, of sufficient generality to allow the use of any three-atom potential energy surface. To save computer time, however, the surface actually used was a highly simplified one involving three separate plateaux (a reactant, an activated complex, and a product plateau). In the numerical procedure, the motion of a wave packet across this surface was analyzed. For comparison, a classical investigation of the reacting system was made for the same potential-energy surface. When the reacting masses were all set equal to that for hydrogen, the classical reaction-probability was five times the quantum reaction-probability.

The immediate conclusion from the above results might be that classical mechanics is inapplicable to chemical reactions, or at least those involving light masses. It must be recalled, however, that the simplified potential-energy surface involved finite discontinuities between the plateaux, whereas actual potential-energy surfaces are thought to be uniformly continuous. Thus, the work of Rubin and Mazur should be repeated for more realistic potential-energy surfaces before any conclusions are drawn concerning the validity of classical mechanics with respect to

collisions of the type A + BC → AB + C.

Mortensen and Pitzer (69) carried out a numerical solution of the time-independent Schroedinger equation for the reacting system H + H_2 → H_2 + H. Employing a realistic potential-energy surface of the London-Eyring-Polanyi-Sato type, they calculated the transmission coefficient, K_{ij}, for several total energies and several values of the initial and vibrational state, i and j. At first, strictly collinear collisions were considered, reducing the Schroedinger equation to a two-variable partial differential equation. Later, a small angle bending term was added to the Hamiltonian and the corresponding transmission coefficients were calculated. The results obtained by Mortensen and Pitzer are presented in Table 1, with K_{ij} tabulated versus i, j, and the total energy E for collinear collisions with and without bending corrections.

Table 1. Transmission Coefficients at Various Total Energies

			K_{ij}	
			With Bending Correction	Without Bending Correction
E(kcal)	i	j		
10	1	1	0.140	0.00586
11	1	1	0.654	
14	1	1	0.999	0.903
17.5	1	1	0.967	
20	1	1	0.762	
20	2	1	0.148	
20	1	2	0.151	
20	2	2	0.360	

From these results they concluded that it was necessary to consider the bending motion in the reactive configuration, especially at low energies.

Recent Contributions

All of the previously discussed quantum mechanical investigations of bimolecular exchange reactions have included approximations with respect to the nuclear motion. In recent years, several complicated treatments (70-71) have accounted more rigorously for the multi-dimensionality of the reactive collisions. For the most part, these efforts were executed in the formalism of the quantum theory of collisions (25).

In studying the reactive collisions of $H + H_2 \rightarrow H_2 + H$, Tang (70) employed both the distorted wave Born approximation and the perturbed stationary state approximation* to derive expressions for the differential reaction cross-sections. Because of the thermal neutrality of the above exchange reaction, Tang intentionally omitted the possibility of vibrational excitation from the formulation but did allow for the possibility of rotational excitation.

Included in the formulas for the cross-sections were six-dimensional transition integrals*, a few of which were evaluated by a high-speed computer. Unfortunately, about forty hours of computer time were required to evaluate only one of these six-dimensional integrals. Thus, to avoid the use of a prohibitive amount of computer time, Tang calculated only a few of the transition integrals by six-dimensional integration. He then introduced what he called the "linear" model which assumes that finite contributions to the transition integral results only from linear configurations of the reacting system $H + H_2$. Before integrating over the relative orientation of the H_2 molecule with respect to the H atom, a Dirac delta

---

* For the definition of this terminology see Chapter III.

function (72) was included in the integrand of the transition integral to insure that only the linear configuration made a finite contribution. This manipulation reduced the dimensionality of the transition integral from six to two, thus decreasing greatly the time required for numerical integration. Tang calculated all of the differential reaction cross-sections of interest by the "linear" model approach and compared the results with the limited results of the more rigorous six-dimensional procedure. He then computed the ratio r_{cs} of the more rigorous cross-section to the corresponding "linear" model cross-section. Tang's assumption was that if all the "linear" model cross-sections were multiplied by r_{cs}, the results would closely approximate the results of the six-dimensional integration procedure.

The results of the analysis just discussed indicated a high probability of back-scattering, i.e., the product H_2 molecule recoils backward in the direction from which the initial H atom approaches. Both the distorted wave approximation and the perturbed stationary state approximation gave the same qualitative results, but the latter method gave values for the differential reactive cross-sections that were generally twenty times greater than those obtained by the former method.

The potential energy surface used by Tang was probably the best available for the $H + H_2$ system--the potential energy surface of Karplus and Porter (48) discussed previously in this chapter.

In conjunction with the molecular beam scattering experiments of Ross, et al., Suplinskas (71) performed a quantum mechanical analysis of the reactive collisions $K + HBr \rightarrow KBr + H$. Beginning with the formal theory of scattering, he developed a chemical analog to the core-core

interaction theory of Greider for nuclear collisions involving rearrangements (73). Suplinskas eventually obtained an expression for the transition integral corresponding to the above reaction that was similar to the results of the distorted wave Born approximation. A more detailed review of this approach will be given in Chapter III.

Suplinskas postulated a potential energy function for the KBr + H system which included no interaction between H and K. An attenuation factor was included in the expression for the potential-energy function which weakened the KBr bond on the approach of H. Morse type interactions (39) were assumed for the unperturbed HBr and KBr bonds.

Before evaluating the transition integrals Suplinskas also neglected the interaction between the product KBr molecule and the departing H atom. This allowed strict separation of the translational motion between H and KBr from the vibrational motion of KBr, and enabled the translational motion to be represented by a plane wave function.

Also, the wave function corresponding to the distorted vibration of KBr was approximated by a harmonic oscillator wave function with a Hooke's law constant dependent on the distance between H and Br. This vibrational wave function resulted from an additional approximation to the perturbed stationary state approximation.

After obtaining an algebraic expression for the transition integral, and therefore for the differential reaction cross-section, Suplinskas integrated over the scattering angles to obtain an expression for the total reaction cross-section. He evaluated the total reaction cross-section for various initial translational and vibrational energies and final rotational and vibrational energies. Only a single initial rotational state (the

third excited state) for HBr was considered since it was assumed that the total reaction cross-section was relatively insensitive to the initial rotational energy.

For an initial translational energy of 2.0 kcal/mole and an initial vibrational energy corresponding to the ground state, Suplinskas calculated the total cross-sections for reaction to form KBr in various vibrational states. The reaction cross-sections corresponding to the ground and first excited vibrational states were about 5.0 $Å^2$ each, but the cross-sections fell off rapidly for the more highly excited states (0.3 $Å^2$ for the fifth excited state and 0.08 $Å^2$ for the seventh excited state). This was expected, of course, since the exothermicity of the reaction (4.2 kcal/mole) is insufficient to produce KBr in the higher excited states. For the same initial conditions, the distribution of the reaction cross-sections with respect to the final rotational states of KBr showed a somewhat sharp peak at the 70th excited rotational state.

When HBr was initially in the ground vibrational state, the total cross-sections into all available states of KBr were determined by Suplinskas to be about 37 $Å^2$ for an initial translational energy $E_{tr,i}$ of 1.0 kcal/mole, 10 $Å^2$ for $E_{tr,i}$ equal to 2.0 kcal/mole, and about 5.0 $Å^2$ for $E_{tr,i}$ equal to three, four, and five kcal/mole. Suplinskas attributed the anomalously high values of the reaction cross-section at low values of $E_{tr,i}$ to the use of a plane wave to describe the relative translational motion of H and KBr. This gave excessively high values for the exact wave corresponding to H in close proximity with KBr. At low values of $E_{tr,i}$, and thus at low values of the total energy, the probability that H can be very close to KBr is negligible, since repulsive forces become dominant at

close range. The cross-sections corresponding to the higher values of $E_{tr,i}$ were considered to be in fair agreement with the experimental cross-section of 32 $Å^2$ (19), considering the many assumptions included in the calculations.

CHAPTER III

THE QUANTUM THEORY OF SCATTERING

In their recent studies of reactive collisions, both Tang (70) and Suplinskas (71) utilized the time-independent approach within the formal theory of scattering. Gerjouy (74) and Lippmann (75) have been the prime developers of the time-independent theory, while some crucial points have been analyzed by Epstein (76). The time-dependent approach, based mainly on the work of Gell-Mann and Goldberger (77), is admirably reviewed by Wu and Ohmura (25) in their recent text on the quantum theory of scattering.

As previously stated, the binary collisions are assumed to occur independently, uninfluenced by any effects external to the colliding molecules. The Hamiltonian governing the behavior of the collision system is therefore not an explicit function of time, and the time-dependent and time-independent formalisms lead to identical expressions for the reaction cross-sections. Because it is less complicated conceptually, the time-independent approach will be used in the present study.

Explicit expressions for the reaction cross-sections derived in this chapter will be used for actual calculations in Chapter V. The development herein closely follows that of Suplinskas (71) and is included as a convenience to those readers unfamiliar with the quantum theory of collisions.

The Hamiltonian Operator

Consider the reactive collision A + BC → AB + C which is diagrammed in Figure 1. For discussion purposes, it is convenient to begin with a classical mechanical description of the collision and to convert later to quantum mechanics by using the appropriate postulates (78).

The Classical Mechanical Hamiltonian

In classical mechanics the time-independent Hamiltonian for the motion of three particles A, B, C of masses m_A, m_B, m_C, respectively, is

$$H = \frac{1}{2m_A}\left(p_{xA}^2 + p_{yA}^2 + p_{zA}^2\right) + \frac{1}{2m_B}\left(p_{xB}^2 + p_{yB}^2 + p_{zB}^2\right) \tag{3-1}$$

$$+ \frac{1}{2m_C}\left(p_{xC}^2 + p_{yC}^2 + p_{zC}^2\right) + V(x_A, y_A, z_A, x_B, y_B, z_B, x_C, y_C, z_C)$$

Here, the coordinates x_A, y_A, ..., z_C are the cartesian coordinates of the particles A, B, and C in a reference frame stationary with respect to an observer, i.e., the laboratory frame. The symbols p_{xA},..., p_{zC} are the linear moments conjugate to these coordinates (79). The potential-energy function V is usually a function only of the three interatomic distances, r_{AB}, r_{AC}, and r_{BC}, so

$$V = V(r_{AB}, r_{BC}, r_{AC}) \tag{3-2}$$

where

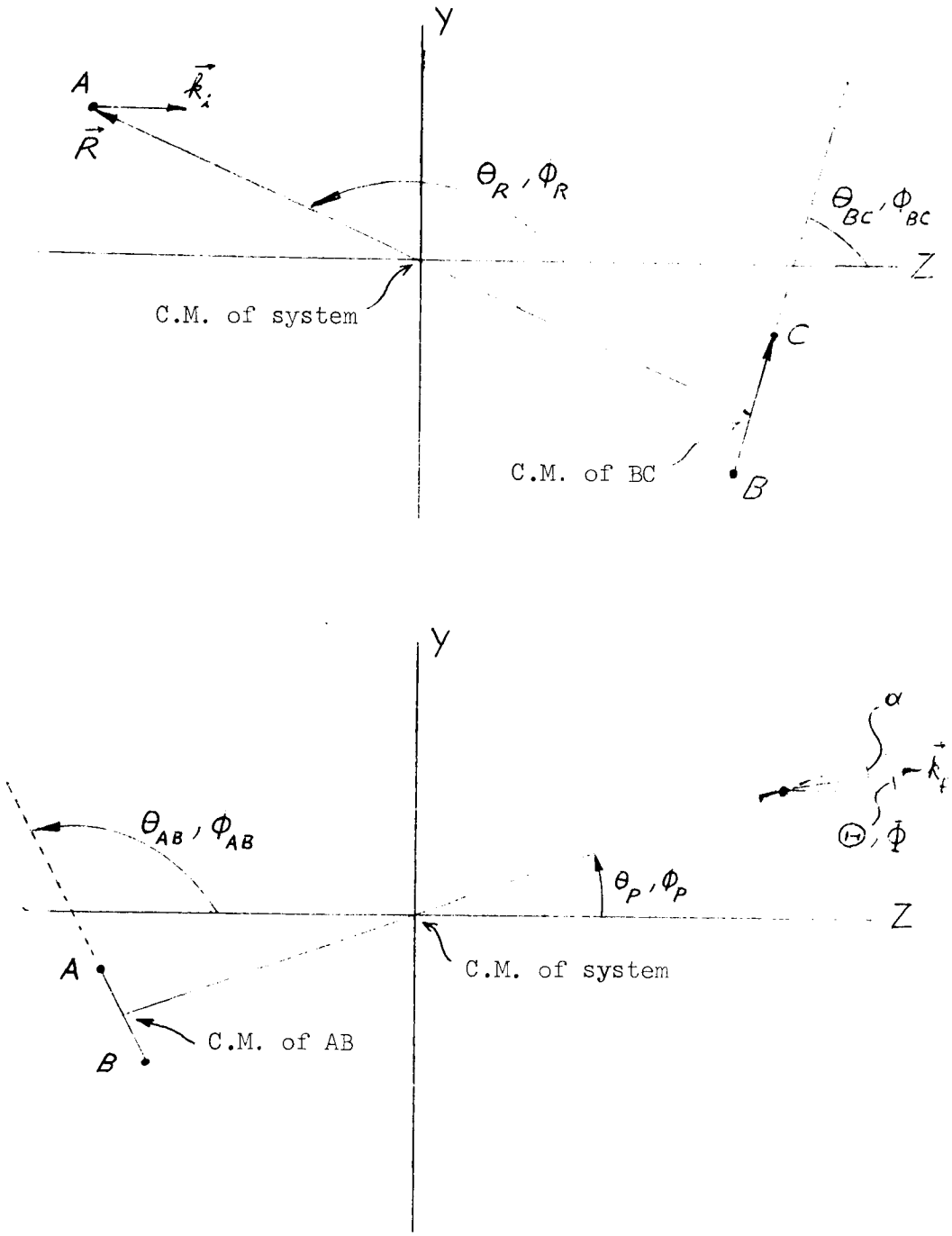

Figure 1. Collision Diagram in Center of Mass System

$$r_{AB} = \left| \left[(X_A - X_B)^2 + (y_A - y_B)^2 + (Z_A - Z_B)^2 \right]^{1/2} \right| \tag{3-3}$$

Expressions similar to Equation (3-3) define r_{BC} and r_{AC}.

The canonical equations of motion are given by (80)

$$\dot{P}_{xi} = -\partial H / \partial x_i \tag{3-4}$$

$$\dot{P}_{yi} = -\partial H / \partial y_i$$

$$\dot{P}_{zi} = -\partial H / \partial Z_i$$

and

$$\dot{X}_i = \partial H / \partial P_{xi} \tag{3-5}$$

$$\dot{y}_i = \partial H / \partial P_{yi}$$

$$\dot{Z}_i = \partial H / \partial P_{zi}$$

If a classical description of the collision is desired, Equations (3-4) and (3-5) can be integrated to yield X_A, Y_A, ..., Z_C and P_{XA}, P_{YA}, ..., P_{ZC} as functions of time, provided the initial values are specified for these variables.

Coordinate System for Initial Stage of Reactive Collision. When considering the collision of a molecule BC with an oncoming atom A, it is convenient to use a different set of coordinates (80). The new set of coordinates are:

1. The center of mass coordinates of the entire system

$$X = (m_A x_A + m_B x_B + m_C x_C)/(m_A + m_B + m_C) \tag{3-6}$$

$$Y = (m_A y_A + m_B y_B + m_C y_C)/(m_A + m_B + m_C)$$

$$Z = (m_A z_A + m_B z_B + m_C z_C)/(m_A + m_B + m_C)$$

2. The components of the vector between atoms B and C, $\vec{r}_{BC}$

$$x_{BC} = x_B - x_C \tag{3-7}$$

$$y_{BC} = y_B - y_C$$

$$z_{BC} = z_B - z_C$$

3. The components of the vector $\vec{R}$ between atom A and the center of mass of BC

$$R_x = x_A - (m_B x_B + m_C x_C)/(m_B + m_C) \tag{3-8}$$

$$R_y = y_A - (m_B y_B + m_C y_C)/(m_B + m_C)$$

$$R_z = z_A - (m_B z_B + m_C z_C)/(m_B + m_C)$$

These new coordinates are such that Hamilton's equations, Equations (3-4) and (3-5), are invariant under the transformation. Also, by selecting a reference frame in which the center of mass coordinates remain constant, i.e., the center of mass system, the new Hamiltonian takes the form (80)

$$H = \frac{1}{2\mu_i}(P_1^2 + P_2^2 + P_3^2) + \frac{1}{2m_{BC}}(P_4^2 + P_5^2 + P_6^2) + V(r_{AB}, r_{BC}, r_{AC}) \tag{3-9}$$

where

$$\mu_i = m_A(m_B + m_C)/(m_A + m_B + m_C) \tag{3-10}$$

$$m_{BC} = m_B m_C/(m_B + m_C) \tag{3-11}$$

The symbols p_1, p_2, ..., p_6 denote the momenta conjugate to the coordinates

$$q_1 = x_{BC} \tag{3-12}$$

$$q_2 = y_{BC}$$

$$q_3 = z_{BC}$$

$$q_4 = R_x$$

$$q_5 = R_y$$

$$q_6 = R_z$$

respectively.

Coordinate System for the Final Stage of Reactive Collisions. To keep track of the motion of the products of the reaction A + BC, AB + C, another coordinate system should be introduced. The coordinate system is the same as that used in the initial stage, except that the set of variables used within that coordinate system is changed. In this case, the vector $\vec{P}$ is defined as the vector between atom C and the center of mass of AB. The components of $\vec{P}$ are

$$P_x = X_c - (m_A x_A + m_B x_B)/(m_A + m_B) \tag{3-13}$$

$$P_y = y_c - (m_A y_A + m_B y_B)/(m_A + m_B)$$

$$P_z = Z_c - (m_A Z_A + m_B Z_B)/(m_A + m_B)$$

and the components of the vector $\vec{r}_{AB}$ between atoms A and B are

$$X_{AB} = x_A - X_B \tag{3-14}$$

$$y_{AB} = y_A - y_B$$

$$Z_{AB} = Z_A - Z_B$$

Then the Hamiltonian governing the motion of A, B, and C can be written (80) as

$$H = \frac{1}{2\mu_f}(p_1^2 + p_2^2 + p_3^2) + \frac{1}{2m_{AB}}(p_4^2 + p_5^2 + p_6^2) \tag{3-15}$$

$$+ V(r_{AB}, r_{Bc}, r_{Ac})$$

where

$$\mu_f = m_c (m_A + m_B)/(m_A + m_B + m_c) \tag{3-16}$$

$$m_{AB} = m_A m_B /(m_A + m_B) \tag{3-17}$$

The momenta $p_1, p_2, \ldots, p_6$ are conjugate to the coordinates

$$q_1 = X_{AB} \tag{3-18}$$

$$q_2 = Y_{AB}$$

$$q_3 = Z_{AB}$$

$$q_4 = P_x$$

$$q_5 = P_y$$

$$q_6 = P_z$$

respectively.

Like the coordinate transformations of Equations (3-7) and (3-8), Equations (3-13) and (3-14) are invariant under the transformations just

described.

The Quantum Mechanical Hamiltonian Operators

The following equations represent well known quantum mechanical postulates (78) for conversion of classical mechanical variables to quantum mechanical operators:

$$p^2 = \hbar^2 \, \partial^2/\partial q^2 \tag{3-19}$$

$$q = q \tag{3-20}$$

where q is a classical position coordinate and p is its conjugate momentum. Subjecting Equations (3-9) and (3-15) to the prescription given by Equations (3-19) and (3-20) yields the following expressions for the quantum mechanical operators appropriate to the initial and final stage of the collision, respectively:

$$\mathcal{H} = -\frac{\hbar^2}{2\mu_i}\nabla_R^2 - \frac{\hbar^2}{2m_{BC}}\nabla_{r_{BC}}^2 + V(\vec{R}, \vec{r}_{BC}) \tag{3-21}$$

$$\mathcal{H} = -\frac{\hbar^2}{2\mu_f}\nabla_P^2 - \frac{\hbar^2}{2m_{AB}}\nabla_{r_{AB}}^2 + V(\vec{P}, \vec{r}_{AB}) \tag{3-22}$$

Here,

$$P = \left| \left[P_x^2 + P_y^2 + P_z^2 \right]^{1/2} \right| \tag{3-23}$$

$$R = \left| \left[R_x^2 + R_y^2 + R_z^2 \right]^{1/2} \right| \tag{3-24}$$

Since the potential energy functions and the Hamiltonian operators are the same,

$$-\frac{\hbar^2}{2\mu_i} \nabla_R^2 - \frac{\hbar^2}{2m_{BC}} \nabla_{r_{BC}}^2 = -\frac{\hbar^2}{2\mu_f} \nabla_P^2 - \frac{\hbar^2}{2m_{AB}} \nabla_{r_{AB}}^2 \tag{3-25}$$

Schroedinger Equation Appropriate to Initial Stage of Collision

Taking note of Equation (3-21), the Schroedinger equation for the reactive collision A + BC → AB + C, can be written as

$$\left[-\frac{\hbar^2}{2\mu_i} \nabla_R^2 - \frac{\hbar^2}{2m_{BC}} \nabla_{r_{BC}}^2 + V(\vec{R}, \vec{r}_{BC}) \right] \Psi(\vec{R}, \vec{r}_{BC}) \tag{3-26}$$

$$= E \, \Psi(\vec{R}, \vec{r}_{BC})$$

where $\Psi(\vec{R}, \vec{r}_{BC})$ is the total wave function for the system, and E denotes the total energy of the system. An important boundary condition imposed on $\Psi(\vec{R}, \vec{r}_{BC})$ is the initial asymptotic condition. Since the interaction between the colliding molecules is negligible for large R, the initial

asymptotic condition for the wave function can be represented as a product of wave functions corresponding to the free relative motion between A and BC and the internal states of A and BC. All molecules are assumed to be in their ground electronic states so A is regarded as a structureless mass. The diatomic molecule can be approximated as a rigid rotator, Morse oscillator (81). Thus, the initial asymptotic condition for $\Psi(\vec{R},\vec{r}_{BC})$ can be written as

$$\varphi_i = \lim_{R\to\infty} \Psi(\vec{R},\vec{r}_{BC}) = \exp(i\vec{k}_i\cdot\vec{R})\, Y_{l_i}^{m_i}(\theta_{BC},\phi_{BC})\, Z_{n_i}(r_{BC}) \qquad (3\text{-}27)$$

where $Y_{l_i}^{m_i}(\theta_{BC}, \phi_{BC})$ denotes the spherical harmonic function ocrresponding to the rigid rotation of BC, and $Z_{n_i}(r_{BC})$ denotes the Morse oscillator function corresponding to the vibration of BC. The symbols n_i, l_i, and m_i denote the vibrational, angular momentum, and Z-component of angular momentum quantum numbers, respectively, for the BC molecule. θ_{BC} and ϕ_{BC} are, of course, the angular components of $\vec{r}_{BC}$ in spherical coordinates (see Figure 1). The vector $\vec{k}_i$, the wave vector, has the direction of $\vec{v}_i$ and the magnitude $(\mu_i/\hbar)\, v_i$.

One of the most familiar results of quantum mechanics is that if the total wave function is a product of wave functions corresponding to different modes of motion, then the total energy is the sum of the separate energies for these particular modes. Thus, in the initial asymptotic case above, the total energy is the sum of the relative translational energy of approach, the vibrational energy of the molecule BC, and the rotational energy of BC, provided the ground electronic states of A and BC are taken

as zero energy.

Schroedinger Equation Appropriate to Final Stage of Collision

The product wave function represents the collision system when the product molecules have reached such large separations that no intermolecular interaction exists. To account for all the various probabilities of the collision results, the post-collision wave function must include the sum of terms corresponding to molecules which are the products of elastic, inelastic, and reactive scattering. After the collision has occurred, the product molecules might still be A and BC, with BC either in a different internal state or not, or some chemical rearrangement might have taken place to form, say, atom C and molecule AB. By visualizing a detector which can distinguish between different chemical types of molecules and their internal states, attention can be focused on a single term in the product wave function representing the particular species of molecule detected.

Consider now the collision leading to the atom C and the diatomic molecule AB with vibrational quantum number n_f and rotational quantum numbers l_f and m_f. Using Equation (3-22) one can write the Schroedinger equation as

$$\left[-\frac{\hbar^2}{2\mu_f}\nabla_P^2 - \frac{\hbar^2}{2m_{AB}}\nabla_{r_{AB}}^2 + V(\vec{P},\vec{r}_{AB})\right]\Psi(\vec{P},\vec{r}_{AB}) \qquad (3\text{-}28)$$

$$= E\,\Psi(\vec{P},\vec{r}_{AB})$$

As P approaches infinity, the interaction between A and BC vanishes so that the final asymptotic expression for the total wave function can be written as

$$\varphi_f = \lim_{P\to\infty} \Psi(\vec{P}, \vec{r}_{AB}) \qquad (3\text{-}29)$$

$$= f_f^i(\Theta, \Phi)\,[\exp(i k_f P)/P]\, Z_{n_f}(r_{AB})\, Y_{l_f}^{m_f}(\theta_{AB}, \phi_{AB})$$

where Θ and Φ are the deflection angles in the center of mass system (see Figure 1). The first two factors on the right side of Equation (3-29) correspond to the relative translational motion of AB and C. Particle flux is conserved by $\exp(ik_fP)/P$, in which the wave vector $\vec{k}_f$ has the direction of the final relative mom velocity $\vec{v}_f$ and the magnitude $(\mu_f/\hbar)v_f$. The factor $f_f^i(\Theta, \Phi)$, called the scattering amplitude, takes into account the anisotropic scattering caused by the peculiarities of the initial conditions and the potential energy function. On $f_f^i(\Theta, \Phi)$, the superscript i denotes the set of initial conditions n_i, l_i, m_i, k_i, and the subscript f denotes the set of final conditions n_f, l_f, m_f.

The Cross-Section and the Scattering Amplitude

A very important relationship between the differential reaction cross-section mentioned in Equation (1-8) and the scattering amplitude of Equation (3-29) will now be presented:

$$\sigma_f^i(\Theta,\Phi) = \frac{k_f}{k_i}\frac{\mu_i}{\mu_f}\left|f_f^i(\Theta,\Phi)\right|^2 \qquad (3\text{-}30)$$

The derivation of this expression will be omitted since it is rather lengthy and is thoroughly treated in most standard textbooks on quantum mechanics (82).

The quantum mechanical treatment of the reaction cross-section is now reduced to the quest for the wave functions, possessing the correct asymptotic form, of the complete system Hamiltonian. Once these wave functions are found, the scattering amplitudes $f_f^i(\Theta, \Phi)$ can be obtained by comparing the wave functions, in the limit of infinite P, with Equation (3-29). Of course, very few wave equations of the type represented by Equations (3-26) and (3-28) are analytically solvable, and suitable methods of approximation must be sought.

It is very difficult to make intelligent and intuitive approximations with the Schroedinger equation in the form of Equation (3-26) or Equation (3-28). A more suitable formalism for analyzing the exact nature of proposed approximations can be obtained by recasting the Schroedinger equation in the form of an integral equation. This is the approach taken in the following section, which contains a discussion on the approximate methods appropriate for exchange collisions of the type A + BC → AB + C.

The Differential Reaction Cross-Section

At this point it is appropriate to present expressions for the scattering amplitude in terms of the solutions to the Schroedinger equation governing the collision A + BC → AB + C. Since extensive derivations

of the equations that follow appear in many sources (83), no attempt will be made to repeat the derivations in the present study. For the purposes here, the two most important expressions for the scattering amplitude are:

$$f_f^i(\Theta,\Phi) = \left(\frac{\mu_f}{2\pi\hbar^2}\right)\iint \varphi_f^*(\vec{r}_{AB}',\vec{P}')\,\bar{U}_i(\vec{r}_{AB}',\vec{P}') \tag{3-31}$$

$$\times\, \Psi_i^+(\vec{r}_{AB}',\vec{P}')\; d^3\vec{r}_{AB}'\; d^3\vec{P}'$$

and

$$f_f^i(\Theta,\Phi) = \left(\frac{\mu_f}{2\pi\hbar^2}\right)\iint \Psi_f^{-*}(\vec{r}_{AB}',\vec{P}')\,\bar{U}_f(\vec{r}_{AB}',\vec{P}') \tag{3-32}$$

$$\times\, \varphi_i(\vec{r}_{AB}',\vec{P}')\; d^3\vec{r}_{AB}'\; d^3\vec{P}'$$

Here, the function Ψ_f^- is the solution to Equation (3-28) having the asymptotic condition

$$\lim_{P\to\infty} \Psi_f^-(\vec{r}_{AB},\vec{P}) = \exp(i\vec{k}_f\cdot\vec{P})\,Z_{n_f}(r_{AB})\,Y_{\ell_f}^{m_f}(\theta_{AB},\phi_{AB}) \tag{3-33}$$

$$+ f(\Theta,\Phi)\left[\exp(-ik_fP)/P\right] Z_{n_f}(r_{AB})\,Y_{\ell_f}^{m_f}(\theta_{AB},\phi_{AB})$$

where the factor $f(\Theta, \Phi)$ multiplying the incoming wave function is an elastic scattering amplitude. The potential functions $\bar{U}_i(r_{AB}, P)$ and $\bar{U}_f(r_{AB}, P)$ are defined as

$$\bar{U}_i(\vec{r}_{AB}, \vec{P}) = V(\vec{r}_{AB}, \vec{P}) - V_{AB}(r_{AB}) \tag{3-34}$$

and

$$\bar{U}_f(\vec{r}_{AB}, \vec{P}) = V(\vec{r}_{AB}, \vec{P}) - V_{BC}(r_{BC}) \tag{3-35}$$

where V_{AB} and V_{BC} are the ground state potentials for molecules AB and BC, respectively.

Using Equation (3-30), one can now write

$$\sigma_f^i(\Theta, \Phi) = \left(\frac{\mu_f}{2\pi\hbar^2}\right)^2 \frac{k_f}{k_i} \frac{\mu_i}{\mu_f} \left| \iint \varphi_f^* \bar{U}_i \Psi_i^+ \, d^3\vec{r}_{AB} \, d^3\vec{P} \right|^2 \tag{3-36}$$

or

$$\sigma_f^i(\Theta, \Phi) = \left(\frac{\mu_f}{2\pi\hbar^2}\right)^2 \frac{k_f}{k_i} \frac{\mu_i}{\mu_f} \left| \iint \Psi_f^{-*} \bar{U}_f \varphi_i \, d^3\vec{r}_{AB} \, d^3\vec{P} \right|^2 \tag{3-37}$$

The remaining task is now to find either of the total wave functions Ψ_i^+ or Ψ_f^-. For realistic potential-energy surfaces, exact solutions to Equations (3-26) or (3-28) are practically unobtainable. Thus, an appropriate method of approximation must be used which avoids the mathematical

barriers of the exact problem but still yields physically meaningful results. Such a method is the perturbed stationary state approximation originally proposed by Mott (84). This approach was taken by Suplinskas (71) in his study of the K + HBr → KBr + H reaction but was only discussed by Tang (70) in his study of the H + H_2 → H_2 + H reaction. Chapters IV and V will demonstrate how the perturbed stationary state approximation can be applied to the study of a highly exothermic reaction such as H + Br_2 → HBr + Br.

Perturbed Stationary State Approximation

The perturbed stationary state approximation was formulated by Mott, Massey, and Bates (84, 85, 86) to attack those problems involving the slow collision of an atom, ion, or molecule with another such particle. Although this method is theoretically rigorous, various approximations must be made to avoid overwhelming mathematical difficulties. Below is an outline of the theory as applied to the reactive collision A + BC → C + AB. First, however, a discussion of the distorted wave method will be given because of its prominence in some of the previous applications of the perturbed stationary state approximation.

The Distorted Wave Method

Sometimes it is possible to obtain an exact solution to Equation (3-26) if some part of the potential can be neglected. For instance, since the Born-Oppenheimer separation has been assumed, the complete potential for the exchange reaction A + BC → AB + C can be written as

$$V = V_{AB} + V_{AC} + V_{BC} + V_{ABC} \qquad (3\text{-}38)$$

The two-body potentials V_{AB}, V_{BC}, V_{AC} are identical to the potentials for the isolated diatomic molecules AB, AC, and BC, respectively. The three-body potential V_{ABC} is defined as the deviation of the sum of the two-body potentials from the complete potential V when all three atoms are in the same vicinity.

Now, suppose the three-body interaction term V_{ABC} can be partitioned into two parts as

$$V_{ABC} = V_a^* + V_b^* \tag{3-39}$$

Here, it is assumed that V_a^* is predominantly an interaction between A and B, while V_b^* is primarily an interaction between B and C.

Now, define the function $\lambda_i^+(\vec{r}_{BC}, \vec{R})$ as the solution to

$$\left[-\frac{\hbar^2}{2\mu_i} \nabla_R^2 - \frac{\hbar^2}{2m_{BC}} \nabla_{r_{BC}}^2 + V_{BC} + V_b^* \right] \lambda_i^+ = E \lambda_i^+ \tag{3-40}$$

with the asymptotic condition given by Equation (3-27). Further, define the function $\lambda_f^-(\vec{r}_{AB}, \vec{P})$ as the solution to

$$\left[-\frac{\hbar^2}{2\mu_f} \nabla_P^2 - \frac{\hbar^2}{2m_{AB}} \nabla_{r_{AB}}^2 + V_{AB} + V_a^* \right] \lambda_f^- = E \lambda_f^- \tag{3-41}$$

with the asymptotic condition given by Equation (3-29). Then, it has been shown by Greider (73) that, to a first order approximation, one can write

$$\sigma_f^i(\Theta,\Phi) = \frac{k_f}{k_i}\left(\frac{\mu_f}{2\pi\hbar^2}\right)^2 \frac{\mu_i}{\mu_f}\left|\iint \lambda_f^{-*}\, \bar{u}_f\, \lambda_i^{+}\, d^3\vec{r}_{AB}\, d^3\vec{P}\right|^2 \qquad (3\text{-}42)$$

This is known as the distorted wave method and is particularly useful if exact solutions to Equations (3-40) and (3-41) can be found.

The "Linear" Model of Tang

Even if the exact wave functions Ψ_i^+ and Ψ_f^- were known, it would be practically impossible to evaluate the integrals of Equation (3-36) and (3-37) due to the unfactorable six-dimensional integrands. Thus, some reasonable approximation designed to simplify this integrand integration would be extremely welcome.

Using the distorted wave method, Tang (70) assumed that both λ_i^+ and λ_f^- essentially vanished unless $\theta_{AB} = \pi - \theta_P$ and $\phi_{AB} = \pi + \phi_P$ (see Figure 1). Thus, he replaced the element of volume $d^3\vec{r}_{AB}$ in Equation (3-42) with $C\,\delta(\pi - \theta_P, \theta_{AB})$, $\delta(\pi + \phi_P, \phi_{AB})\, r_{AB}^2\, dr_{AB}$. Here, $\delta(a, b)$ is a Dirac delta function defined as

$$\int_1^2 F(b)\,\delta(a,b)\,db = F(a) \qquad (3\text{-}43)$$

and C is a constant. Tang discovered that this model resulted in considerable simplification of the integral of Equation (3-42). The parameter C was adjusted so that $\sigma_f^i(\Theta, \Phi)$ agreed with the results of a long, tedious, six-dimensional integration of Equation (3-42) by high-speed computer.

The "Two-Dimensional Interaction" Model of Suplinskas

Suplinskas (71), in his study of the K + HBr → KBr + H reactive

collision, neglected the interaction between the potassium and the hydrogen atoms, thus reducing the potential $\bar{U}_f$ in Equation (3-35) from a three-dimensional to a two-dimensional function. This approximation also implies the unhindered rotation of KBr in the proximity of H. Thus, considerable simplification of Equation (3-37) resulted from the use of this model.

The "Linear Complex" Model

The "linear complex" model will be applied to the study of triatomic, exothermic, bimolecular reactions in the next chapter. It is based on the same assumption as the "linear" model of Tang; that is, the chemical forces tend to align the system A + B + C as A approaches BC. When the AB interatomic distance becomes approximately that of a free, unperturbed AB molecule, the three atoms ABC are assumed to be rigidly locked in a linear configuration. Since the complicated electronic and nuclear motions leading to reaction are assumed to occur when the atoms are in this compact arrangement, the effective potential of the "reactive" configuration is $V_L(r_{AB}, P)$, the potential-energy function for three atoms constrained to a straight line. Thus, as will be shown in the next chapter, it should be valid to replace Ψ_f^- in Equation (3-37) by χ_f^-, the solution to the problem

$$\left[K_p + K_{AB} + V_L \right] \chi_f^- = E \chi_f^- \qquad (3\text{-}44)$$

Here, K_p is the relative translational kinetic energy operator $-(\hbar^2/2\mu_f)$ ∇_p^2, K_{AB} is the vibrational kinetic energy operator $-(\hbar^2/2m_{AB})$ $\nabla_{r_{AB}}^2$, and E is the total energy of the colliding system. The asymptotic condition for

χ_f^- is Equation (3-33).

The guiding concept of the perturbed stationary state approximation is that the relative translational velocities of the colliding aggregates are extremely slow compared to the internal motions of the particles. Thus, the relative motion of AB and C is assumed to be adiabatic with respect to the vibrational motion of AB, and χ_f^- will be most appropriately expanded in terms of the molecular wave functions $z_n(\vec{r}_{AB}; P)$ which are the eigenfunctions, for fixed P, of

$$\left[K_{AB} + V_L(r_{AB}, P) \right] Z(\vec{r}_{AB}; P) = \epsilon_n(P) \; Z(\vec{r}_{AB}; P) \tag{3-45}$$

$\epsilon_n(P)$ denotes the internal energies of AB at a given P, and the $z_n(\vec{r}_{AB}; P)$ form a complete set of functions of r_{AB} for any fixed P. Asymptotically, for large P,

$$\lim_{P \to \infty} \epsilon_n(P) = E_n \tag{3-46}$$

$$\lim_{P \to \infty} z_n(\vec{r}_{AB}; P) = \zeta_n(\vec{r}_{AB}) \tag{3-47}$$

where E_n, $\zeta_n(\vec{r}_{AB})$ are the energy and eigenfunction of the unperturbed molecule AB in the state n. The boundary conditions for the $z_n(\vec{r}_{AB}; P)$ are the same as those for the $\zeta_n(\vec{r}_{AB})$.

Since

$$V_L(r_{AB}, P) = V_{AB}(r_{AB}) + U_{i,L}(r_{AB}, P) \tag{3-48}$$

where $U_{i,L}(r_{AB}, P)$ is the linear configuration form of the three-dimensional potential U_i, Equation (3-45) would be the Schroedinger equation for the $\zeta_n(\vec{r}_{AB})$ functions if the atom C were sufficiently removed from AB to cause $U_{i,L}(r_{AB}, P)$ to vanish. This perturbation of AB by C gives the perturbed stationary state approximation its name, although the perturbing potential $U_{i,L}$ is generally too large to handle by straightforward application of perturbation theory (87).

If $\epsilon_n(P)$ and $z_n(\vec{r}_{AB}; P)$ can be obtained by solving Equation (3-45), then the function χ_f^- may be expanded in terms of the $z_n(\vec{r}_{AB}; P)$ as

$$\chi_f^-(\vec{r}_{AB}; \vec{P}) = \sum_{n'} G_{n'}(\vec{P})\, z_{n'}(\vec{r}_{AB}; P) \tag{3-49}$$

Substituting Equation (3-49) into Equation (3-44), multiplying by $z_n^*(\vec{r}_{AB}; P)$ and integrating over r_{AB}, yields

$$\left[\frac{\hbar^2}{2\mu_f}\nabla_P^2 + E - \epsilon_n(P)\right] G_n(\vec{P}) = \sum_{n'} \frac{\hbar^2}{2\mu_f} C_{nn'}(P)\, G_{n'}(\vec{P}) \tag{3-50}$$

where the $C_{nn'}$ are the operators

$$C_{nn'}(P) = -\int z_n^* \nabla_P z_{n'}\, d^3\vec{r}_{AB} \cdot \nabla_P - \int z_n^* \nabla_P^2 z_{n'}\, d^3\vec{r}_{AB} \tag{3-51}$$

The functions $z_n(\vec{r}_{AB}; P)$ can be appropriately named the static field diatomic wave functions since they represent the rotational and vibrational motion of AB which is stationary relative to the atom C. On the other hand, the functions $G_n(\vec{P})$ should be called the translational motion coefficients since they account for the motion of C relative to AB.

In Chapter IV, suitable approximations will be made to facilitate the solution of both Equation (3-45) and Equation (3-50) for the case of the highly exothermic reactions of the type $A + BC \rightarrow AB + C$.

CHAPTER IV

DETERMINATION OF REACTION CROSS-SECTIONS FOR TRIATOMIC, EXOTHERMIC REACTIONS

Perturbed Morse Oscillator Method

As mentioned in the last few paragraphs of the previous chapter, the wave function of Equation (3-44) will be applicable to the method presented herein for determination of the reaction cross-sections. The discussion in the present chapter will be concerned first with obtaining the solutions $z_n(\vec{r}_{AB},P)$ to Equation (3-45). Even though the variable P is treated as a parameter in the perturbed stationary state method, the functional complexity of $V_L(r_{AB},P)$ discourages an analytical attack on Equation (3-45). On the other hand, a direct numerical procedure, such as the Numerov method (88), would consume a considerable amount of computer time since the solutions $z_n(\vec{r}_{AB},P)$ are required for many closely-spaced values of P. A possible answer to this dilemma could lie in the affinity of atom A for B. In highly exothermic reactions A + BC → AB + C, one might expect the A atom to remain tightly bound to the B atom even when C is in fairly close proximity. A recent semiempirical calculation (9) of the potential-energy surface for $H + X_2 \rightarrow HX + X$ (where X = F, Cl, Br, and I) indicated that this was the case. Furthermore, even when the distance between B and C approached zero (that is to say, P → 0), the function $V_L(r_{AB},P)$ still re ained the Morse function form shown in Figure 2. Thus, the standard perturbation theory for eigenvalue problems in quantum mechanics can be made applicable to the solution of Equation (3-45) in the

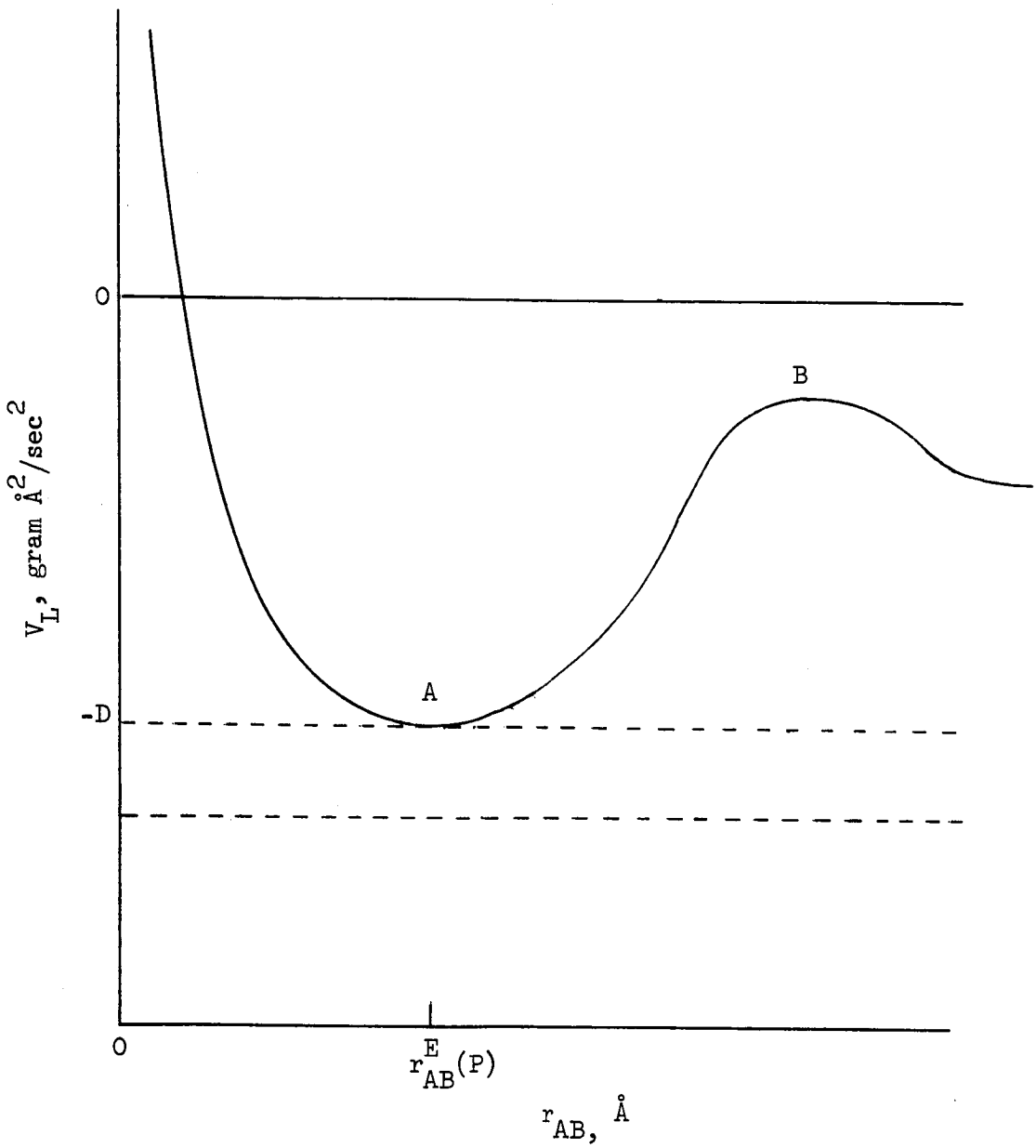

Figure 2. Perturbed AB Interaction When C is in Close Proximity.

manner to be outlined below.

The magnitude of $V_L(r_{AB},P)$ for small values of P is such that these configurations are classically inaccessible. In the perturbed stationary state approximation, this phenomenon should be manifested by high values of the eigenvalues $\epsilon_n(P)$ when P is small.

"Linear Complex" Model Wave Function

From Equation (3-48) it is seen that, for sufficiently small-valued $U_{i,L}(r_{AB},P)$, ordinary perturbation theory (87) could be applied easily and directly to the solution of Equation (3-45). The zero-order wave functions required in the calculation would merely be the solutions $\zeta_n(\vec{r}_{AB})$ of Equation (3-47). However, as mentioned in Chapter IV, the interaction $U_{i,L}$ is seldom negligible compared to V_{AB}, and, based on the work of Ellison (9), this seems to be the case for several exothermic reactions.

Partitioning of the Potential-Energy. Perturbation theory can be made applicable to the solution of Equation (3-45) by taking a different approach. As a beginning, the potential-energy function $V_L(r_{AB},P)$ should be partitioned into

$$V_L(r_{AB},P) = V_M(r_{AB},P) + V_P(r_{AB},P) \tag{4-1}$$

where

$$V_P(r_{AB},P) \equiv V_L(r_{AB},P) - V_M(r_{AB},P) \tag{4-2}$$

and

$$V_M(r_{AB},P) = D(P)\left\{1 - \exp\left[-a(P)\left(r_{AB} - r_{AB}^E(P)\right)\right]\right\}^2 + U_m(P) \qquad (4\text{-}3)$$

For constant P, $V_M(r_{AB},P)$ has the form of a Morse potential with P-dependent parameters, and since the Schroedinger equation for a Morse function oscillator has been solved by ter Haar (81), the solutions to the boundary value problem

$$\left[K_{AB} + V_M(r_{AB},P)\right] Z_n^\circ(\vec{r}_{AB};P) = \epsilon_n^\circ(P)\, Z_n^\circ(\vec{r}_{AB};P) \qquad (4\text{-}4)$$

$$Z_n^\circ(\vec{r}_{AB};P) = 0 \quad \text{when} \quad r_{AB} = 0 \qquad (4\text{-}5)$$

$$Z_n^\circ(\vec{r}_{AB};P) = 0 \quad \text{when} \quad r_{AB} = \infty \qquad (4\text{-}6)$$

can be obtained at every value of constant P from ter Haar's solutions. The $z_n^\circ(\vec{r}_{AB};P)$ can be used as zero-order wave functions in a second-order perturbation calculation of the solutions $z_n(\vec{r}_{AB};P)$ of Equation (3-45).

The physical meaning of the parameters D(P), $r_{AB}^E(P)$, and $U_m(P)$ is indicated in Figure 3, which depicts a typical curve of $V_L(r_{AB},P)$ at constant P from Ellison's treatment of $H + Br_2 \rightarrow HBr + Br$ (9).

Assuming that $V_L(r_{AB},P)$ retains definite Morse curve features for exothermic, triatomic reactions in general, it should be possible to partition the potential-energy surface for a large number of these reac-

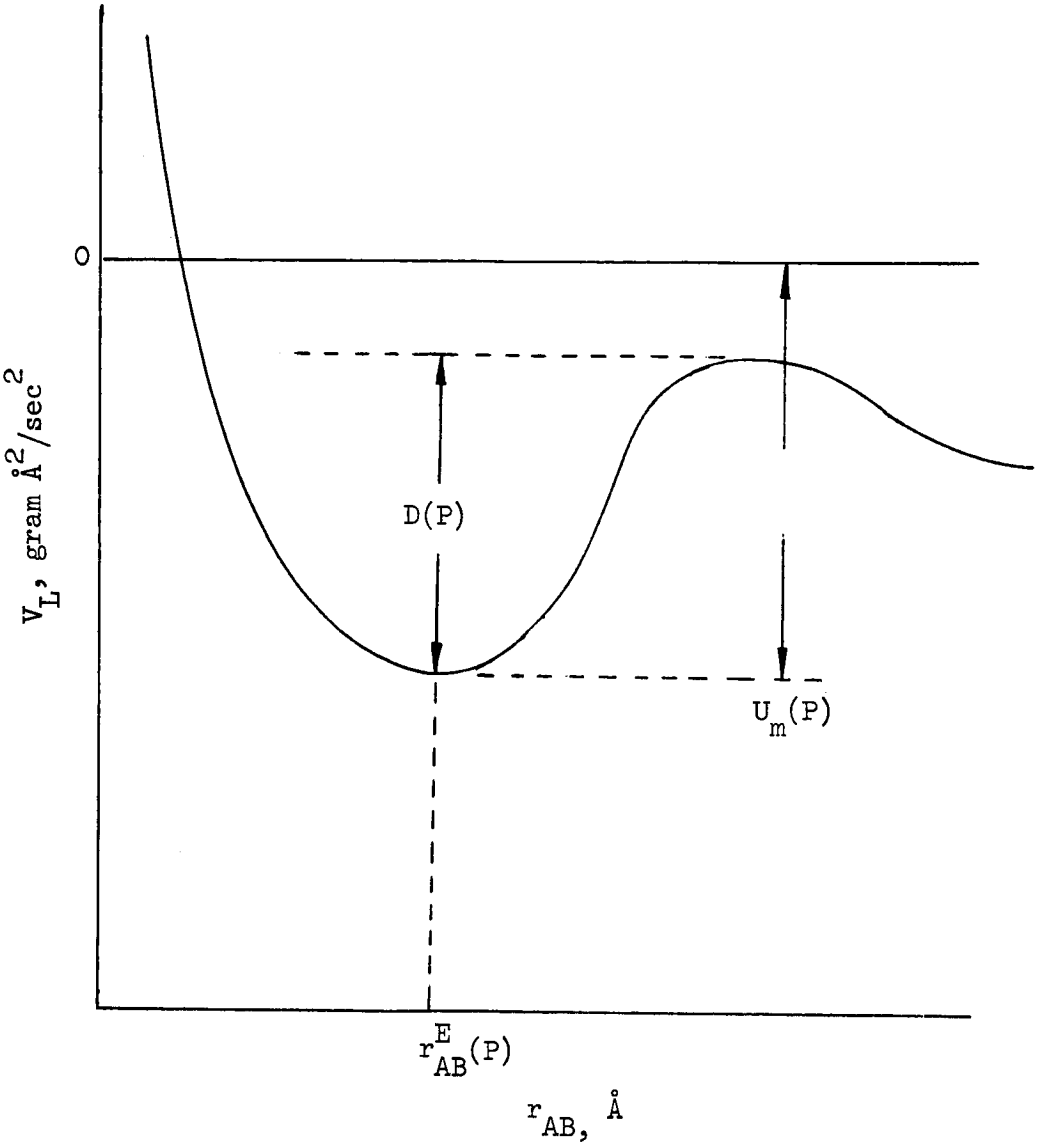

Figure 3. Parameters Used to Fit V_M to V_L.

tions. Furthermore, proper adjustment of the parameters D(P), a(P), $r_{AB}^{E}(P)$, and $U_m(P)$ can render $V_P(r_{AB},P)$ negligible compared with $V_M(r_{AB},P)$. Very good values for $U_M(P)$, $r_{AB}^{E}(P)$, and D(P) can be obtained by reading directly from the plot of $V_L(r_{AB},P)$ versus r_{AB} for fixed P. The parameter a(P) can then be calculated from points on the $V_L(r_{AB},P)$ curve by the relationship

$$a(P) = \frac{\pm \sqrt{\frac{V_L(r_{AB},P) - U_m(P)}{D(P)}} - 1}{r_{AB} - r_{AB}^{E}(P)} \qquad (4\text{-}7)$$

obtained from Equation (4-3). The plus sign is to be used for points to the right of $r_{AB}^{E}(P)$, and the negative sign is used for points to the left of $r_{AB}^{E}(P)$. Preferably, the point used in Equation (4-7) should be at some distance r_{AB} to the left of $r_{AB}^{E}(P)$. Then the function $V_M(r_{AB},P)$ will fit snugly to the function $V_L(r_{AB},P)$ in the region of steepest slope ($r_{AB} \leq r_{AB}^{E}$) and fairly close to $V_L(r_{AB},P)$ in the region of more gradual slope $r_{AB} \geq r_{AB}^{E}$). Fitting the function $V_M(r_{AB},P)$ to the function $V_L(r_{AB},P)$ in this manner has the effect of minimizing $V_P(r_{AB},P)$. If some point at $r_{AB} \geq r_{AB}^{E}$ is used to determine a(P), the slope of $V_M(r_{AB},P)$ to the left of r_{AB}^{E} will not coincide as well with that of $V_L(r_{AB},P)$ as in the former case. Thus, due to the steepness of the slope in this region, a small deviation in slope corresponds to a large valued function $V_P(r_{AB},P)$. In the limit of large P, the parametric functions a(P), D(P), $U_m(P)$, and $r_{AB}^{E}(P)$ should approach the corresponding Morse parameters for the unper-

turbed AB molecule.

The Zero-Order Wave Functions. As mentioned above, ter Haar (81) obtained an almost analytical solution to the system of equations

$$\left\{-\frac{\hbar^2}{2\mu}\nabla_r^2 + D\left[1-\exp(-a(r-r^E))\right]^2 - D\right\}\psi_n(r) = E_n\,\psi_n(r) \qquad (4\text{-}8)$$

$$\psi_n(0) = \psi_n(\infty) = 0$$

which describes the motion of a rigid rotator-Morse oscillator. Here, r is the interatomic distance, μ is the reduced mass, r^E is the equilibrium interatomic distance, and D and a are the Morse parameters. Since the derivation of the solutions to Equation (4-8) is rather lenghty, the reader is referred to the original paper by ter Haar (81). In this work the results will be written down in the form of solutions to Equation (4-8) as follows:

$$Z_n^\circ(\vec{r}_{AB};P) = N_{n_f}^\circ(P)\;\; R_{n_f}^\circ(r_{AB};P)\;\; Y_{l_f}^{m_f}(\theta_{AB},\phi_{AB}) \qquad (4\text{-}9)$$

$$\epsilon_n^\circ(P) = \frac{2\sqrt{D(P)}}{A(P)}(n_f+\tfrac{1}{2}) - \frac{(n_f+\tfrac{1}{2})^2}{A^2(P)} + U_m(P) + \epsilon_{rot} \qquad (4\text{-}10)$$

where $N_{n_f}^{o}(P)$ is a normalizing constant and $Y_{l_f}^{m_f}(\theta_{AB}, \phi_{AB})$ is the wave

function corresponding to the assumed rigid rotation of AB in the field of C. From standard textbooks in quantum chemistry (89), it is shown that

$$Y_{l_f}^{m_f}(\theta_{AB}, \phi_{AB}) = (-1)^{m_f} \left[\frac{(2l_f-1)(l_f-m_f)!}{4\pi\ (l_f+m_f)!}\right]^{1/2} P_{l_f}^{m_f}(\cos\theta_{AB}) \qquad (4\text{-}11)$$

$$\times \exp(i\, m_f\, \theta_{AB})$$

where $P_{l_f}^{m_f}(\cos\theta_{AB})$ is the associated Legendre polynomial defined as

$$P_l^{m_f}(u) = \frac{(1-u^2)^{m_f/2}}{2^{l_f}\ l_f!} \frac{d^{l_f+m_f}}{du^{l_f+m_f}} (u^2-1)^{l_f}, \quad |u| \geq 1 \qquad (4\text{-}12)$$

The radially dependent factor $R^{o}_{n_f}(r_{AB};P)$ is

$$R^{o}_{n_f}(r_{AB};P) = \exp(-X/2)\,(X/2)^{A(P)\sqrt{D(P)}-(n_f+1/2)}\, M_{n_f}(n_f,\beta;X)/r_{AB} \qquad (4\text{-}13)$$

where

$$X = 2\,A(P)\,\sqrt{D(P)}\,\exp\left[-a(P)\,(r_{AB}-r^{E}_{AB}(P))\right] \qquad (4\text{-}14)$$

$$A(P) = \left[2\left(\frac{m_A m_B}{m_A + m_B}\right)/\hbar^2\right]^{1/2} / a(P) \tag{4-15}$$

and

$$M(n_f, \beta; X) = 1 + \frac{(-n_f)}{\beta} X + \frac{(-n_f)(-n_f+1)}{\beta(\beta+1)} \frac{X^2}{2}$$

$$+ \frac{(-n_f)(-n_f+1)(-n_f+2)}{\beta(\beta+1)(\beta+2)} \frac{X^3}{3!} + \cdots \tag{4-16}$$

Here,

$$\beta = 2A(P)\sqrt{D(P)} - 2n_f \tag{4-17}$$

Equation (4-16) is the confluent hypergeometric function (90)

$$M(\alpha, \beta; X) = 1 + \frac{\alpha}{\beta} X + \frac{\alpha(\alpha+1)}{\beta(\beta+1)} \frac{X^2}{2!}$$

$$+ \frac{\alpha(\alpha+1)(\alpha+2)}{\beta(\beta+1)(\beta+2)} \frac{X^3}{3!} + \cdots \tag{4-18}$$

for the case where

$$\alpha = -n_f \ , \ n_f = 0, 1, 2, \cdots \tag{4-19}$$

The normalizing factors are obtained by numerical integration of

$$N^{\circ}_{n_f}(P) = 1/\left\{\int \left[R^{\circ}_{n_f}(r_{AB};P)\right]^2 r_{AB}^2 \, dr_{AB}\right\}^{1/2} \tag{4-20}$$

Assuming that the equilibrium interatomic distance $r^E_{AB}(P)$ does not differ greatly from $r^E_{AB}(\infty)$, the last term on the right side of Equation (4-10) can be approximated as (91)

$$\epsilon_{rot} = B_{AB} \, \ell_f(\ell_f+1) - \alpha_{AB}(n_f+1/2)\,\ell_f(\ell_f+1) - T_{AB}\,\ell_f^2(\ell_f+1)^2 \tag{4-21}$$

where B_{AB}, α_{AB}, and T_{AB} are the spectroscopic rotational constants (92) of AB. On the right side of Equation (4-21), the first term corresponds to the energy levels of a rigid rotor, the second term corrects for the anharmonicity of a Morse oscillator, and the third term corrects for centrifugal force.

Improvement of the Zero-Order Eigenfunctions and Eigenvalues. The results of Equations (4-9) and (4-10) can be used in conjunction with second-order perturbation theory to correct for the nonvanishing of $V_P(r_{AB},P)$. Only second-order perturbation theory need be considered since rapid convergence is assured by the careful adjustment of the parameters a(P), $r^E_{AB}(P)$, D(P), and $U_m(P)$ to make $V_P(r_{AB},P)$ negligible compared to

$V_M(r_{AB},P)$.

Since the perturbing potential $V_P(r_{AB},P)$ does not depend on the angles θ_{AB}, ϕ_{AB}, only the radially dependent eigenfunctions $\bar{R}^{o}_{n_f}(r_{AB};P)$ where $\bar{R}^{o}_{n_f}(r_{AB};P)$ denotes the orthonormal product $N^{o}_{n_f}(r_{AB};P)\, R^{o}_{n_f}(r_{AB};P)$, must be subjected to the perturbation treatment. From Equation (4-10), the zero-order eigenvalues corresponding to the $\bar{R}^{o}_{n_f}(r_{AB};P)$ are

$$\epsilon^{o}_{n_f,vib}(P) = 2\frac{\sqrt{D(P)}}{A(P)}(n_f+1) - \frac{(n_f+1)^2}{A^2(P)} + U_m(P) \qquad (4\text{-}22)$$

which are nondegenerate. Thus, due to the orthogonality of the zero-order eigenfunctions $\bar{R}^{o}_{n_f}(r_{AB};P)$, the radially dependent factor of the static field diatomic eigenfunctions may be approximated by the second-order perturbation relations for nondegenerate states (93) as

$$R_{n_f}(r_{AB};P) = \bar{R}^{o}_{n_f}(r_{AB};P) + \sum_{i}^{N\prime}\frac{V^{P}_{i,n_f}(P)}{\epsilon^{o}_{n_f,vib}(P) - \epsilon^{o}_{i,vib}(P)}\bar{R}^{o}_{i}(r_{AB};P) \qquad (4\text{-}23)$$

$$+\sum_{j}^{N\prime}\left[\sum_{i}^{N\prime}\frac{V^{P}_{j,i}(P)\;V^{P}_{i,n_f}(P)}{\left[\epsilon^{o}_{n_f,vib}(P)-\epsilon^{o}_{j,vib}(P)\right]\left[\epsilon^{o}_{n_f,vib}(P)-\epsilon^{o}_{i,vib}(P)\right]}\right.$$

$$\left.-\frac{V^{P}_{n_f,n_f}(P)\;V^{P}_{j,n_f}(P)}{\left[\epsilon^{o}_{n_f,vib}(P)-\epsilon^{o}_{j,vib}(P)\right]^2}\right]\bar{R}^{o}_{j}(r_{AB};P)$$

and the corresponding eigenvalues are

$$\epsilon_{n_f,vib}(P) = \epsilon^{\circ}_{n_f,vib}(P) + V^{P}_{n_f,n_f}(P) + \sum_{i}^{N'} \frac{\left[V^{P}_{n_f,i}(P)\right]^2}{\epsilon^{\circ}_{n_f,vib}(P) - \epsilon^{\circ}_{i,vib}(P)} \qquad (4\text{-}24)$$

where

$$V^{P}_{i,j}(P) = \int_0^{\infty} \bar{R}^{\circ *}_{i}(r_{AB};P)\, V_P(r_{AB},P)\, \bar{R}^{\circ}_{j}(r_{AB};P)\, r^2_{AB}\, dr_{AB} \qquad (4\text{-}25)$$

A prime following a summation symbol specifies the omission from the summation of the term corresponding to the vibrational state n_f. The symbol N denotes the highest vibrational state included in the set of basis functions $\bar{R}^{\circ}_{n_f}(r_{AB};P)$ used in the perturbation treatment.

The static field diatomic eigenfunctions and eigenvalues are now approximated as

$$Z_n(\vec{r}_{AB};P) = N_{n_f}(P)\, R_{n_f}(r_{AB};P)\, Y^{m_f}_{l_f}(\theta_{AB},\phi_{AB}) \qquad (4\text{-}26)$$

and

$$\epsilon_n(P) = \epsilon_{n_f,vib}(P) + B_{AB}\, \ell_f(\ell_f+1) - \alpha_{AB}(n_f+1/2)\,\ell_f(\ell_f+1) \qquad (4\text{-}27)$$

$$- T_{AB}\, \ell_f^2(\ell_f+1)^2$$

where $N_{n_f}(P)$ is the normalization constant computed numerically from

$$N_{n_f}(P) = \left[\int_0^\infty \left[R_{n_f}(r_{AB};P)\right]^2 r_{AB}^2\, dr_{AB}\right]^{-1/2} \qquad (4\text{-}28)$$

For convenience, the perturbed vibrational functions will be written hereafter in the normalized form $\bar{R}_{n_f}(r_{AB};P) = N_{n_f}(P)\, R_{n_f}(r_{AB};P)$.

Approximation of the Translational Motion Coefficients

After expressions for the static field diatomic eigenfunctions and eigenvalues have been obtained from Equations (4-23) and (4-24), respectively, they can be substituted into Equation (3-51) in order to determine the translational motion coefficients $G_n(\vec{P})$. To avoid mathematical mayhem, however, some way must be found to uncouple the system of differential equations represented by Equation (3-50).

The analysis of Equation (3-50) begins by operating upon $z_n(\vec{r}_{AB};P)$ with ∇_P and then ∇_P^2 to obtain

$$\nabla_P\, Z_n(\vec{r}_{AB};P) = Y_{\ell_f}^{m_f}(\theta_{AB},\phi_{AB})\, \frac{d\bar{R}_{n_f}}{dP}\, \vec{\delta}_P \qquad (4\text{-}29)$$

where $\vec{\delta}_p$ is the unit vector in the direction $\vec{P}$, and

$$\nabla_P^2 \, Z_n(\vec{r}_{AB}; P) = Y_{l_f}^{m_f}(\theta_{AB}, \phi_{AB}) \, \frac{d^2 \bar{R}_{n_f}}{dP^2} \tag{4-30}$$

Since the scalar product of $\nabla_P \, z_n(\vec{r}_{AB};P)$ and $\nabla_P \, G_n(\vec{P})$ within Equation (3-) can be written as

$$\nabla_P \, Z_n(\vec{r}_{AB}; P) \cdot \nabla_P \, G_{n'}(\vec{P}) = Y_{l_f}^{m_f}(\theta_{AB}, \phi_{AB}) \, \frac{d\bar{R}_{n_f}}{dP} \, \frac{d G_{n'}}{dP} \tag{4-31}$$

the action of the operators $C_{n,n'}(P)$ upon $G_n(\vec{P})$ can be expressed as

$$C_{n,n'}(P) \, G_{n'}(\vec{P}) = \int_0^\infty \bar{R}_{n_f} \, \frac{d R_{n'_f}}{dP} \, r_{AB}^2 \, dr_{AB} \cdot \frac{d G_{n'}(\vec{P})}{dP} \tag{4-32}$$

$$- \int_0^\infty \bar{R}_{n_f} \, \frac{d^2 R_{n'_f}}{dP^2} \, r_{AB}^2 \, dr_{AB} \cdot G_{n'}(\vec{P})$$

Equation (3-) can now be written

$$\left[\nabla_P^2 + k_n^2 - \tilde{U}_n(P)\right] G_n(\vec{P}) = -\sum_{n'} \int_0^\infty \bar{R}_{n_f} \frac{d\bar{R}_{n_f'}}{dP} r_{AB}^2 \, dr_{AB} \cdot \frac{dG_{n'}(\vec{P})}{dP} \qquad (4\text{-}33)$$

$$-\sum_{n'} \int_0^\infty \bar{R}_{n_f} \frac{d^2 R_{n_f'}}{dP^2} r_{AB}^2 \, dr_{AB} \cdot G_{n'}(\vec{P})$$

where

$$k_n^2 = \frac{2\mu_f}{\hbar^2} \left[E - \epsilon_n(\infty)\right] \qquad (4\text{-}34)$$

and

$$\tilde{U}_n(P) = \frac{2\mu_f}{\hbar^2} \left[\epsilon_n(P) - \epsilon_n(\infty)\right] \qquad (4\text{-}35)$$

Here, the $\epsilon_n(\infty)$ are the eigenvalues E_n for the unperturbed molecule AB in the state n.

The Coupling Operators. At this point it is appropriate to discuss the action of the coupling operators $C_{nm}(P)$ on the set of functions $\bar{R}_{n_f}(r;P)$. For the case of $H + Br_2 \rightarrow HBr + Br$, the integrals on the right side of Equation (4-33) were evaluated numerically for $n_f' = 3,5$ and $n_f = 0$ to $n_f = 7$. The results are listed in Table 2, where

Table 2. Maximum Absolute Values of the Coupling Integrals With Respect to P, the Distance Between AB and C

n_f'	n_f	I_1, $Å^{-1}$	I_2, $Å^{-2}$
3	0	0.08762	0.00532
3	1	0.31132	0.07224
3	2	0.47521	0.08147
3	3	0.02775	0.00031
3	4	1.66391	0.09382
3	5	0.69823	0.07182
3	6	0.39168	0.04229
3	7	0.21797	0.02799
5	0	0.07359	0.00388
5	1	0.17225	0.04211
5	2	0.19625	0.05223
5	3	0.31462	0.07616
5	4	0.56684	0.05179
5	5	0.98992	0.10017
5	6	0.33423	0.04718
5	7	0.22965	0.02994

$$I_1(P) = \int_0^\infty \bar{R}_{n_f} \frac{d\bar{R}_{n'_f}}{dP} r_{AB}^2 \, dr_{AB} \tag{4-36}$$

$$I_2(P) = \int_0^\infty \bar{R}_{n_f} \frac{d^2\bar{R}_{n'_f}}{dP^2} r_{AB}^2 \, dr_{AB} \tag{4-37}$$

To save space only the maximum absolute values of I_1 and I_2 with respect to P are reported. As can be seen, none of the integrals I_1 exceed 1.664 $Å^{-1}$ in absolute value, and the integrals I_2 are even smaller. Because the value of $k_n^2 - \tilde{U}_n(P)$ will usually exceed 1000 $Å^{-2}$, and since the maximum absolute value of $\partial G_n(\vec{P})/\partial P$ is not expected to be greater than 10 $Å^{-1}$, approximations to $G_n(\vec{P})$ could be obtained from

$$\left[\nabla_P^2 + k_n^2 - \tilde{U}_n(P)\right] G_n(\vec{P}) = 0 \tag{4-38}$$

Of course, it is difficult to evaluate the effect of neglecting all the coupling coefficients. As in the closely related two-state approximation (94-95), the reasonable assumption that coupling can be neglected is due primarily to mathematical necessity.

Partial Wave Analysis. It is now convenient to restate the asymptotic condition for $\chi_f^{-*}(r_{AB};P)$ corresponding to the formation of AB in the state n:

$$\lim_{P\to\infty} \chi_f^{-*}(r_{AB};P) = \left[e^{-i\vec{k}_n\cdot\vec{P}} + \frac{\exp(ik_nP)}{P} f(\Theta,\Phi)\right] \zeta_n^*(\vec{r}_{AB}) \quad (4\text{-}39)$$

Now, in Equation (3-) $\chi_f^{-*}(r_{AB};P)$ has also been written as an expansion in the complete set of functions $z_n^*(\vec{r}_{AB};P)$, and since

$$\lim_{P\to\infty} Z_n^*(\vec{r}_{AB};P) = \zeta_n^*(\vec{r}_{AB}) \quad (4\text{-}40)$$

one can write the following asymptotic equation:

$$G_m^*(\vec{P}) = \exp(-i\vec{k}_n\cdot\vec{P}) + f(\Theta,\Phi)\exp(ik_nP)/P \quad (4\text{-}41)$$

Now the problem of the translational motion coefficients has been reduced to the task of solving Equation (4-38) subject to the asymptotic condition given in Equation (4-41). A partial wave method (96) similar to that for elastic scattering by a central potential is the most straightforward procedure. If α represents the common-plane angle between the vectors $\vec{P}$ and $\vec{k}_n$, then

$$\exp(-i\vec{k}_n\cdot\vec{P}) = \exp(-ik_nP\cos\alpha) \quad (4\text{-}42)$$

As P approaches infinity, α tends to zero and θ_P and ϕ_P approach Θ and Φ, respectively (see Figure 1). Expansion of the incoming wave function in

Equation (4-42) in terms of Legendre polynomials (96) and subsequent use of the addition theorem of spherical harmonics (97) results in

$$e^{-i\vec{k}_n\cdot\vec{P}} = 4\pi \sum_{\ell=0}^{\infty} \sum_{m=-\ell}^{\ell} i^{-\ell} j_\ell(k_n P)\, Y_\ell^m(\theta_p,\phi_p)\, Y_\ell^{m*}(\Theta,\Phi) \qquad (4\text{-}43)$$

Also, for very large P, but where θ_P and ϕ_P have not quite become equal to Θ and Φ, respectively, the elastic scattering amplitude can be expanded as

$$f(\Theta,\Phi) = 4\pi \sum_{\ell=0}^{\infty} \sum_{m=-\ell}^{\ell} i^{-\ell} a_\ell \frac{1}{2k_n} Y_\ell^m(\theta_p,\phi_p) Y_\ell^{m*}(\Theta,\Phi) \qquad (4\text{-}44)$$

where the a_l's are constants to be determined. The same type of expansion can be carried out for $G_n^*(\vec{P})$:

$$G_n^*(P) = 4\pi \sum_{\ell=0}^{\infty} \sum_{m=-\ell}^{\ell} i^{-\ell} C_\ell \frac{u_\ell(k_n P)}{k_n P} Y_\ell^m(\theta_p,\phi_p) Y_\ell^{m*}(\Theta,\Phi) \qquad (4\text{-}45)$$

Here, the functions $u_l(k_n P)$ are the solutions to the problem

$$\frac{d^2 u_\ell}{dP^2} + \left[k_n^2 - \tilde{U}_n(P) - \frac{\ell(\ell+1)}{P^2} \right] u_\ell = 0 \qquad (4\text{-}46)$$

$$\lim_{\rho \to \infty} C_\ell \, u_\ell(k_n \rho) = C_\ell \sin\left(k_n \rho - \frac{\ell\pi}{2} + \eta_\ell\right) \tag{4-47}$$

where C_1 and η_1 are constant for a given 1.

Substitution of the above expansions into Equation (4-41), and utilization of the asymptotic form of u_1 and the spherical Bessel function

$$j_\ell(k_n \rho) = \frac{\sin\left(k_n \rho - \ell\pi/2\right)}{k_n \rho} \tag{4-48}$$

yields the following expression:

$$\frac{4\pi}{2 i k_n \rho} \sum_{\ell=0}^{\infty} \sum_{m=-\ell}^{\ell} i^{-\ell} \left\{ \left[e^{i(k_n \rho - \ell\pi/2)} - e^{-i(k_n - \ell\pi/2)} \right] \right. \tag{4-49}$$

$$\left. - a_\ell \, e^{i k_n \rho} \right\} Y_\ell^m(\theta_\rho, \phi_\rho) \, Y_\ell^{m*}(\Theta, \Phi)$$

$$= \frac{4\pi}{2 i k_n \rho} \sum_{\ell=0}^{\infty} \sum_{m=-\ell}^{\ell} i^{-\ell} C_\ell \left[e^{i(k_n \rho - \ell\pi/2 + \eta_\ell)} \right.$$

$$\left. - e^{-i(k_n \rho - \ell\pi/2 + \eta_\ell)} \right] Y_\ell^m(\theta_\rho, \phi_\rho) \; Y_\ell^{m*}(\Theta, \Phi)$$

The left- and right-hand coefficients of the ingoing waves must be equal so

$$C_\ell \exp(-i\eta_\ell) = 1 \tag{4-50}$$

or

$$C_\ell = \exp(i\eta_\ell) \tag{4-51}$$

and therefore

$$G_n^*(P) = 4\pi \sum_{\ell=0}^{\infty} \sum_{m=-\ell}^{\ell} i^{-\ell} e^{i\eta_\ell} \frac{u_\ell(k_n P)}{k_n P} Y_\ell^m(\theta_p, \phi_p) \tag{4-52}$$

$$\times Y_\ell^{m*}(\Theta, \Phi)$$

For large P, Equations (4-47) and (4-48) show that $u_1(k_n P)$ differs from $j_1(k_n P)$ only by the constant η_1 which is called the phase shift corresponding to 1.

Equation (4-46) has been studied extensively in the theory of elastic collisions (98), and the methods of its solution are well established for potential functions $U_n(P)$ which decrease faster than $1/P^2$ as P increases.

Semiclassical Method. For sufficiently high values of k_n and l such that

$$l(H) = unity \tag{4-53}$$

$$\frac{\mu_f}{k^2} \quad \frac{\left| \frac{d\tilde{U}_n(P)}{dP} \right|}{k_n^3} \ll unity \tag{4-54}$$

and for potential functions $\tilde{U}_n(P)$ decreasing faster than P^{-2} as P increases, the semiclassical approximation may be employed. Thus, when the above criteria are met, the solutions $u_l(k_n P)$ can be approximated as (99)

$$u_l(k_n P) = \frac{k_n}{\sqrt{k_n K_{n,l}(P)}} \sin\left[\int_{P_o}^{P} K_{n,l}(P)\, dP + \pi/4\right] \tag{4-55}$$

where P_o is the classical "turning point" shown on Figure 4, and $K_{n,l}(P)$ is defined as

$$K_{n,l}(P) = \left[\left| k_n^2 - \tilde{U}_n(P) - (l-1/2)^2/P^2 \right|\right]^{1/2} \tag{4-56}$$

Numerov Method. For low values of k_n and l, Equations (4-53) and (4-54) will not generally hold true. If the potential function $\tilde{U}_n(P)$

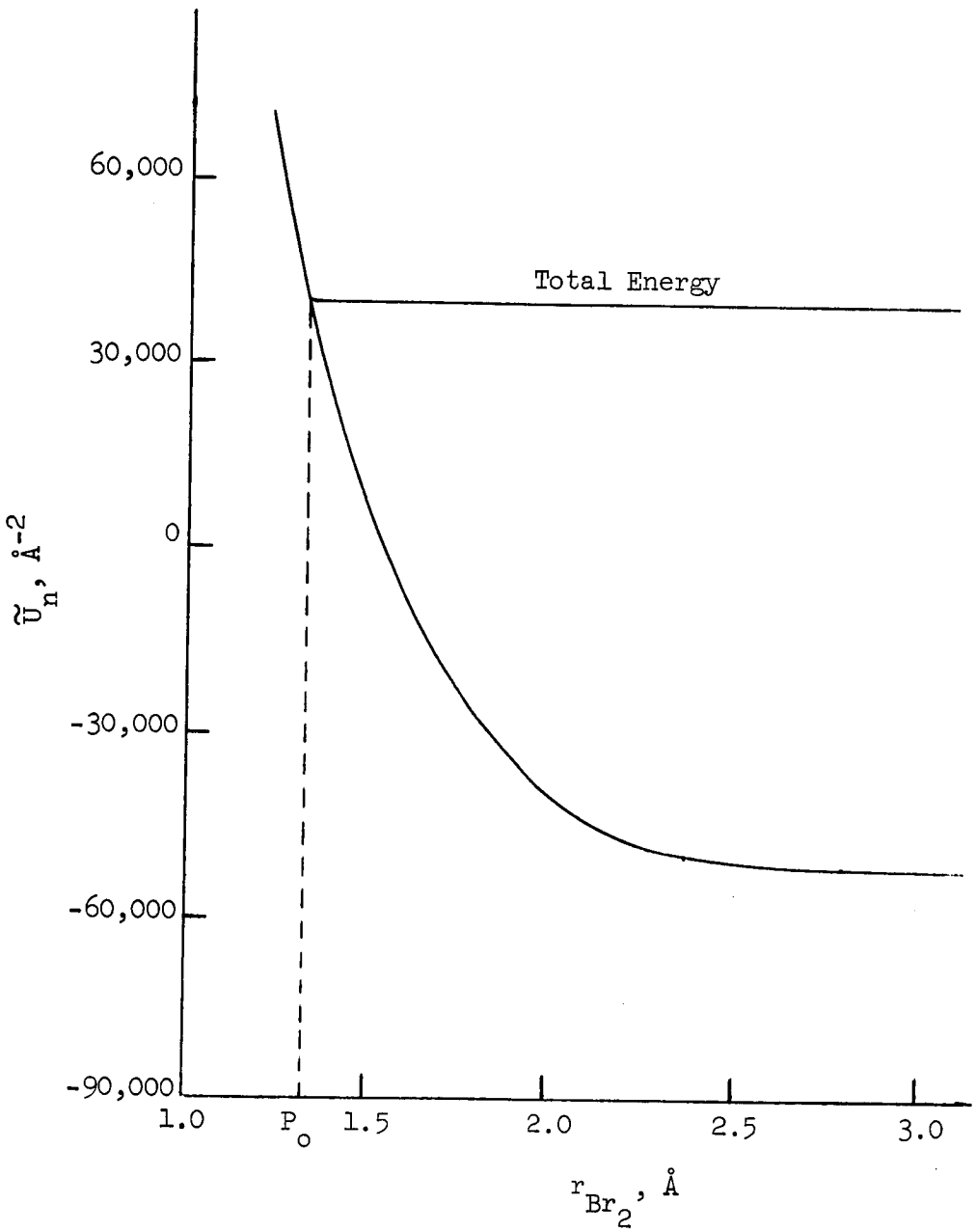

Figure 4. Interaction Between HBr and Br Versus r_{Br_2} for n_f = 1.

decreases faster than $1/P^2$ with increasing P, one can still obtain the solutions $u_l(k_n P)$ by resorting to the numerical integration of Equation (4-46). As shown by Mason, et al. (100), proper utilization of the Numerov method (88) can generate values for $u_l(k_n P)$ almost as rapidly as Equation (4-55).

With the Numerov method a linear differential equation of the type represented by Equation (4-46), or

$$\frac{d^2y}{dx^2} = f(x)\, y \tag{4-57}$$

can be integrated by using the step-by-step relation (88)

$$y_n = \frac{2y_{n-1} - y_{n-2} - (H^2/12) f(x_{n-2}) y_{n-2} - 10(H^2/12) f(x_{n-1}) y_{n-1}}{1 - (H^2/12) f(x_n)} \tag{4-58}$$

Here, the constant H is given by

$$H = x_{n-1} - x_n \tag{4-59}$$

Of course one needs to know the starting values y_o and y_1, but Mason's group found that this requirement can be avoided provided:

(a) The potential $\tilde{U}_n(P)$ has a strongly repulsive core of the type shown in Figure 4.

(b) The integration is begun at a point just to the left of the

classical "turning point", P_o.

(c) The starting values are taken to be about equal and at some low value (about 10^{-9}).

This approximate rule was verified by several sample calculations for the case of HBr - Br.

As will be demonstrated later, the value of the phase shifts, η_l, will be unnecessary in light of the model to be used and the calculations to be made. Hence, no mention will be made of their method of calculation.

The Transition Integral

Combining Equations (3-49), (4-26), and (4-52), the function χ_f^{-*} can be written as

$$\chi_f^{-*} = \sum_n 4\pi \, Y_{l_f}^{m_f}(\theta_{AB}, \phi_{AB}) \, \bar{R}_{n_f}(r_{AB}; \rho) \sum_{l_1=0}^{\infty} \sum_{m_1=-l_1}^{l_1} i^{-l_1} \qquad (4\text{-}60)$$

$$e^{i\eta_{l_1}} \, \frac{u_{l_1}(k_n \rho)}{k_n \rho} \, Y_{l_1}^{m_1}(\theta_\rho, \phi_\rho) \, Y_{l_1}^{m_1 *}(\Theta, \Phi)$$

Now, $f_n^i(\Theta,\Phi)$ is the scattering amplitude for the reaction of A and BC, in state n_i, l_i, m_i, k_i to form C and AB, in the state n (n_f, l_f, m_f, k_n). In the first-order approximation, only that term in Equation (3-49) corresponding to the state n should be included in any calculation of $f_n^i(\Theta,\Phi)$. This is consistent with the neglect of coupling between different vibrational states.

Linear Complex Model

Attention will now be focused on the transition integral of Equation (3-37) which is defined as

$$T_n^i = \iint \Psi_f^{-*} \bar{U}_f \varphi_i \, r_{AB}^2 \, dr_{AB} \sin\theta_{AB} \, d\theta_{AB} \, d\phi_{AB} \, P^2 dP \sin\theta_P \, d\theta_P \, d\phi_P \qquad (4\text{-}61)$$

These integrals can be evaluated rigorously only by expending many hours on a high speed computer (70). Thus, it is desirable to attempt to simplify the computation of T_n^i through the use of some plausible model, such as the "linear complex" model. The "linear complex" model, as mentioned in Chapter III, assumes that valence interactions rigidly align the configuration of the A-B-C reacting system at interatomic distances close to r_{AB}^E and r_{BC}^E. The applicability of this approach to the system $H + Br_2 \rightarrow Br + HBr$ will be discussed in the next chapter.

Let $\bar{\chi}_f^{-*}$ represent the function χ_f^{-*} when the system A-B-C is restricted to a straight line, i.e., $\theta_{AB} = \pi - \theta_P$ and $\phi_{AB} = \phi_P + \pi$, and

$$\bar{\chi}_f^{-*} = \chi_f^{-*}(r_{AB}, \pi - \theta_P, \pi + \phi_P, P, \theta_P, \phi_P) \qquad (4\text{-}62)$$

Also, because of the nature of valence-type interactions, $\bar{U}_f$ takes on significant values when the order of magnitude of P is about r_{BC}^E, the equilibrium bond length of molecule BC, and tends to vanish faster than P^{-2} as P increases. Thus, most of the contribution to the integral T_n^i will come from the region in which Ψ_f^{-*} can be replaced by $\bar{\chi}_f^{-*}$. It is

reasonable to assume, therefore, that the integral T_n^i can be approximated as

$$T_n^i = \iint \bar{\chi}_f^{-*}\ \bar{u}_f\ \varphi_i\ r_{AB}^2\ dr_{AB}\ \sin\theta_{AB}\ d\theta_{AB}\ d\phi_{AB} \qquad (4\text{-}63)$$

$$\times\ P^2\ dP\ \sin\theta_P\ d\theta_P\ d\phi_P$$

Expansion of Wave Functions

Because the coupling between final states was neglected when the translational motion coefficients $G_n^*(\vec{P})$ were being obtained, the only term of χ_f^{-*} of concern in the calculation of T_n^i is $G_n^*(P)\ z_n^*(\vec{r}_{AB};P)$. From Equation (4-60) the expansion of this term is

$$4\pi\ Y_{\ell_f}^{m_f}(\theta_{AB},\phi_{AB})\ \bar{R}_{n_f}(r_{AB};P) \sum_{\ell_1=0}^{\infty} \sum_{m_1=-\ell_1}^{\ell_1} i^{-\ell_1}\ e^{i\eta_{\ell_1}} \qquad (4\text{-}64)$$

$$\times\ \frac{u_{\ell_1}(k_n P)}{k P}\ Y_{\ell_1}^{m_1}(\theta_P,\phi_P)\ Y_{\ell_1}^{m_1 *}(\Theta,\Phi)$$

and that of the corresponding term in $\bar{\chi}_f^{-*}$ is

$$4\pi\, Y_{\ell_f}^{m_f}(\pi-\theta_p,\pi+\phi_p)\,\bar{R}_{n_f}(r_{AB};p)\sum_{\ell_2=0}^{\infty}\sum_{\ell_3=0}^{\infty} i^{-\ell_1}\, e^{i\eta_{\ell_1}} \qquad (4\text{-}65)$$

$$\times\ \frac{u_{\ell_1}(k_n p)}{k_n p}\ Y_{\ell_1}^{m_1}(\theta_p,\phi_p)\, Y_{\ell_1}^{m_1 *}(\Theta,\Phi)$$

Here, the subscript on l and m has the purpose of associating these two quantities with the orbital angular momenta of the final state. Also, the initial asymptotic wave function φ_i can be expanded as

$$\varphi_i = Z_{n_i}(r_{BC})\, Y_{\ell_i}^{m_i}(\theta_{BC},\phi_{BC})\sum_{\ell_2=0}^{\infty}\sum_{\ell_3=0}^{\infty} 4\pi\sqrt{(2\ell_2+1)(2\ell_3+1)} \qquad (4\text{-}66)$$

$$\times\ i^{\ell_2+\ell_3}\ j_{\ell_2}(k_i r_{AB})\, j_{\ell_3}(M_i k_i r_{BC})\, Y_{\ell_2}^{0}(\theta_{AB},\phi_{AB})\, Y_{\ell_3}^{0}(\theta_{BC},\phi_{BC})$$

by virtue of the relation

$$\varphi_i = \exp(i\vec{k}_i\cdot\vec{R})\, Y_{\ell_i}^{m_i}(\theta_{BC},\phi_{BC})\, Z_{n_i}(r_{BC}) \qquad (4\text{-}67)$$

$$= \exp\left(i\vec{k}_i\cdot(\vec{r}_{AB}+M_i\vec{r}_{BC})\right) Y_{\ell_i}^{m_i}(\theta_{BC},\phi_{BC})\, Z_{n_i}(r_{BC})$$

Here, M_i denotes $m_C/(m_B + m_C)$.

Substitution of Equations (4-65) and (4-66) into Equation (4-63) yields the following expression for T_n^i:

$$T_n^i = 16\pi^2 \sum_{\ell_1=0}^{\infty} \sum_{\ell_2=0}^{\infty} \sum_{\ell_3=0}^{\infty} \sum_{m_1=-\ell_1}^{\ell_1} i^{-\ell_1} \exp(i\eta_{\ell_1})\, i^{\ell_2+\ell_3} \qquad (4\text{-}68)$$

$$\times \sqrt{(2\ell_2+1)(2\ell_3+1)}\; Y_{\ell_1}^{m_1*}(\Theta, \Phi) \iint \frac{u_{\ell_1}(k_n P)}{k_n P}\, Y_{\ell_1}^{m_1}(\theta_P, \phi_P)\, j_{\ell_2}(k_i r_{AB})$$

$$\times j_{\ell_3}(M_i k_i r_{BC})\, \bar{u}_f(r_{AB}, P)\, \bar{R}_{n_f}(r_{AB}; P)\, Z_{n_i}(r_{BC})\, Y_{\ell_i}^{m_i}(\theta_{BC}, \phi_{BC})$$

$$\times Y_{\ell_f}^{m_f*}(\pi - \theta_P, \pi + \phi_P)\, Y_{\ell_2}^{0}(\theta_{AB}, \phi_{AB})\, Y_{\ell_3}^{0}(\theta_{BC}, \phi_{BC})\, d^3\vec{r}_{AB}\, d^3\vec{P}$$

The above equation, in conjunction with the relation

$$f_n^i(\Theta, \Phi) = \frac{\mu_f}{2\pi\hbar^2}\, T_n^i \qquad (4\text{-}69)$$

can be used as the starting point in the calculation of reaction cross-sections for specific bimolecular, highly exothermic exchange reactions.

In the next chapter, the foregoing development will be applied to the calculation of reaction cross-sections for the reaction $H + Br_2 \rightarrow HBr + Br$.

CHAPTER V

REACTION CROSS-SECTIONS FOR $H + Br_2 \rightarrow HBr + Br$ CORRESPONDING TO ELLISON'S POTENTIAL-ENERGY SURFACE

There are several reasons why the $H + Br_2 \rightarrow HBr + Br$ was selected to test the methods outlined in the previous chapter. First, infrared chemiluminescence experiments have yielded information on the manner in which the energy of reaction (about 41 kilocalories per mole) is distributed among the product molecules. By performing relative intensity measurements of the infrared emission spectra of the $H + Br_2 \rightarrow HBr + Br$ reacting mixture, Polanyi and his co-workers (10) were able to estimate the relative values of the detailed reaction rate constants $\bar{K}(n_{HBr}, l_{HBr})$. Here, n_{HBr} and l_{HBr} represent the vibrational and rotational quantum numbers, respectively, of the product HBr. The detailed rate constants provide information on the relative rates at which reactive collisions are forming HBr molecules in the state n_{HBr}, l_{HBr}. By summing their results over all possible rotational states l_{HBr}, Polanyi, et al., obtained detailed rate constants $\bar{\bar{K}}(n_{HBr})$ for reaction into the specified vibrational states n_{HBr}. In Table 3, the values of these rate constants are reported relative to $\bar{\bar{K}}(n_{HBr} = 3) = 1$. The significance of this experiment is that various potential-energy surfaces for the reaction $H + Br_2 \rightarrow HBr + Br$ can be assumed, and then some preliminary quantum mechanical calculations can be made until agreement with the results of Table 3 is reached. The most successful potential-energy function can be used to continue the calculations until the total rate constant K_t is obtained for several temperatures.

Comparison of the theoretical rate constant can then be made with the experimental value.

Table 3. Detailed Rate Constants for Formation of HBr in Various Vibrational States; Normalized to the Detailed Rate Constant for the Third Vibrational State (from Infrared Chemiluminescent Experiments of Polanyi (10)).

Vibrational Quantum Number of HBr	Detailed Reaction Rate Constant
3	1.00
4	0.64
5	0.19
6	0.05

A second reason for the study of $H + Br_2 \rightarrow HBr + Br$ is that the diatomics-in-molecules method of Ellison (41) has been used to derive a potential-energy function for this system (9). Thus, certain features of this function can be retained and others varied in order to accomplish the task of fitting the infrared chemiluminescent data.

A third reason for considering $H + Br_2 \rightarrow HBr + Br$ is that the light mass of hydrogen relative to that of bromine reduces by an order of magnitude the amount of calculations required to determine the reaction cross-sections.

A fourth reason is one that deals with the applicability of the linear complex model to $H + Br_2 \rightarrow HBr + Br$. In his classical mechanical study of this reaction (60,111), Polanyi noticed that the collinear trajectory was a fairly good description of the typical $H + Br_2$ trajectory.

In this reaction, the light H atom tends to come right up to the nearest Br atom before the more distant Br atom has time to leave; in other words, $r_{H\text{-}Br_2}$ decreases first, then $r_{HBr\text{-}Br}$ increases--as is implied in a rectilinear trajectory.

Finally, experimental rate constants are available for $H + Br_2 \rightarrow HBr + Br$, although the stationary state hypothesis is necessary to extract these constants from the measurable rate of the reaction $H_2 + Br_2 \rightarrow 2\ HBr$ (101).

Ellison's Potential-Energy Function

As discussed in Chapter II, the diatomics-in-molecules method of Ellison's is designed to calculate potential-energy surfaces for simple molecular systems without evaluating exchange or coulombic integrals or resorting to adjustable parameters. Instead, one is confronted with the problem of obtaining experimental energies for the ground and excited electronic states of all the possible diatomic and monatomic combinations present in the molecular system.

By beginning with conventional valence-bond structures for HBr, Br_2, and H--Br--Br, Ellison (9) obtained expressions of the type represented by Equations (2-24) and (2-25). The resulting H_{nm}^{PQ} and H_{nm}^{P} were substituted into the secular equation, Equation (2-15), and an expression for $V_L(r_{HBr},P)$ was obtained.

Valence-Bond Structures

Ellison began with two valence-bond structures for HBrBr, the canonical (102) structures (1) H-BrBr and (2) HBr-Br. The associated wave functions can be represented by

$$\Psi_1 = |a\bar{b}c| - |\bar{a}bc| \tag{5-1}$$

$$\Psi_2 = |a\bar{b}c| - |ab\bar{c}|$$

The symbol a represents a 1s orbital located on the hydrogen atom, and b and c denote 4p orbitals on each of the bromine atoms. It shall be understood that the nonbonding $1s^2\ 2s^2\ 2p^6\ 3s^2\ 3p^6\ 4s^2\ 3d^{10}\ 4p^4$ electron orbitals should also be written into the determinantal wave functions. A bar over an orbital symbolizes β-spin, while no bar means α-spin. The notation $|\ a\bar{b}c\ |$ is shorthand for the determinant

$$\begin{vmatrix} a(1)\alpha(1) & b(1)\ \beta(1) & c(1)\ \alpha(1) \\ a(2)\alpha(2) & b(2)\ \beta(2) & c(2)\ \alpha(2) \\ a(3)\alpha(3) & b(3)\ \beta(3) & c(3)\ \alpha(3) \end{vmatrix} \tag{5-2}$$

According to Ellison, the diatomics-in-molecules theory is easier to execute if the wave functions are not normalized, even for infinite separation of the nuclei.

Ellison utilized the simplest valence-bond structures for HBr and Br_2. If A denotes the H atom, B denotes the Br atom closest to the H atom, and C denotes the Br atom farthest from the H atom, the diatomic valence-bond structures may be written

$$\Psi_1^{AB} = |a\bar{b}| + |\bar{a}b| \tag{5-3}$$

$$\Psi_2^{AB} = |a\bar{b}| - |\bar{a}b| \tag{5-4}$$

$$\Psi_3^{AB} = |ab| \tag{5-5}$$

$$\Psi_4^{AB} = |\bar{a}\bar{b}| \tag{5-6}$$

Equation (5-3) represents the ground singlet state, whereas Equations (5-4), (5-5), and (5-6) represent the excited triplet states for AB; analogous expressions for the AC and BC molecules are also needed.

The Energy Matrix Elements H_{nm}

To illustrate the diatomics-in-molecules theory presented in Chapter II, two integrals, H_{12}^{AB} and H_{22}^{AB}, necessary for the solution of Equation (2-15) will now be evaluated. From Equation (2-31)

$$H_{nm}^{PQ} = \int \Psi_n^* A_{PQ}^{(PQ)} H_{PQ} A_{PQ} A_{(PQ)} \Psi_m \, d\tau \tag{5-7}$$

The primitive function corresponding to the canonical structure Ψ_2 is written

$$\Psi_2 = |a_1 \bar{b}_2 c_3| - |a_1 b_2 \bar{c}_3| \tag{5-8}$$

Operation on Ψ_2 with the antisymmetrizer $A_{AB}A_{(AB)}$ results in

$$A_{AB} A_{(AB)} \Psi_2 = |a\bar{b}|c - |ab|\bar{c} \tag{5-9}$$

Solving Equations (5-3) and (5-4) for $a\bar{b}$ in terms of Ψ_1^{AB} and Ψ_2^{AB} and utilizing the identity in Equation (5-5), one can rewrite Equation (5-9) as

$$A_{AB} A_{(AB)} \Psi_2 = \frac{1}{2}(\Psi_1^{AB} + \Psi_2^{AB})c - \Psi_3^{AB}\bar{c} \tag{5-10}$$

Employment of the diatomic Hamiltonian H_{AB} yields

$$H_{AB} A_{AB} A_{(AB)} \Psi_2 = \frac{1}{2}(E_1^{AB}\Psi_1^{AB} + E_2^{AB}\Psi_2^{AB})c - E_2^{AB}\Psi_3^{AB}\bar{c} \tag{5-11}$$

By Equations (5-3) to (5-5), the above expression can be rewritten as

$$H_{AB} A_{AB} A_{(AB)} \Psi_2 = \frac{1}{2}\left[E_1^{AB}(|\bar{a}b| - |a\bar{b}|)c \right. \tag{5-12}$$

$$\left. + E_2^{AB}(|\bar{a}b| - |a\bar{b}|)c\right] - E_2^{AB}|ab|c$$

Consequent application of the supplementary antisymmetrizer results in

$$A_{AB}^{(AB)} H_{AB} A_{AB} A_{(AB)} \Psi_2 = \frac{1}{2}\left[E_1^{AB}(|a\bar{b}c| - |\bar{a}bc|)\right. \tag{5-13}$$

$$\left. + E_2^{AB}(|\bar{a}bc| + |a\bar{b}c|)\right] - E_2^{AB}|ab\bar{c}|$$

Denoting $A_{AB}^{(AB)} H_{AB} A_{AB} A_{(AB)}$ by H_{AB} and employing Equations (5-1) and (5-2), one obtains

$$H_{AB} \Psi_2 = \frac{1}{2}\left[E_1^{AB} \Psi_1 + E_2^{AB}(2\Psi_2 - \Psi_1)\right] \tag{5-14}$$

Reference to Equation (5-7) yields

$$H_{12}^{AB} = \left[E_1^{AB} S_{11} + E_2^{AB}(2S_{12} - S_{11})\right]/2 \tag{5-15}$$

and

$$H_{22}^{AB} = \left[E_1^{AB} S_{21} + E_2^{AB}(2S_{22} - S_{21})\right]/2 \tag{5-16}$$

where

$$S_{nm} = \int \Psi_n^* \Psi_m \, d\tau \tag{5-17}$$

By carrying out a similar procedure for each of the other $H_{PQ}\ \Psi_n$ and the $H_P\ \Psi_n$, it can be shown that

$$\mathcal{H}_{AB}\ \psi_1 = E_1^{AB}\ \Psi_1 \tag{5-18}$$

$$\mathcal{H}_{Ac}\ \psi_1 = \left[E_1^{Ac}(\Psi_1 - \Psi_2) + E_2^{Ac}(\Psi_1 + \Psi_2)\right]/2 \tag{5-19}$$

$$\mathcal{H}_{Bc}\ \psi_1 = \left[E_1^{Bc}\ \Psi_2 + E_2^{Bc}(2\Psi_1 - \Psi_2)\right]/2 \tag{5-20}$$

$$\mathcal{H}_{Ac}\ \psi_2 = \left[E_1^{Ac}(\Psi_2 - \Psi_1) + E_2^{Ac}(\Psi_1 + \Psi_2)\right]/2 \tag{5-21}$$

$$\mathcal{H}_{Bc}\ \psi_2 = E_1^{Bc}\ \Psi_2 \tag{5-22}$$

$$H_p\ \Psi_n = E_p\ \Psi_n \tag{5-23}$$

All the integrals H_{nm}^{PQ} and H_{n}^{P} can thus be obtained by substitution of Equations (5-18) through (5-23) into Equation (5-7), and the energy matrix elements H_{nm} calculated according to Equation (2-27).

The Overlap Matrix Elements S_{nm}

Substitution of Equations (3-1) and (5-2) into Equation (5-17) results in

$$S_{11} = 2 + 2\bar{S}_{AB}^{2} - \bar{S}_{AC}^{2} - \bar{S}_{BC}^{2} - 2\bar{S}_{AB}\bar{S}_{AC}\bar{S}_{BC} \qquad (5\text{-}24)$$

$$S_{12} = S_{21} = 1 - 2\bar{S}_{AC}^{2} + \bar{S}_{BC}^{2} + \bar{S}_{AB}^{2} - \bar{S}_{AB}\bar{S}_{AC}\bar{S}_{BC}$$

$$S_{22} = 2 + 2\bar{S}_{BC}^{2} - \bar{S}_{AB}^{2} - \bar{S}_{AC}^{2} - 2\bar{S}_{AB}^{2}\bar{S}_{AC}^{2}\bar{S}_{BC}^{2}$$

In his diatomics in molecules method calculations for the H_2O, H_3, and H_3^+ molecules, Ellison (103) discovered that the energy results obtained for neglected overlap between atomic orbitals, i.e., $\bar{S}_{PQ} = 0$, did not differ significantly (less than 0.4 kcal) from those obtained when overlap between atomic orbitals was included. Thus, to avoid the insurmountable task of correctly calculating the overlap between atomic orbitals for a molecule containing bromine atoms, he neglected all the $\bar{S}_{PQ}$. Therefore, overlap integrals between structures simplified to

$$S_{11} = S_{22} = 2 \tag{5-25}$$

$$S_{12} = S_{21} = 1$$

The Ground State Energy Curves E_1^{PQ}

Since no sufficiently accurate theoretical or empirical potential-energy curves are available for the ground singlet states of HBr and Br_2, one must resort to more approximately formulated potential-energy functions. The best approximate function available for ground singlet states is probably the Hulburt-Hirschfelder curve (104), which has been thoroughly reviewed by Steele, et al. (105). Mathematically, this potential-energy function is written as

$$V(r) = D\left[\left(1 - e^{-x}\right)^2 + cx^3 e^{-2x}(1 + bx)\right] - D \tag{5-26}$$

where

$$x = a\,(r - r_e) \tag{5-27}$$

Here, D is the sum of the dissociation and ground state energies for the diatomic molecule, r_e is its equilibrium distance, and a, b, and c are experimentally determined parameters. The molecular parameters a, A, D, r_e, B, α, and T for Br_2 and HBr are taken from the work of Herzberg (106), whereas the parameters b and c are taken from the work of Hulburt

and Hirschfelder (104). Table 4 includes these spectroscopic constants.

Table 4. Spectroscopic Constants for Br_2 and HBr to be Used in Ellison's Potential-Energy Function

Molecule	a, $Å^{-1}$	A, sec/Å $\sqrt{gram}$	D, gram $Å^2/sec^2$
Br_2	1.962	0.6861	31898
HBr	1.809	0.1054	62753

Molecule	r_e, Å	B, gram $Å^2/sec^2$	α, gram $Å^2/sec^2$
Br_2	2.284	0.16071	0.00054
HBr	1.414	16.826	0.449

Molecule	T, gram $Å^2/sec^2$
Br_2	4.028×10^{-8}
HBr	6.585×10^{-4}

It should be noted that Hulburt- Hirschfelder curves are usually very accurate in the region near equilibrium, and thus should not adversely affect the potential energy for those interatomic configurations contributing most heavily to the reaction cross-sections.

The Excited State Energy Curves

To circumvent the nonavailability of even semiempirical potential-energy curves for the excited triplet states of HBr and Br_2, Ellison (9) postulated that the final polyatomic molecule energies should be relatively insensitive to diatomic excited state energies and devised a simple scheme for approximating these potentials. In elementary valence-bond theory (102), the ground singlet and excited triplet state energies

(relative to separate atoms) for the equilibrium internuclear distance r_e are given by the expressions

$$E_{1e} = J + K \tag{5-28}$$

$$E_{2e} = J - K \tag{5-29}$$

where J and K represent the coulomb and exchange energy, respectively. Taking $J = p\, E_{1e}$, where p is a parameter, equal to the fraction of the total energy that is coulombic at the equilibrium distance, and substituting into Equation (5-29) gives

$$E_{2e} = E_{1e}\,(2p-1) \tag{5-30}$$

The values of p were varied from about 0.1 to 0.4. Ellison supposed that the excited triplet state is repulsive for all distances, and proposed to represent it by the simple exponential expression

$$E_2 = \alpha\, exp(-\beta r) \tag{5-31}$$

where Equation (5-30) is utilized to evaluate one of the two constants α and β. For large R, Ellison assumed that the coulomb energy is a negligible fraction of the total energy. By taking $J = 0$ at $r = 4r_e$ ($r = 3r_e$ for Br_2), Ellison obtained the relationship

$$(E_1)_{r=4r_e} = -(E_2)_{r=4r_e} \tag{5-32}$$

from which the second of the constants α and β was determined.

Ellison found that modification of the parameter p in the range 0.1 to 0.4 causes only small (0-2 kcal) changes in the activation energies for all of the reactions studied, and that for the specific reaction $H + Br_2 \rightarrow HBr + Br$, changing p only causes the downhill slopes to change in shape. Thus, he settled on the value 0.15 for p since it has often been assumed that the total binding energy is approximately 12-15 percent coulombic (107).

Algebraic Expression for the Potential-Energy Surface

Utilizing all the appropriate expressions presented previously in this chapter, and employing Equation (2-15), one obtains the following expression for $V_L(r_{HBr}, r_{Br_2})$:

$$V_L = \frac{2H_{11}H_{22} - H_{12} - H_{21} - \{[H_{12} - H_{21} - 2(H_{11} - H_{22})]^2 - 12(H_{12}H_{21} - H_{11}H_{22})\}^{1/2}}{6} \tag{5-33}$$

where

$$H_{11} = 2E_1^{AB} + \frac{1}{2}E_1^{AC} + \frac{3}{2}E_2^{AC} + \frac{1}{2}E_1^{BC} + \frac{3}{2}E_2^{BC} \tag{5-34}$$

$$H_{12} = H_{21} = E_1^{AB} - \tfrac{1}{2} E_1^{AC} + \tfrac{3}{2} E_2^{AC} + E_1^{BC} \tag{5-35}$$

$$H_{22} = \tfrac{1}{2} E_1^{AB} + \tfrac{3}{2} E_2^{AB} + \tfrac{1}{2} E_1^{AC} + \tfrac{3}{2} E_2^{AC} + 2 E_1^{BC} \tag{5-36}$$

Here the H_{nm}^{P} do not appear since, according to Equation (2-47),

$$H_{nm}^{P} = E_1^{P} S_{nm} \tag{5-37}$$

The separated atoms are assumed to be in their ground electronic states, for which the energies are taken as zero.

Special Features of Ellison's Potential-Energy Surface

Values of $V_L(r_{HBr}, r_{Br_2})$ were calculated in the manner just described over the region $0 \leq r_{HBr} \leq 5.0$ Å, $0 \leq r_{Br_2} \leq 7.0$ Å at intervals of 0.05 Å for each interatomic distance. Figure 5 contains plots of V_L versus r_{HBr} for different constant values of r_{Br_2}. The retention of definite Morse curve features by V_L, with respect to r_{HBr}, even when r_{Br_2} takes on small values lends some justification to the perturbed Morse oscillator model developed in the previous chapter for bimolecular, highly exothermic exchange reactions.

Plots of V_L versus r_{Br_2} for various constant values of r_{HBr} are shown in Figure 6. Note that the Br-Br interaction is greatly distorted by the presence of the H atom, being only slightly attractive when H

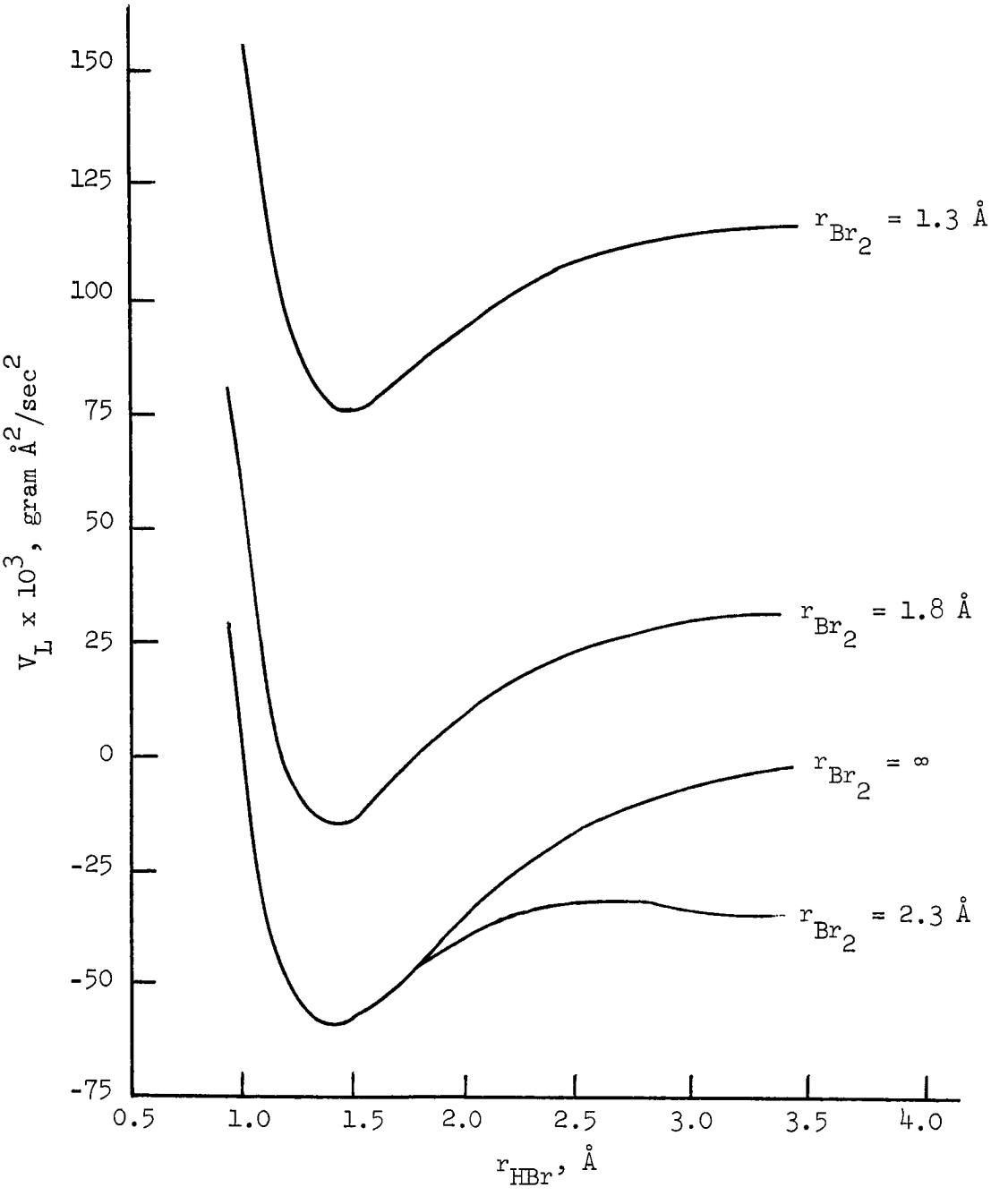

Figure 5. V_L Versus r_{HBr} for Constant Values of r_{Br_2}.

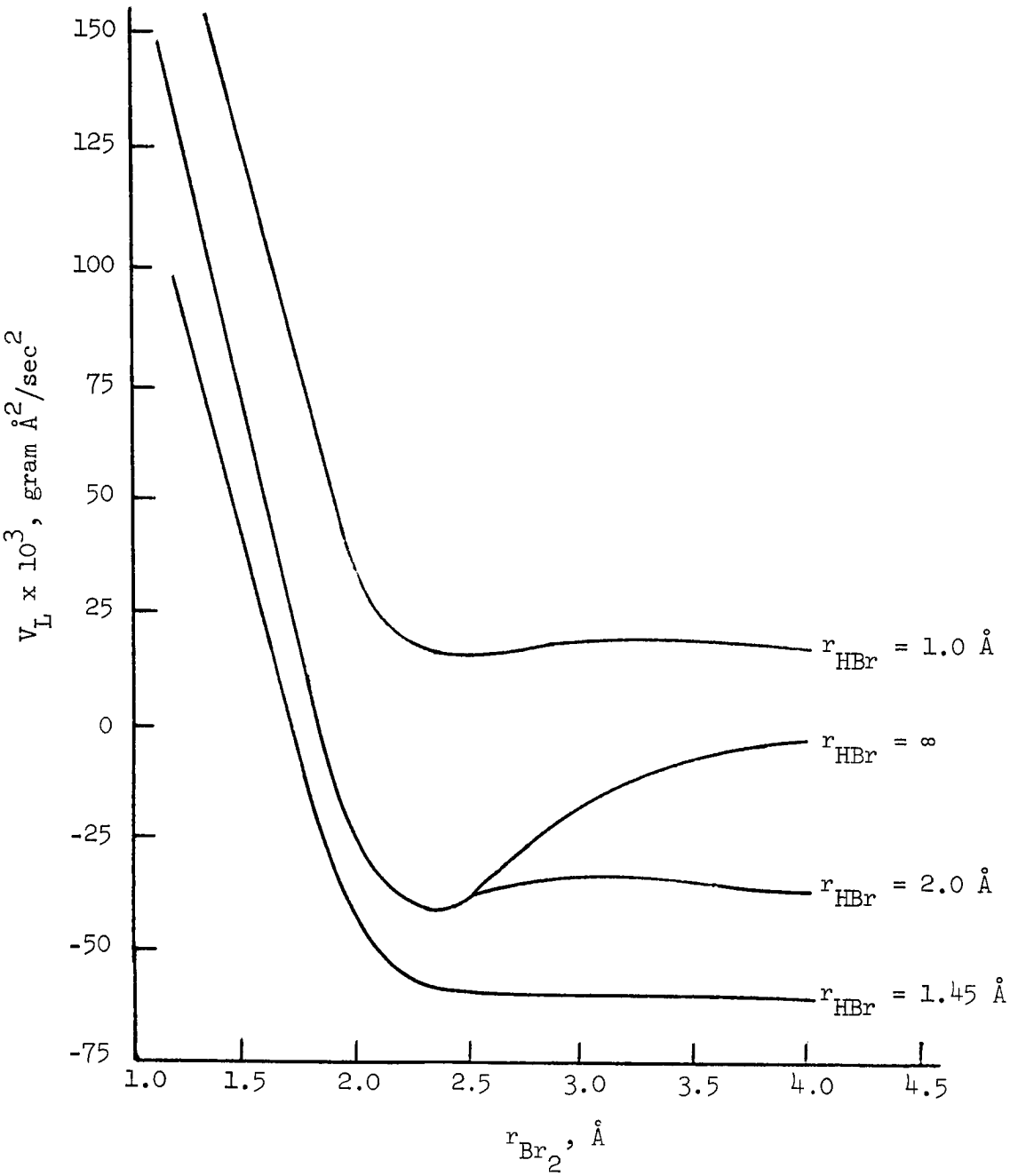

Figure 6. V_L Versus r_{Br_2} for Constant Values of r_{HBr}.

approaches within 2.0 Å of the closer Br atom.

Fitting of Ellison's Potential-Energy Surface to Morse Curves

To apply the methods developed for the perturbed Morse potential model to the reaction $H + Br_2 \rightarrow HBr + Br$, the curves represented in Figure 5 were fitted as closely as possible to Morse curves. As suggested in the previous chapter, the Morse parameters $D(r_{Br_2})$, $r^E_{HBr}(r_{Br_2})$, and $U_M(r_{Br_2})$ can be taken directly from the plots of V_L versus r_{HBr} at constant r_{Br_2}. Then the remaining Morse parameter $a(r_{Br_2})$ can be obtained from Equation (4-7) by using a value of V_L at a point to the left of $r^E_{HBr}(r_{Br_2})$. The Morse parameters obtained by this procedure for Ellison's potential-energy surface are listed in Table 5. The point used to calculate $a(r_{Br_2})$ was taken at 1.0 Å.

Reference to the original paper by ter Haar (81) reveals a certain criterion to be met by the parameters A(P), a(P), D(P), $r^E_{HBr}(P)$, if ter Haar's solution is to be applicable to the Scroedinger equation for the perturbed Morse oscillator, Equation (4-4). This criterion can be expressed by the equation

$$A(P)\sqrt{D(P)}\left[e^{a(P)\,r^E_{HBr}(P)} - a(P)\,r^E_{HBr}(P) - 1\right] \geq 1 \qquad (5\text{-}38)$$

The parameters listed in Table 5 meet this criterion for all values of P.

Simplification of the Reaction Cross-Section

The Reactive Scattering Amplitude

Beginning with Equation (4-68), the "linear model" relation for

Table 5. Parameters Used to Fit Morse Type Functions V_M to V_L for the System H-Br-Br

r_{Br_2}, Å	r^E_{HBr}, Å	D, gram Å^2/sec^2	U_m, gram Å^2/sec^2	a, Å^{-1}
0.0	1.4750	73423	1017876	1.828
0.1	1.4300	72803	847603	1.832
0.2	1.4000	71026	705247	1.834
0.3	1.3775	68319	586393	1.854
0.4	1.3675	64993	487193	1.860
0.5	1.3750	61376	404339	1.863
0.6	1.3850	57760	335026	1.866
0.7	1.3950	54361	276916	1.862
0.8	1.4075	51314	228086	1.892
0.9	1.4175	48686	186961	1.856
1.0	1.4250	46493	152252	1.844
1.1	1.4325	44738	122885	1.841
1.2	1.4350	43437	97936	1.844
1.3	1.4325	42696	76539	1.841
1.4	1.4350	42819	57744	1.849
1.5	1.4325	44526	40289	1.862
1.6	1.4225	49153	22380	1.892
1.7	1.4175	47695	2637	1.844
1.8	1.3925	46695	-16898	2.128
1.9	1.4275	33921	-33202	2.163
2.0	1.4325	28768	-44838	2.241
2.1	1.4325	27149	-52591	2.275
2.2	1.4325	27500	-57357	2.264
2.3	1.4300	29139	-59981	2.387
2.4	1.4275	31668	-61200	2.195
2.5	1.4250	34777	-61595	2.147
2.6	1.4200	38191	-61582	2.111
2.7	1.4200	41649	-61416	2.055
2.8	1.4175	44937	-61240	2.017
2.9	1.4175	48031	-61114	1.974
3.0	1.4150	50716	-61060	1.951
3.1	1.4150	53011	-61074	1.922
3.2	1.4150	54942	-61141	1.899
3.3	1.4150	56500	-61248	1.880
3.4	1.4150	57783	-61379	1.866
3.5	1.4150	58790	-61524	1.855
3.6	1.4150	59596	-61673	1.846
3.7	1.4150	60228	-61818	1.839
3.8	1.4150	60727	-61956	1.834
3.9	1.4150	61122	-62084	1.829
4.0	1.4150	61435	-62201	1.825
4.1	1.4150	61686	-62304	1.823
4.2	1.4150	61886	-62395	1.821
4.3	1.4150	62052	-62475	1.819
4.4	1.4150	62185	-62543	1.818
4.5	1.4150	62297	-62602	1.817

the transition integral, a convenient expression for the reaction cross-sections of $H + Br_2 \rightarrow HBr + Br$ will be derived. First, the notation of Equation (4-68) should be altered for the sake of symbological brevity. Let the components of $\vec{P}$ in spherical coordinates be symbolized as follows: $P = P$, $\theta = \theta_P$, and $\phi = \phi_P$. Likewise, change the notation for the spherical components of $\vec{r}_{AB}$ so that $r = r_{AB}$, $\xi = \theta_{AB}$, $\delta = \phi_{AB}$.

Now since

$$\vec{P} = \vec{r}_{Br_2} + \frac{m_H}{m_H + m_{Br}} \vec{r}_{HBr} \tag{5-39}$$

the vector $\vec{r}_{Br_2}$ is tentatively approximated as $\vec{P}$ because of the smallness of $m_H/(m_H + m_{Br})$. The validity of this approximation will be discussed later. Incorporating this assumption and the aforementioned notation into Equation (4-68) gives

$$T_n^i = 16\pi^2 \sum_{l_1=0}^{\infty} \sum_{l_2=0}^{\infty} \sum_{l_3=0}^{\infty} \sum_{m_1=-l_1}^{l_1} i^{-l_1} e^{i m_1 \xi} \sqrt{(2l_2+1)(2l_3+1)}\; i^{l_2+l_3} \tag{5-40}$$

$$Y_{l_1}^{m_1 *}(\Theta, \Phi) \int_{r=0}^{\infty} \int_{P=0}^{\infty} \frac{u_{l_1}(k_n P)}{k_n P}\, j_{l_2}(k_n r)\, j_{l_3}(M_i k_n P)\, \bar{U}_f(r, P)$$

$$\bar{R}_n(r; P)\, Z_{n_i}(P)\, P^2 dP\, r^2 dr \int_{\delta=0}^{2\pi} \int_{\xi'=0}^{\pi} Y_{l_2}^{0}(\xi', \delta) \sin\xi'\, d\xi'\, d\delta$$

$$\int_{\phi=0}^{2\pi} \int_{\theta=0}^{\pi} Y_{l_f}^{m_f *}(\pi - \theta, \pi + \phi)\, Y_{l_i}^{m_i}(\theta, \phi)\, Y_{l_1}^{m_1}(\theta, P)\, Y_{l_3}^{0}(\theta, P) \sin\theta\, d\theta\, d\phi$$

Integration over the angular coordinates results in

$$T_n^i = (4\pi)^{3/2} \sum_{l_1=0}^{\infty} \sum_{l_2=0}^{\infty} \sum_{l_3=0}^{\infty} \sum_{m_1=-l_1}^{l_1} i^{-l_1} e^{i\eta_n} \sqrt{(2l_2+1)(2l_3+1)} \tag{5-41}$$

$$i^{l_2+l_3} Y_{l_1}^{m_1*}(\Theta,\Phi)\, I(l_1,l_2,l_3) \sqrt{2l_2+1}\, \delta_{l_2,0}\, (-1)^{m_1} \sqrt{2l_1+1}$$

$$\sqrt{(2l_3+1)(2l_2+1)(2l_1+1)} \sum_{l_4} (2l_4+1)^{-1} C(l_1,l_3,l_4;-m_1,0,-m_1)$$

$$C(l_1,l_3,l_4;0,0,0)\, C(l_1,l_2,l_4;m_1,m_2,-m_1)\, C(l_1,l_2,l_4;0,0,0)$$

The symbol $\delta_{a,b}$ represents the Kronecker delta defined by

$$\delta_{a,b} = 0 \quad , \quad a \neq b \tag{5-42}$$

$$\delta_{a,b} = 1 \quad , \quad a = b$$

and the expression $I(l_1, l_2, l_3)$ is shorthand notation for the integral

$$\int_{r=0}^{\infty}\int_{\rho=0}^{\infty} dr\, d\rho\, r^2\,\rho^2\,\frac{u_{\ell_1}(k_n\rho)}{k_n\rho}\, j_{\ell_2}(k_i r)\, j_{\ell_3}(M_i k_i \rho)\,\bar{u}_{\ell_f}(r,\rho) \qquad (5\text{-}43)$$

$$\times\, \bar{R}_{n_f}(r;\rho)\; Z_{n_i}(\rho)$$

The symbols $C(l_1, l_2, l_3; m_1, m_2, m_3)$ represent the Clebsch-Gordan coefficients (108) and have certain properties that provide for conservation of angular momentum and parity in Equation (5-41). The principal properties of the Clebsch-Gordan coefficients are summarized in Appendix B, and reference to them will be made frequently.

Finally, summation over l_2 yields, in conjunction with Equation (4-69), the following expression for the reactive scattering amplitude:

$$f_n^i(\Theta,\Phi) = \frac{\mu_f}{2\pi\hbar^2}\,(4\pi)^{3/2}\sum_{\ell_1=0}^{\infty}\sum_{\ell_3=0}^{\infty}\sum_{m_1=-\ell_1}^{\ell_1} i^{-\ell_1}\, e^{i\eta_{\ell_1}}\,(2\ell_3+1)\, i^{\ell_3} \qquad (5\text{-}44)$$

$$I(\ell_1,0,\ell_3)\,(-1)^{m_f}\sqrt{(2\ell_f+1)(2\ell_i+1)(2\ell_1+1)}\sum_{\ell_4=|\ell_f-\ell_3|}^{\ell_f+\ell_3}(2\ell_4+1)^{-1}$$

$$C(\ell_f,\ell_3,\ell_4;-m_f,0,-m_f)\,C(\ell_f,\ell_3,\ell_4;0,0,0)$$

$$C(\ell_1,\ell_i,\ell_4;m_1,m_i,-m_f)\;C(\ell_1,\ell_i,\ell_4;0,0,0)$$

The Total Reaction Cross-Section

The differential reaction cross-section is obtained by substitution of Equation (5-44) into Equation (3-30), or

$$\sigma_n^i(\Theta, \Phi) = \frac{k_n}{k_i} \frac{\mu_i}{\mu_f} \left| f_n^i(\Theta, \Phi) \right|^2 \tag{5-45}$$

and the total reaction cross-sec on is obtained from $\sigma_n^i \Theta, \Phi)$ by integration over Θ, Φ.

Now, referring to Equation (1-8), the expression for the detailed specific rate constant is

$$K(n_f, l_f, m_f; n_i, l_i, m_i) = \int \left(P/\mu_i \right) \sigma(k_i, n_i, l_i, m_i; k_n, n_f, l_f, m_f) \tag{5-46}$$

$$\times F_{Br_2}^{\circ}(n_i, l_i, m_i, \vec{P}_{Br_2}) \quad F_H^{\circ}(\vec{P}_H) \; d^3\vec{P}_H \; d^3\vec{P}_{Br_2}$$

By assuming $F_{Br_2}^{\circ}(n_i, l_i, m_i, p_{Br_2})$ is independent of m_i, the specific detailed rate constant can be averaged over m_i and then summed over m_f to get

$$\bar{K}(n_f, l_f; n_i, l_i) = \int \left(P/\mu_i \right) \sigma(k_i, n_i, l_i; k_n, n_f, l_f) \, F_H^{\circ}(\vec{P}_H) \tag{5-47}$$

$$\times F_{Br_2}^{\circ}(n_i, l_i, \vec{P}_{Br_2}) \; d^3\vec{P}_H \; d^3\vec{P}_{Br_2}$$

where

$$\sigma(k_i, n_i, l_i; k_n, n_f, l_f) = \frac{1}{(2l_i+1)} \tag{5-48}$$

$$\times \sum_{m_i=-l_i}^{l_i} \sum_{m_f=-l_f}^{l_f} \sigma(k_i, n_i, l_i, m_i; k_n, n_f, l_f, m_f)$$

Thus, the cross-section defined by Equation (5-48) is really the cross-section of interest with regard to rate constant determinations.

From Equation (5-44) the reaction cross-section of Equation (5-48) is

$$\sigma = \frac{k_n}{k_i} \frac{\mu_i}{\mu_f} \left(\frac{\mu_f}{2\pi\hbar^2}\right)^2 (4\pi)^3 \sum_{l_1=0}^{\infty} \sum_{l_3=0}^{\infty} \sum_{l_3'=0}^{\infty} \sum_{m_1=-l_1}^{l_1} \sum_{l_4} \sum_{l_4'} \tag{5-49}$$

$$\sum_{m_f} \sum_{m_i} (2l_3+1)(2l_3'+1)\, i^{l_3-l_3'}\, I(k_1, 0, l_3)\, I(k_1, 0, l_3')$$

$$\frac{(2l_f+1)(2l_1+1)}{(2l_4+1)(2l_4'+1)}\, C(l_f, l_3, l_4; -m_f, 0, -m_f)\, C(l_f, l_3', l_4'; -m_f, 0, -m_f)$$

$$C(l_f, l_3, l_4; 0, 0, 0)\, C(l_f, l_3', l_4'; 0, 0, 0)\, C(l_1, l_i, l_4; m_1, m_i, -m_f)$$

$$C(l_1, l_i, l_4'; 0, 0, 0)\, C(l_1, l_i, l_4; 0, 0, 0)\, C(l_1, l_i, l_4'; 0, 0, 0)$$

By the orthogonality relations given in Equation (B-20) of Appendix B

$$\sum_{m_1=-l_1}^{l_1} \sum_{m_2=-l_2}^{l_2} C(l_1, l_2, l_4; m_1, m_2, -m_f)\, C(l_1, l_2, l_4'; m_1, m_2, -m_f) \tag{5-50}$$

so summation over m_i, m_1, and l_4' yields

$$\sigma(k_2, m_2, l_2; k_m, m_f, l_f) = \frac{k_m}{k_2} \frac{\mu_2}{\mu_f} \left(\frac{\mu_f}{2\pi\hbar^2}\right)^2 (4\pi)^3 \sum_{l_1} \sum_{l_3} \sum_{l_3'} \sum_{l_4} \tag{5-51}$$

$$\sum_{m_f} \frac{(2l_3+1)(2l_3'+1)}{(2l_2+1)}\, i^{l_3-l_3'}\, I(l_1, 0, l_3)\, I(l_1, 0, l_3')\, \frac{(2l_f+1)(2l_1+1)}{(2l_4+1)^2}$$

$$C(l_f, l_3, l_4; -m_f, 0, -m_f)\, C(l_f, l_3', l_4; -m_f, 0, -m_f)\, C(l_f, l_3, l_4; 0, 0, 0)$$

$$C(l_f, l_3', l_4; 0, 0, 0)\; C^2(l_1, l_2, l_4; 0, 0, 0)$$

Using the symmetry properties of Clebsch-Gordan coefficients (see Appendix B), one can write

$$C(l_f, l_3, l_4; -m_f, 0, -m_f)\, C(l_f, l_3', l_4; -m_f, 0, -m_f) = (-1)^{l_3 + l_3'} \qquad (5\text{-}52)$$

$$\times \frac{2l_4 + 1}{\sqrt{(2l_3+1)(2l_3'+1)}}\, C(l_f, l_4, l_3; m_f, -m_f, 0)\, C(l_f, l_4, l_3'; m_f, -m_f, 0)$$

Invoking once more the orthogonality relation of Equation (B-21) in Appendix B, one obtains

$$\sum_{l_f = |l_4 - l_3|}^{l_4 + l_3} \sum_{m_f = -l_f}^{l_f} C(l_f, l_4, l_3; m_f, -m_f, 0)\, C(l_f, l_4, l_3'; m_f, -m_f, 0) \qquad (5\text{-}53)$$

$$= \delta_{l_3, l_3'}$$

Thus, summation over m_f and l_3' in Equation (5-51) results in

$$\mathcal{T} = \frac{k_n}{k_i} \frac{\mu_i}{\mu_f} \left(\frac{\mu_f}{2\pi\hbar^2}\right)^2 (4\pi)^3 \sum_{l_1} \sum_{l_3} \sum_{l_4} \frac{(2l_3+1)(2l_f+1)(2l_1+1)}{(2l_4+1)} \qquad (5\text{-}54)$$

$$C^2(l_f, l_3, l_4; 0, 0, 0)\, C^2(l_1, l_i, l_4; 0, 0, 0)\, I^2(l_1, 0, l_3)$$

The discussion on computational procedure will show that the summation over l_1 is bounded by l_i and l_4, the summation over l_4 is bounded by l_3 and l_f, and the summation over l_3 is bounded effectively between two finite values. Thus, it is convenient to rearrange the Clebsch-Gordan factor $C^2(l_1, l_i, l_4; 0, 0, 0)$ by the symmetry properties in Appendix B. The result is

$$C^2(l_1, l_i, l_4; 0, 0, 0) = \frac{2l_4+1}{2l_1+1} C^2(l_4, l_i, l_1; 0, 0, 0) \tag{5-55}$$

The total reaction cross-section can then be written as

$$\sigma(k_i, n_i, l_i; k_n, n_f, l_f) = \frac{k_n}{k_i} \frac{\mu_i}{\mu_f} \left(\frac{\mu_f}{2\pi\hbar^2}\right)^2 (4\pi)^3 \sum_{l_3=0}^{\infty} \tag{5-56}$$

$$\sum_{l_4=|l_3-l_f|}^{|l_3+l_f|} \sum_{l_1=|l_4-l_i|}^{l_4+l_i} I^2(l_1, 0, l_3)\,(2l_3+1)(2l_f+1)$$

$$C^2(l_f, l_3, l_4; 0, 0, 0)\; C^2(l_4, l_i, l_1; 0, 0, 0)$$

where

$$I(l_1, 0, l_3) = \int_{r=0}^{\infty} \int_{P=0}^{\infty} dr\, dP\, r^2\, P^2 \frac{U_{l_1}(k_n P)}{k_n P} j_0(k_i r) \qquad (5\text{-}57)$$

$$\cdot j_{l_3}(M_i k_i P)\, \bar{U}_f(r, P)\, \bar{R}_{n_f}(r; P)\, Z_{n_i}(P)$$

Indistinguishability of Bromine Atoms

The acceptable practice in scattering theory (109) is to treat the collision as if all the particles involved were completely distinguishable, and then modify the resulting cross-sections to account for the indistinguishability. Thus, the role of indistinguishability in the study of the reaction H + Br_2 → HBr + Br has not been mentioned until now. When it is taken into account (see Appendix C) the resulting expression for the reaction cross-section is twice the cross-section in Equation (5-56). This is the expected result since an H atom approaching a Br_2 molecule from a large distance will attach to either Br atom with equal probability.

Computational Procedure

Computational Formula for Total Reaction Cross-Section

The vibrational wave functions $R_{n_f}(r;P)$ and $Z_{n_i}(P)$ were found to be negligible outside of the ranges $0.9 \leq r \leq 2.5$ Å and $1.8 \leq P \leq 3.0$ Å, respectively. Therefore, the integration of $I(l_1, 0, l_3)$ was carried out for the region

$$0.9 \leq r \leq 2.5 \text{ Å} \qquad (5\text{-}58)$$

$$1.8 \leq P \leq 3.0\ \text{Å} \tag{5-59}$$

only. With this restriction placed on the integration of $I(l_1, 0, l_3)$, it is seen that the maximum value of the argument of $j_{l_3}(M_i\ k_i\ P)$ is $(3/2)k_i$, since $M_i = \frac{1}{2}$. Based on a Maxwell-Boltzmann distribution, more than 99 percent of the collisions between H and Br_2 at 1000°K occur with k_i less than 20 $Å^{-1}$, so the maximum argument of $j_{l_3}(M_i\ k_i\ P)$ that will be of concern is 30. Now, an important property of spherical Bessel functions is that, for fixed x and increasing l, $j_l(x)$ reaches a maximum at about $l = x$, and then decreases rapidly until, at $l = \frac{4}{3}x$, it is only a negligible fraction of its maximum. Hence, the summation over l_3 will be terminated in Equation (5-56) after $l_3 = 40$ without incurring serious error.

Next, one of the selection rules in Appendix B for the Clebsch-Gordan coefficients states that $C(l_4, l_i, l_1; 0, 0, 0)$ vanishes identically until l_1 is in the range $| l_i - l_4 | \leq l_1 \leq l_4 + l_i$. This provides for conservation of angular momentum. And, finally, the Clebsch-Gordan coefficients $C(l_f, l_3, l_4; 0, 0, 0)$ and $C(l_4, l_i, l_1; 0, 0, 0)$ insure conservation of parity by vanishing except when $(l_f + l_3 + l_4)$ and $(l_4 + l_i + l_1)$, respectively, are even integers. Thus, the expression for $\sigma(k_i, n_i, l_i; k_n, n_f, l_f)$ to be used for computational purposes is

$$\tau(k_i, n_i, l_i; k_n, n_f, l_f) = \frac{2k_n}{k_i} \frac{\mu_{l_i}}{\mu_{l_f}} \left(\frac{\mu_{l_f}}{2\pi k^2}\right)^2 (4\pi)^3 \qquad (5\text{-}60)$$

$$\sum_{l_3=0}^{40} \sum_{l_4=|l_3-l_f|}^{l_3+l_f} \sum_{l_1=|l_4-l_i|}^{l_4+l_i} (2l_3+1)\ (2l_f+1)$$

$$C^2(l_f, l_3, l_4; 0,0,0)\ C^2(l_4, l_i, l_1; 0,0,0)$$

$$I^2(l_1, 0, l_3)$$

where the summations over l_4 and l_1 are to be carried out in steps of two. Also, because of the effective range of integration of $I(l_1,0,l_3)$ mentioned above, one can now use the relation

$$I(l_1, 0, l_3) = \int_{P=1.8}^{3.0} \int_{r=0.9}^{2.5} dP\, dr\, P^2 r^2 \frac{u_{l_1}(k_n, P)}{k_n P} \qquad (5\text{-}61)$$

$$\times j_{l_3}\left(\tfrac{1}{2} k_i P\right)\ j_0(k_i r)\ Z_{n_i}(P)$$

$$\times \bar{R}_{n_f}(r; P)\ \bar{u}_f(r, P)$$

Calculation of the Integral $I(l_1,0,l_3)$

Using the trapezoidal rule, Equation (5-61) was integrated with an interval of 0.025 Å for both r and P. The integration was carried out on the B-5500 computer of the Rich Electronic Computer Center, Georgia Institute of Technology. Before the actual integration was performed, the functions $\bar{U}_f(r,P)$, $u_{l_1}(k_n P)$, $Z_{n_i}(P)$, $\bar{R}_{n_f}(r;P)$, $j_o(k_i r)$, $j_{l_3}(\frac{1}{2} k_i P)$ were computed separately for the appropriate values of r and P.

The Potential-Energy Function. The function $V_L(r,P)$ was computed from Equation (5-33) and the function $\bar{U}_f(r,P)$ was then obtained from

$$\bar{U}_f(r,P) = V_L(r,P) - V_{Br_2}(P) \qquad (5\text{-}62)$$

where $V_{Br_2}(P)$ is the ground state intermolecular potential for an isolated Br_2 molecule. Utilizing the parameters of Table 4, the function $V_{Br_2}(P)$ was calculated using the Hulburt-Hirschfelder function, Equation (5-27). After the appropriate values of $\bar{U}_f(r,P)$ were computed, they were punched out on cards to be used later in the integration program.

The Initial Vibrational Wave Functions. The vibrational wave functions $Z_{n_i}(P)$ were calculated from the equation given by ter Haar for the Morse oscillator (81):

$$Z_n(P) = \frac{N_n \, W^{A\sqrt{D}-(n+\nu_2)} \, e^{-X} \, M(-n, 2A\sqrt{D}-2n; 2X)}{P} \qquad (5\text{-}63)$$

where

$$A = (m_{Br}/\hbar^2)^{1/2}/a \tag{5-64}$$

$$X = 2A\sqrt{D}\ \exp[-a(P-P^E)] \tag{5-65}$$

$$W = X/2 \tag{5-66}$$

After taking the parameters a, P^E, and D from Table 4, the confluent geometric function $M(-n, A\sqrt{D} - 2n; 2X)$ was calculated from Equation (4-16), and the normalizing constant N_n obtained by numerical integration of

$$N_n = \left[\int_{P=1.8}^{3.0} W^{2A\sqrt{D}-2(n+1/2)} e^{-2X} M^2(-n, 2A\sqrt{D}-2n; 2X)dP\right]^{-1/2} \tag{5-67}$$

Using Equation (5-63), the necessary values of $Z_{n_i}(P)$ were calculated for $n_i = 0$, to $n_i = 8$ and then punched out on cards to be used in the integration program.

The Vibrational Wave Functions for Perturbed HBr. Using the parameters in Table 5, the functions $\bar{R}_{n_f}(r;P)$ were obtained from Equations (4-13) and (4-23) for $n_f = 0$ to $n_f = 9$. The normalization factors $N_{n_f}(P)$ were calculated from Equation (4-28), the integrals of which were evaluated by the trapezoidal rule. The results of these calculations were stored on cards as $\bar{R}_{n_f}(r;P)$ for later use.

The Spherical Bessel Functions. The necessary values of the

spherical Bessel functions $j_o(k_i r)$ and $j_{l_3}(\frac{1}{2} k_i P)$ were calculated in the early stages of the actual integration program for $I(l_1,0,l_3)$ and stored in the computer memory for later use. Since the arguments of these functions depend on k_i, the initial energy of approach was specified prior to their calculation. The function $j_{l_3}(\frac{1}{2} k_i P)$ was computed for $l_3 = 0$ to $l_3 = 40$ by the Miller recurrence algorithm (110) as follows.

For fixed P, values of zero and one were assigned to F_{L+1} and F_L, respectively, where L is some integer larger than $\frac{1}{2} k_i P$. Taking L equal to 80, the recurrence relation (110)

$$F_{L-1}(X) = F_L(X) - \frac{X^2}{4(L+1)L} F_{L+1}(X) \tag{5-68}$$

for spherical Bessel functions was generate a sequence of numbers $\{F_L\}$ down to L = 0. The exact value of $j_0(\frac{1}{2} k_i P)$ was computed from

$$j_0(X) = \sin(X)/X \tag{5-69}$$

and compared with $F_0(x)$. Every $F_L(x)$ was multiplied by the ratio $j_0(x)/F_0(x)$ to form a sequence $\{G_L(x)\}$. Comparison with tables of spherical Bessel functions for x = 10, 50 (110) showed the disagreement between $G_L(x)$ and $j_L(x)$ to be less than 0.0001 percent.

The function $j_0(k_i r)$ was computed from the exact relation given by Equation (5-69).

The Final Translational Wave Functions. After specifying the initial and final states and the initial energy of approach, the final

wave constant k_n was determined from conservation of energy (see later discussion). When the criteria represented by Equations (4-53) and (4-54) were met, Equation (4-55) was used to generate values for $u_{l_1}(k_nP)$. Otherwise, the program shifted into the Numerov method previously described in Chapter V. Equation (4-58) was used to compute values for $u_{l_1}(k_nP)$ where H equaled 0.001. At P = 1.8, 1.825, ..., 2.575, 2.600 Å, the corresponding values of $u_{l_1}(k_nP)$ were stored in the computer memory to be used in Equation (5-61).

Additional Comment. To check the accuracy of using an interval of 0.025 Å for r and P in the numerical calculation of $I(l_1,0,l_3)$, the foregoing procedure was carried out for k_i = 10 $Å^{-1}$, n_i = 4, l_i = 60, n_f = 3, l_f = 10, l_3 = 40, l_4 = 40, l_1 = 100 at intervals of integration of 0.025 Å and 0.0025 Å. The value $I(l_1,0,l_3)$ obtained by using the smaller interval of integration differed by less than three percent from the value corresponding to the larger interval.

When the subprogram for $u_{l_1}(k_nP)$ was written, the value of H was decreased to 0.0001 in order to insure that Equation (4-58) gave fairly accurate results when the larger value of H, 0.001, was used. The values of $u_{l_1}(k_nP)$ corresponding to H = 0.001 differed from those values corresponding to H = 0.0001 by less than five percent.

The Clebsch-Gordan Coefficients

Before summing over l_3, l_4, and l_1 in Equation (5-60), the Clebsch-Gordan coefficients $C(l_f, l_3, l_4; 0, 0, 0)$ and $C(l_4, l_i, l_1; 0, 0, 0)$ had to be calculated. From Equation (B-27) in Appendix B,

$$C^2(l_1, l_2, l_3; 0, 0, 0) = (2l_3+1)\ \frac{(l_1+l_2-l_3)!\ (l_1+l_3-l_2)!\ (l_2+l_3-l_1)!}{(l_1+l_2+l_3+1)!} \qquad (5\text{-}70)$$

$$\times \left[\ \frac{Q!}{(Q-l_1)!\ (Q-l_2)!\ (Q-l_3)!}\ \right]^2$$

where

$$Q = (l_1+l_2+l_3)/2 \qquad (5\text{-}71)$$

Since $C(l_1, l_2, l_3; 0, 0, 0)$ for Q not an integer, Equation (5-70) was used only when Q is an integer.

The method used to computer $C^2(l_f, l_3, l_4; 0, 0, 0)$ and $C^2(l_4, l_i, l_1; 0, 0, 0)$ was as follows:

(a) The logarithms of n! for n = 0, 1, 2, 3, ..., 300 were calculated and stored in the memory of the computer.

(b) The squares of the Clebsch-Gordan coefficients were computed from the relation

$$C^2(\ell_1,\ell_2,\ell_3;0,0,0) = \exp\left\{\ln[(\ell_1+\ell_2-\ell_3)!] - 2\ln[(Q-\ell_3)!]\right. \quad (5\text{-}72)$$

$$\ln[(\ell_1+\ell_3-\ell_2)!] + \ln[(\ell_2+\ell_3-\ell_1)!] - \ln[(\ell_1+\ell_2+\ell_3+1)!]$$

$$\left. - 2\ln(Q!) - 2\ln[(Q-\ell_1)!] - 2\ln[(Q-\ell_2)!]\right\}(2i_3+1)$$

as needed. Equation (5-72) was used to avoid exceeding the maximum number limit (about 10^{64}) of the computer. Thus, it is desirable to use a relation in which the logarithm of 300! appears rather than 300! itself.

Conservation of Energy

Because reactive collisions under consideration are assumed to be adiabatic, the total energy is conserved during the collision. Assuming that H and Br_2 initially approach each other with a relative translational energy of $(\hbar^2/2\mu_i)k_i^2$, the total energy E of the collision can be expressed as

$$E = \frac{\hbar^2}{2\mu_i} k_i^2 + E_{vib,i} + E_{rot,i} \quad (5\text{-}73)$$

where $E_{vib,i}$ and $E_{rot,i}$ represent the initial vibrational and rotational

energies, respectively, of Br_2. The final translational energy is then given by

$$\frac{\hbar^2}{2\mu_f} k_n^2 = \frac{\hbar^2}{2\mu_i} k_i^2 + E_{vib,i} + E_{rot,i} - E_{vib,f} - E_{rot,f} \tag{5-74}$$

by conservation of energy.

Notice that the requirement of a positive final relative translational energy effectively limits the magnitude of the internal energy of HBr. Thus, the maximum allowable value of n_f is the largest integer satisfying the inequality

$$\frac{2\sqrt{D}}{A}(n_f + 1/2) - (n_f + 1/2)^2/A^2 < E + D \tag{5-75}$$

Also, for each final vibrational state n_f, the maximum rotational quantum number l_f is the largest integer satisfying

$$\left[B - \alpha(n_f + 1/2)\right] l_f(l_f+1) - T l_f^2 (l_f+1)^2 \tag{5-76}$$

$$< E + D - \frac{2\sqrt{D}}{A}(n_f + 1/2) + (n_f + 1/2)^2/A^2$$

The parameters A, B, D, α, and T for HBr are taken from Table 4.

Results of Calculations

Relation of Reaction Cross-Sections to Final State

Using the procedure just outlined, values of $\sigma(k_i, n_i, l_i; k_n, n_f, l_f)$ were first calculated for $E_{tr,i}$ = 1000 gram $Å^2/sec^2$, $n_i = 0$, $l_i = 60$. For conservation of energy, the maximum allowable value of n_f was six. The maximum allowable value of l_f for each vibrational state is listed in Table 6.

Table 6. Maximum Rotational State Allowed for Each Allowed Final Vibrational State When $E_{tr,i}$ = 1000 gram $Å^2/sec^2$, $n_i = 0$, and $l_i = 60$.

Vibrational State Quantum Number	Quantum Number of Maximum Rotational State
0	43
1	40
2	37
3	32
4	27
5	20
6	12

For n_f = 1, 3, and 6, the results for $\sigma(k_i, n_i, l_i; k_n, n_f, l_f)$ are given in Tables 7, 8, and 9 for all of the possible values of l_f. Notice that the larger values of σ correspond to the higher rotational states possible for a given vibrational state.

To save space, the remaining reaction cross-sections are reported as sums over all the possible rotational states corresponding to a given n_f, or

Table 7. Reaction Cross-Section σ_2 Versus l_f for $n_f = 1$ When $E_{tr,i} = 1000$ gram $Å^2/sec^2$, $n_i = 0$, and $l_i = 60$.

l_f	σ, $Å^2$	l_f	σ, $Å^2$
0	0.00017	20	0.00346
1	0.00025	21	0.00377
2	0.00033	22	0.00409
3	0.00041	23	0.00442
4	0.00050	24	0.00474
5	0.00060	25	0.00508
6	0.00071	26	0.00545
7	0.00083	27	0.00585
8	0.00096	28	0.00628
9	0.00110	29	0.00671
10	0.00125	30	0.00716
11	0.00141	31	0.00760
12	0.00158	32	0.00815
13	0.00176	33	0.00863
14	0.00195	34	0.00913
15	0.00215	35	0.00960
16	0.00237	36	0.01513
17	0.00262	37	0.01626
18	0.00289	38	0.02621
19	0.00317	39	0.08500
		40	0.00899

Table 8. Reaction Cross-Section σ Versus l_f for $n_f = 3$ When $E_{tr,i} = 1000$ gram $Å^2/sec^2$, $n_i = 0$, and $l_i^f = 60$.

l_f	σ, $Å^2$	l_f	σ, $Å^2$
0	0.00049	16	0.00319
1	0.00057	17	0.00346
2	0.00066	18	0.00375
3	0.00076	19	0.00404
4	0.00089	20	0.00431
5	0.00101	21	0.00460
6	0.00115	22	0.00491
7	0.00129	23	0.00528
8	0.00144	24	0.00561
9	0.00161	25	0.00597
10	0.00179	26	0.00632
11	0.00198	27	0.00669
12	0.00220	28	0.00711
13	0.00243	29	0.02628
14	0.00268	30	0.06794
15	0.00293	31	0.29479
		32	0.07721

Table 9. Reaction Cross-Section σ_2 Versus l_f for $n_f = 6$ When $E_{tr,i} = 1000$ gram $Å^2/sec^2$, $n_i = 0$, and $l_i = 60$.

l_f	σ, $Å^2$
0	0.007
1	0.016
2	0.035
3	0.076
4	0.158
5	0.281
6	0.387
7	0.447
8	0.501
9	0.567
10	0.652
11	3.525
12	1.291

$$\bar{\sigma}(k_i, n_i, l_i; k_n, n_f) = \sum_{l_f=0}^{l_f^{max}} \sigma(k_i, n_i, l_i; k_n, n_f, l_f) \qquad (5\text{-}77)$$

Table 10 contains values of $\bar{\sigma}$ for $n_f = 0$ to 6. It is apparent that the larger values of $\bar{\sigma}$ correspond to the higher vibrational states allowed by the conservation of energy requirement.

Table 10. Reaction Cross-Section $\bar{\sigma}$ Versus n_f When $E_{tr,i}$ = 1000 gram $Å^2/sec^2$, $n_i = 0$, and $l_i = 60$.

n_f	$\bar{\sigma}$, $Å^2$
0	0.109
1	0.278
2	0.407
3	0.555
4	0.962
5	2.031
6	7.943

The Effect of the Initial Conditions

The reaction cross-sections required for calculation of the total reaction rate constant (see Chapter I) are the quantities

$$S(k_i, n_i, l_i) = \sum_{n_f=0}^{n_f^{max}} \bar{\sigma}(k_i, n_i, l_i; k_n, n_f) \qquad (5\text{-}78)$$

Therefore, the analysis of the effect of the initial conditions on the reaction A + BC → AB + C is most conveniently carried out by calculations of $S(k_i, n_i, l_i)$ versus k_i, n_i, l_i. Table 11 summarizes some of the results of these calculations, and apparently the initial conditions cause little or no effect on S.

In order to make comparisons with the results of Polanyi given in Table 3, values of the reaction cross-section $\bar{\sigma}(k_i, n_i, l_i; k_n, n_f)$ corresponding to various initial conditions are presented in Table 12. The symbol $E_{tr,i}$ in Table 12 denotes the initial relative translational energy. Since values for $\bar{\sigma}$ are reported in Table 10 for the initial conditions $E_{tr,i}$ = 1000 gram $Å^2/sec^2$, $n_i = 0$, $l_i = 60$, these values are exluded in Table 12.

It is apparent that $\bar{\sigma}$ is peaked around n_f = 6, 7 for most initial conditions, and therefore the rate constant

$$\bar{\bar{K}} = \text{const} \sum_{t,j} \iint (k_i/\mu_A)\, \bar{\sigma}(k_i, n_i, l_i; k_n, n_f) \tag{5-79}$$

$$\times F_t(\vec{p}_A)\, F_j(\vec{p}_{BC})\, d^3\vec{p}_A\, d^3\vec{p}_{BC}$$

will be higher for n_f = 6 or 7 than for n_f = 3; this is in direct contrast with Polanyi's results in Table 3.

Discussion of Results

An examination will now be made of the physical significance of the foregoing results, especially with regard to the nature of the potential-

Table 11. Reaction Cross-Section S Versus $E_{tr,i}$, n_i, l_i.

$E_{tr,i}$ gram $Å^2/sec^2$	n_i	l_i	S, $Å^2$
500	0	30	10.223
500	0	60	10.769
500	0	100	10.930
500	2	30	10.118
500	2	60	9.824
500	2	100	10.421
500	5	30	10.928
500	5	60	11.421
500	5	100	10.872
1000	0	30	11.848
1000	0	60	12.285
1000	0	100	12.227
1000	2	30	12.627
1000	2	60	12.511
1000	2	100	12.750
1000	5	30	12.433
1000	5	60	12.789
1000	5	100	12.962
2000	0	30	10.991
2000	0	60	12.082
2000	0	100	13.174
2000	2	30	14.004
2000	2	60	14.117
2000	2	100	14.328
2000	5	30	13.724
2000	5	60	13.661
2000	5	100	12.962

Table 12. Reaction Cross-Section $\bar{\sigma}$ for Various Initial Conditions

$E_{tr,i}$, gram Å^2/sec^2	n_i	l_i	n_f	$\bar{\sigma}$, Å^2
500	0	60	0	0.101
500	0	60	1	0.263
500	0	60	2	0.391
500	0	60	3	0.532
500	0	60	4	0.947
500	0	60	5	1.986
500	0	60	6	6.549
500	5	60	0	0.097
500	5	60	1	0.283
500	5	60	2	0.413
500	5	60	3	0.558
500	5	60	4	1.186
500	5	60	5	2.221
500	5	60	6	6.663
1000	5	60	0	0.104
1000	5	60	1	0.286
1000	5	60	2	0.412
1000	5	60	3	0.588
1000	5	60	4	1.301
1000	5	60	5	2.424
1000	5	60	6	7.674
2000	0	60	0	0.056
2000	0	60	1	0.202
2000	0	60	2	0.350
2000	0	60	3	0.505
2000	0	60	4	0.704
2000	0	60	5	1.221
2000	0	60	6	2.112
2000	0	60	7	6.932
2000	5	60	0	0.061
2000	5	60	1	0.215
2000	5	60	2	0.362
2000	5	60	3	0.523
2000	5	60	4	0.814
2000	5	60	5	1.527
2000	5	60	6	2.628
2000	5	60	7	7.531

energy surface. From this analysis, one hopes to discover which features of Ellison's potential-energy surface should be altered in order to bring the calculated reaction cross-sections into agreement with the experimental results of Polanyi (10).

The Influence of Initial Conditions

The weak dependence of the reaction cross-sections on the initial conditions k_i, n_i, l_i is due in part to the low activation energy for the reaction $H + Br_2 \rightarrow HBr + Br$, at least for Ellison's potential-energy surface (about 2.0 kilocalories per mole). Furthermore, even the effect of this small activation energy is minimized by the perturbed Morse oscillator method used to approximate the functions $\overline{R}_{n_f}(r;P)$. In Figure 5, for instance, the small hump to the right of the equilibrium interatomic distance is roughly attributable to the activation energy between Br_2 and the oncoming H atom. In fitting the curve in Figure 5 to a Morse-type function, this small hump was neglected. The inclusion of this small barrier, however, would lead to only one or two additional vibrational states of limited stability.

The presence of the activation energy hump has a very slight effect on the value of the integral $I(l_1,0,l_3)$ in Equation (5-61). In Figure 7, a plot of the potential $\overline{U}_f(r,P)$ for P = 2.283 Å shows that the contribution to $I(l_1,0,l_3)$ resulting from the activation energy (which lies between points b and c) will subtract from the major contribution to $I(l_1,0,l_3)$ coming from the region between points a and b. But because the wave function $\overline{R}_{n_f}(r;P)$ is so small in the region between b and c, this offsetting effect is very slight.

Another reason for the weak dependence of the reaction cross-sections

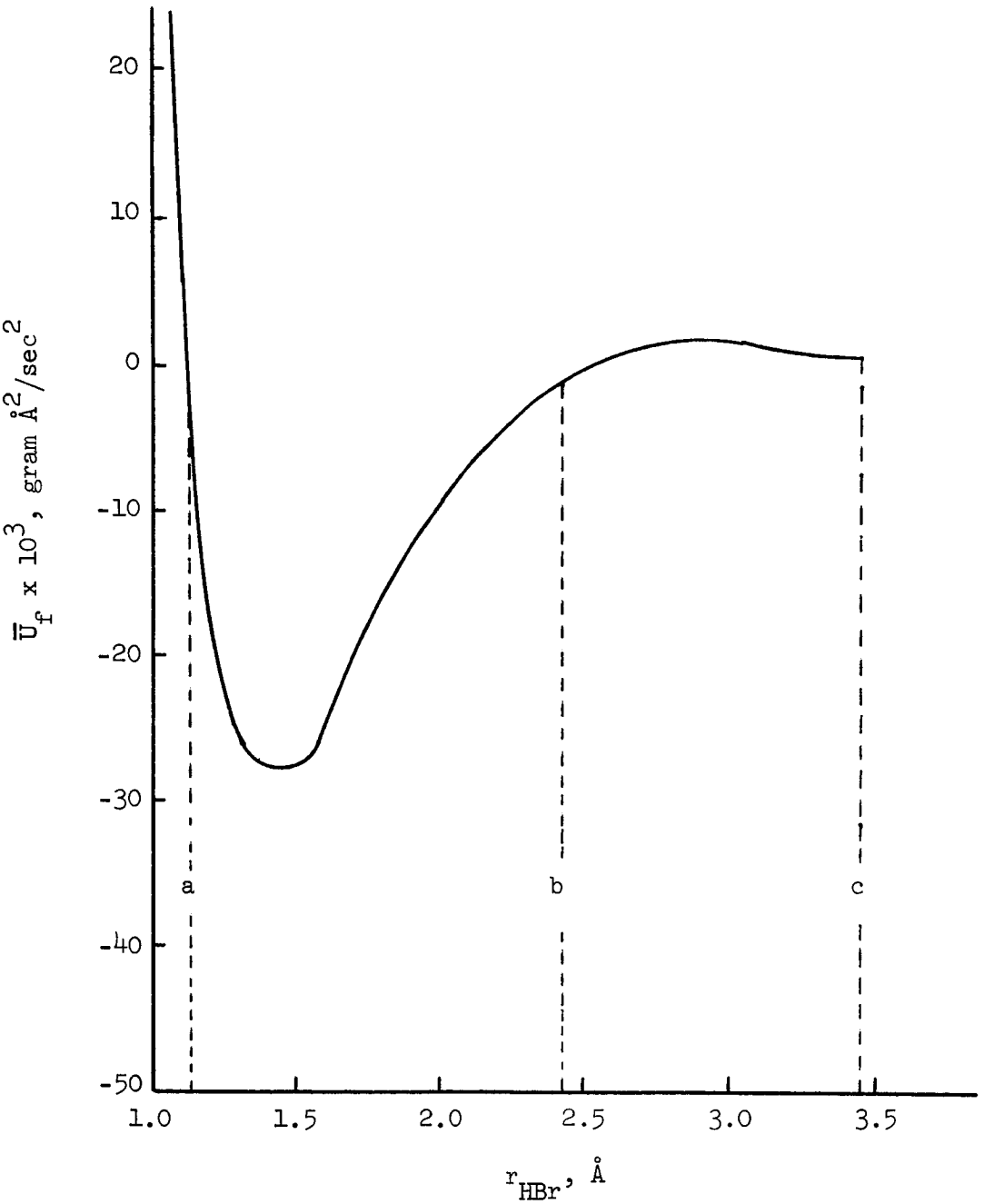

Figure 7. Plot of $\bar{U}_f$ Versus r_{HBr} for r_{Br_2} = 2.283 Å Showing Activation Energy.

upon the initial conditions involves the use of Equation (3-37). Because the wave function Ψ_f^- is a solution to the complete Scroedinger equation, it should reflect, implicitly at least, the influence of the activation energy. Even this implicit dependence on the activation energy was obscured however, when the "linear complex" form of Ψ_f^-, $\overline{\chi}_f^-$, was approximated by the expansion given in Equation (3-49). As mentioned in the first paragraph of this section, the activation energy was neglected completely in the calculation of $\overline{R}_{n_f}(r;P)$; hence, as indicated by Equation (4-9), the functions $z_n(\vec{r};P)$ are uninfluenced by activation energy. Also, the other functions in Equation (3-49), the translational motion coefficients $G_n(\vec{P})$, are independent of the vector $\vec{r}$, along which occurs the approach of H toward Br_2; thus, the functions $G_n(\vec{P})$, cannot account for any effect of the activation energy.

If Equation (3-36) were used for the differential reaction cross-section, the wave function Ψ_i^+ could be expanded as

$$\Psi_i^+ = \sum_n J_n(\vec{R})\, W_n(\vec{r}_{BC};\vec{R}) \qquad (5\text{-}80)$$

where $J_n(\vec{R})$ are the initial translational motion coefficients and $W_n(\vec{r}_{BC};\vec{R})$ are perturbed stationary state functions for Br_2. Because of their explicit dependence on $\vec{R}$, the vector along which the activation energy takes effect, the functions $J_n(\vec{R})$ can be made to account for the influence of activation energy. On the other hand, according to Figure 6, the potential-energy between the two bromine atoms is rendered non-bonding upon the approach of H. This destruction of the Br_2 bond makes

the approximation of the functions by the perturbed stationary state approximation virtually impossible.

Distribution of the Total Collision Energy Among the Products

Tables 7, 8, 9, and 11 show that the reaction cross-sections $\sigma(k_i, n_i, l_i; k_n, n_f, l_f)$ tend to be larger for the higher internal energy states of HBr. For each vibrational state, the major contribution to the reaction cross-section appears to come from the higher possible rotational states, i.e., the rotational states which barely satisfy the inequality in Equation (5-76). Furthermore, the reaction cross-sections $\sigma(k_i, n_i, l_i; k_n, n_f)$ for scattering into the higher possible vibrational states are obviously greater than the cross-sections for the lower vibrational states.

Influence of the Final Translational Wave Functions. An explanation of the product energy distribution lies in the character of Ellison's potential-energy surface and its influence on the functions $u_{l_1}(k_n P)$. Equation (5-61) indicates that a rapidly oscillating $u_{l_1}(k_n P)$ would have a canceling effect on the value of $I(l_1,0,l_3)$ when integration over P is performed. Now, suppose a reactive collision (with initial conditions $E_{tr,i} = 2000$ gram $\text{Å}^2/\text{sec}^2$, $n_i = 0$, $l_i = 0$) results in a moderately excited HBr molecule (say, $n_f = 1$, $l_f = 10$).

From Equations (4-34) and (4-35) it is seen that

$$\left(\hbar^2/2\mu_f\right)\left[k_n^2 - \tilde{U}_n(P)\right] = E - \epsilon_n(P) \qquad (5\text{-}81)$$

For discussion purposes, a less cumbersome notation will be adopted. Let $w = u_{l_1}$, and

$$\tau = k_n^2 - \tilde{U}_n(P) - l_1(l_1+1)/\rho^2 \qquad (5\text{-}82)$$

Thus,

$$\tau = (2\mu_f/\hbar^2)\left[E - \epsilon_n(P)\right] - l_1(l_1+1)/\rho^2 \qquad (5\text{-}83)$$

In order to envision how τ varies with P, the effective potential $\epsilon_n(P) + (\hbar^2/2\,\mu_f)\left[\, l_1(l_1+1)/P^2 \,\right]$ in Equation (4-46) and the total energy E were plotted versus P in Figure 8. The function $\epsilon_n(P)$, which is characteristic of the potential-energy surface, was calculated from Equation (4-27). For illustrative purposes, l_1 was arbitrarily set equal to 60, although the curve in Figure 8 is typical for any appropriate value of l_1.

For $P < P_o$, τ is less than zero, and the solution w of Equation (4-46) is a very small function, decreasing exponentially as P decreases. As τ barely becomes greater than zero, d^2w/dP^2 becomes negative and the slope dw/dP begins to decrease, causing w to go through a maximum at point a. As w decreases below zero, d^2w/dP^2 becomes positive, and dw/dP begins to increase from negative to positive values, thereby causing w to increase from negative to positive values. But, when w is positive, d^2w/dP^2 becomes negative once again. This cyclic variation in the sign of d^2w/dP^2 leads to an oscillating function w. As P increases further beyond P_o, τ becomes much greater, causing the function w to oscillate more rapidly. An important conclusion, therefore, is that the more slowly oscillating values of w occur in the region just to the right of point P_o.

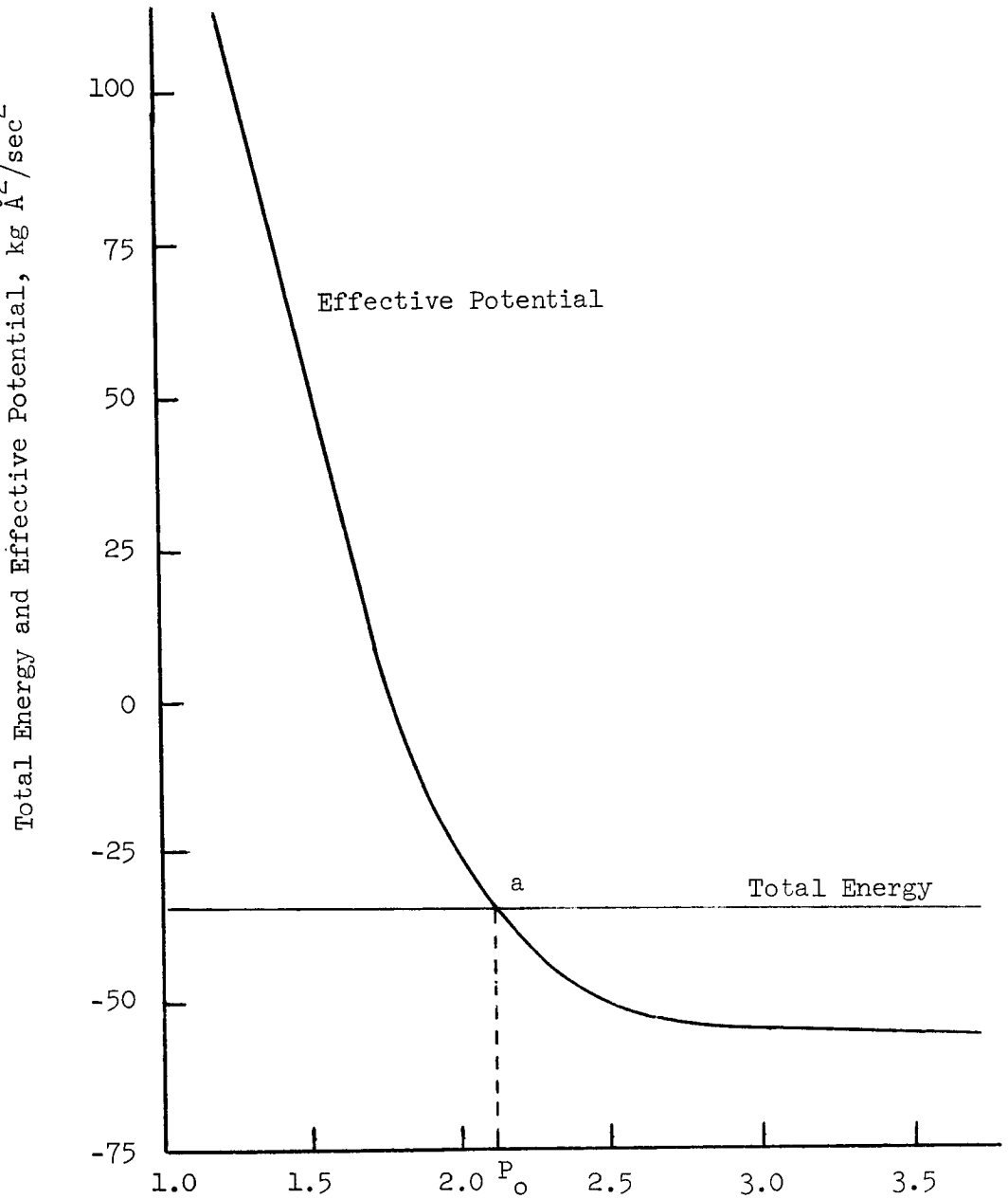

Figure 8. Total Energy and Effective Potential Versus P.

Now, it is also true that the initial vibrational wave function $Z_{n_i}(P)$ in Equation (5-61) is peaked around P = 2.284 Å. Then the region of more slowly oscillating w will coincide with the region of large $Z_{n_i}(P)$ if P_o is slightly to the left of P = 2.284 Å. If such is the case, the resulting values of $I(l_1,0,l_3)$ will be much higher than those values corresponding to a rapidly oscillating w in the region around P = 2.284 Å.

If τ is to be small and positive around P = 2.284 Å, it is evident from Equation (5-83), that the function $\epsilon_n(P)$ must lie slightly below $E - l_1(l_1 + 1)/P^2$. For Ellison's potential-energy surface, the functions $\epsilon_n(P)$ at P = 2.284 Å are approximately equal to the energy levels E_n for unperturbed HBr (see Figure 8). Because of the relative smallness of $l_1(l_1 + 1)/P^2$, the requirement that $E = \epsilon_n(P) - l_1(l_1 + 1)/P^2$ be small at P = 2.284 Å is met approximately by those combinations of n_f and l_f such that E_n is slightly below E in magnitude.

The Peaking of the Reaction Cross-Sections σ at the Higher Possible Rotational States. For the case where $(\hbar^2/2\,\mu_i)\,k_i^2 = 1000$ gram Å^2/sec^2, $n_i = 0$, $l_i = 60$, $n_f = 3$, $l_f = 30$, the value of τ at P = 2.284 Å is so large (about 1900 Å^{-2} at $l_1 = 60$) that the reaction cross-section $\sigma(k_i, n_i, l_i; k_n, n_f, l_f)$ is only 0.06794 Å^2 (see Table 8). On the other hand, if $l_f = 31$ with the other conditions the same, τ is small and positive at P = 2.284 Å (about 500 Å^{-2} for $l_1 = 60$), and the resulting value of $\sigma(k_i, n_i, l_i; k_n, n_f, l_f)$ is 0.29479 Å^2.

When $l_f = 32$ and the other conditions are the same, τ is negative for most values of l_1; the corresponding values of w are small and positive in the vicinity of P = 2.284 Å. Thus, the reaction cross-section corresponding to $l_f = 32$ is not as high as the reaction cross-section corre-

sponding to $l_f = 31$.

The Peaking of the Reaction Cross-Section $\bar{\sigma}$ About the Higher Possible Vibrational States. The major factor contributing to the peaking of $\bar{\sigma}(k_i, n_i, l_i; k_n, n_f)$ about the higher possible vibrational states is the closeness of the rotational levels for low quantum numbers l_f. From Equation (4-27), the energy difference $\Delta\epsilon_n$ between a rotational state l_f and the next highest state is, for constant n_f,

$$\Delta \epsilon_n = \left[B_{AB} - \alpha_{AB}(n_f + \tfrac{1}{2})\right](2l_f + 3) - T_{AB}(4l_f^3 + 12l_f^2 + 12l_f + 4) \qquad (5\text{-}84)$$

Now, as l_f increases from zero in steps of one, $\epsilon_n(P = 2.284\ \text{Å})$ changes by discrete amounts. For a given total energy E and final partial wave l_1, the quantity

$$\tau = (2\mu_f/\hbar^2)\left[E - (\hbar^2/2\mu_f)\, l_1(l_1+1)/P^2 - \epsilon_n(P)\right] \qquad (5\text{-}85)$$

becomes smaller as l_f increases. Assume that the vibrational state n_f is such that

$$\epsilon_n(P = 2.284\,\text{Å}) < E - (\hbar^2/2\mu_f)\, l_1(l_1+1)/P^2 \qquad (5\text{-}86)$$

for $l_f = 0$. Then there exists some crucial rotational state l_f' below l_f^{max} such that

$$\tau\,(P = 2.284\ \text{Å}) > 0 \qquad \text{when } l_f = l_f' \tag{5-87}$$

$$\tau\,(P = 2.284\ \text{Å}) < 0 \qquad \text{when } l_f = l_f' + 1 \tag{5-88}$$

On the average, $\tau(P = 2.284\ \text{Å})$ will be smaller for smaller $\Delta\epsilon_n(P)$, since the smallest positive value of τ (occurring when $l_f = l_f'$) is indicated by Equations (5-87) and (5-88) to be less than $\Delta\epsilon_n(P)$. From Equation (5-84) it is apparent that smaller l_f' s contribute to smaller values of τ at $P = 2.284$ Å, resulting in more slowly oscillating functions $u_{l_l}(k_n P)$. By Equation (5-75), the larger the value of n_f, the smaller the associated l_f' s. Therefore, the higher vibrational states for which Equation (5-75) is satisfied have more slowly oscillating functions $u_{l_l}(k_n P)$, which correspond to larger values of the reaction cross-section $\bar{\sigma}(k_i, n_i, l_i; k_n, n_f)$.

For Ellison's potential-energy surface

$$E_n \sim \epsilon_n(P) - (\hbar^2/2\mu_f)\, l_l (l_l + 1)/P^2 \tag{5-89}$$

when $P = 2.284$ Å. Thus, it is now apparent why the reaction cross-sections $\bar{\sigma}$ are peaked around the higher possible rotational states.

Comparison with Experimental and Classical Mechanical Results of Polanyi

It was mentioned that the calculated results for $\bar{\sigma}(k_i, n_i, l_i; k_n, n_f)$ in Tables 10 and 12 will yield, in conjunction with Equation (5-79), values of $\bar{\bar{K}}$ that are higher for $n_f = 6$ or 7 than for $n_f = 3$. In contrast, from the infrared chemiluminescence of a reacting $H + Br_2$ mixture, Polanyi and

his associates (10) were able to show exactly the opposite effect (see Table 3).

"Repulsive" Potential-Energy Surface. Polanyi's group was able to account for this experimental behavior by reference to a "repulsive" potential-energy surface (60). A "repulsive" surface, in the parlance of Polanyi, was one which resulted in the following kinematical pattern upon the use of classical mechanics:

(1) From a region of negligible interaction, the lighter H atom approaches the Br_2 molecule. The Br_2 interatomic distance remains about 2.3 Å until the distance between the H atom and the nearer bromine atom decreases to about 1.45 Å. This forms an "activated state" configuration which is very short-lived (the "activated state" is in existence for about the same time required for H to fly by Br_2 if no interaction were present).

(2) Very little of the energy of reaction is released at this point; that is, the "activated state" energy is only slightly below that of the reactants.

(3) The furthermost Br atom begins to depart, thus breaking up the "activated state" configuration. As the bromine atom recedes from the HBr molecule, most of the reaction energy is released; that is, the "activated state" energy is much greater than that of the products.

The use of this "repulsive" potential-energy surface in the classical Hamiltonian for three body planar motion resulted in only fifteen percent of the energy of reaction appearing as internal energy of HBr. The initial conditions in these studies were varied systematically rather than by the Monte Carlo method (22).

The reason given by Polanyi and his colleagues for the low degree

of vibrational excitation of HBr is that the HBr interatomic distance in the "activated state" is essentially the normal bond length. Because of their near-equilibrium separation, the hydrogen and nearer bromine atoms tend to recoil together as the furthermost bromine atom is repelled away.

"Attractive" Potential-Energy Surface. By using an "attractive potential-energy surface, Polanyi's group (60) obtained substantial internal excitation of HBr (about 88 percent of the energy of reaction appeared as internal energy of HBr). According to Polanyi, an "attractive" potential-energy surface is one which results in the following classical mechanical behavior:

(1) The "activated state" is formed with the release of most of the energy of reaction; that is, the energy of the "activated state" is far below that of the reactants.

(2) The departure of the furthermost Br atom results in very little release of energy of reaction.

The explanation given for the high vibrational excitation of HBr was that the HBr bond was under stress when the furthermost Br atom was being repelled. Thus, the hydrogen and nearer bromine atoms tended to recoil separately rather than as a diatomic aggregate.

Comparison with Quantum Mechanics. Examination of Figures 5 and 6 and Table 5 reveals that Ellison's potential-energy surface for $H + Br_2$ is an "attractive" potential-energy surface. About 95.5 percent of the energy of reaction has been released by the time the "activated state" is formed. With respect to the effect of an "attractive" potential-energy surface upon product energy distribution, it is apparent that the foregoing quantum mechanical results are in qualitative agreement with Polanyi's classical

mechanical results.

It is now appropriate to examine the form the potential-energy surface for $H + Br_2 \rightarrow HBr + Br$ must have so that the perturbed Morse oscillator calculation will be in qualitative agreement with Polanyi's experimental results in Table 3. In previous sections of this chapter, it was clearly demonstrated that when τ is positive positive at $P = 2.283$ Å, the smaller values of τ give rise to larger values of the reaction cross-section $\sigma(k_i, n_i, l_i; k_n, n_f, l_f)$. Thus, from Equation (5-83), it is apparent that the closer $\epsilon_n(P)$ comes to $E - (\hbar^2/2\mu_f)l_1(l_1 + 1)/P^2$ at $P = 2.283$ Å, the higher will be the resulting reaction cross-section $\sigma(k_i, n_i, l_i; k_n, n_f, l_f)$. An examination of the form of $\epsilon_n^o(P)$ in Equation (4-10) indicates that for constant n_f and l_f, higher values of the parametric function $U_m(P)$ at $P = 2.283$ Å will result in higher values of $\epsilon_n^o(P)$. From the perturbation relation in Equation (4-24), it is evident that the higher values of $\epsilon_n^o(P)$ contribute, in turn, to higher values of $\epsilon_n(P)$. Furthermore, from Figure 3, it is obvious that higher values of $U_m(P)$ at $P = 2.283$ Å result in a potential-energy surface which is more "repulsive"; that is, the energy of the configuration $r = 1.45$ Å, $P = 2.283$ Å (the "activated state") is closer to the energy of the reactants. It is conceivable, therefore, that by making Ellison's potential-energy surface more "repulsive", smaller values of τ at $P = 2.283$ Å will occur for less energetic states of HBr. As a result, larger reaction cross-sections $\sigma(k_i, n_i, l_i; k_n, n_f, l_f)$ will correspond to lower internal states of HBr.

The above analysis indicates that if a "repulsive" potential-energy surface were used in the "linear complex" calculations outlined earlier in this chapter, the resulting reaction cross-sections would have been in

closer agreement with the experimental data of Polanyi.

CHAPTER VI

REACTION CROSS-SECTIONS FOR H + Br_2 → HBr + Br CORRESPONDING TO "REPULSIVE" POTENTIAL-ENERGY SURFACE

The qualitative analysis of the results of the previous chapter suggested that a potential-energy more "repulsive" than Ellison's should yield reaction cross-sections in agreement with Polanyi's experimental findings. To verify this conclusion, a repetition of the foregoing reaction cross-section calculations for a "repulsive" potential-energy surface seems appriate. If the quantum mechanically calculated reaction cross-sections are found to be in agreement with experiment, Polanyi's conclusions regarding the true nature of the H-Br-Br potential-energy surface (60) will be reinforced.

Construction of a "Repulsive" Potential-Energy Surface

The perturbed Morse oscillator method can be retained if the "repulsive" potential-energy surface has Morse-like features. Thus, as discussed in Chapter IV, a plot of the potential-energy function versus r for constant P should possess the shape of a Morse curve, regardless of the value of P. If Morse-like features are incorporated into its construction, the "repulsive" potential-energy surface can be partitioned in the manner of Equation (4-1); that is,

$$V_L(r,P) = V_M(r,P) + (V_L - V_M) \qquad (6\text{-}1)$$

where

$$V_M(r,P) = D(P)\left\{1 - \exp\left[a(P)(r - r_E(P))\right]\right\}^2 + U_m(P) \qquad (6\text{-}2)$$

As pointed out in Chapter IV, proper adjustment of the parametric functions D(P), a(P), $r_E(P)$, and $U_m(P)$ can render $(V_L - V_M)$ extremely small in comparison with V_M, especially in the vicinity of the potential well (see Figure 3).

Now, it is recalled that the functions $\bar{R}_{n_f}(r;P)$ depend essentially on the form of V(r,P) within the potential well (that is, within the interval 0.9 Å ≤ r ≤ 2.5 Å). Also, in the evaluation of $I(l_1,0,l_3)$ in Equation (5-61), the form of the potential-energy function

$$\bar{U}_f(r,P) = V_L(r,P) - V_{Br_2}(P) \qquad (6\text{-}3)$$

is important only within the region 0.9 Å ≤ r ≤ 2.5 Å. Thus, the potential-energy function $V_L(r,P)$ influences the reaction cross-section calculations of Chapter V only over the domain 0.9 Å ≤ r ≤ 2.5 Å, 0 ≤ P ≤ ∞. Since $V_L - V_M$ is small in this domain, a convenient approach would be to approximate $V_L(r,P)$ by the form in Equation (6-2). This approximation is necessitated by the lack of detailed information concerning the actual potential-energy surface. Furthermore, only the gross characteristics of the potential-energy surface, such as its "repulsiveness", are of interest in the present analysis.

The Parametric Functions

As mentioned in the latter part of the previous chapter, a potential-energy surface of the form

$$V_L(r,P) = D(P)\left\{1 - \exp\left[a(P)\,(r - r_E(P))\right]\right\}^2 + U_m(P) \qquad (6\text{-}4)$$

is more "repulsive" the higher the function $U_m(P)$ at P = 2.3 Å. For Ellison's potential-energy function, plots of $V_L(r,P)$ versus P for constant r look like the curve in Figure 6. Curves of this form can be represented fairly accurately over the domain $0 \le P \le \infty$, 0.9 Å $\le r \le$ 2.5 Å by the function

$$V_L(r,P) = \delta\, e^{-\epsilon P} + D(P)\left\{1 - \exp\left[a(P)\,(r - r_E(P))\right]\right\}^2 - D_{HBr} \qquad (6\text{-}5)$$

It is obvious that $V_L(r,P)$ has the Morse-like form of Equation (6-2) with

$$U_m(P) = \delta\, e^{-\epsilon P} - D_{HBr} \qquad (6\text{-}6)$$

When r equals $r^E_{HBr}(P)$, the function $V_L(r,P)$ approaches $-D_{HBr}$ as P approaches infinity. Thus, $V_L(r,P)$ has the correct asymptotic form with respect to P. On the other hand, $V_L(r,P)$ does not have the correct asymptotic form with respect to r. This defect in Equation (6-5) is not serious, however, since the function $V_L(r,P)$ will not be utilized for large values of r. Therefore, by proper selection of the functions D(P),

$a(P)$, $r_E(P)$ and the constants δ, ϵ, β, and γ, the function $V_L(r,P)$ can be molded into a plausible "repulsive" potential-energy function for the $H + Br_2 \rightarrow HBr + Br$ reaction.

The Functions $U_m(P)$ and $r_E(P)$. Because the potential-energies of vibrationless Br_2 and HBr are - 31,898 gram $Å^2/sec^2$ and - 62,753 gram $Å^2/sec^2$, respectively, the energy of reaction $H + Br_2 \rightarrow HBr + Br$ is about 30,855 gram $Å^2/sec^2$. If the potential-energy of the "activated state" associated with the above reaction is - 41,000 gram $Å^2/sec^2$, then the potential-energy function governing the reaction is considered to be about two-thirds "repulsive". That is, 10,000 gram $Å^2/sec^2$ of the energy of reaction is released during the approach of H toward Br_2 to form the "activated state". As a beginning, the function $U_m(P)$ will be adjusted to make $V_L(r,P)$ about two-thirds "repulsive".

From his classical mechanical studies, Polanyi (60,111) discovered that the "activated state" for H-Br-Br corresponds roughly to the linear configuration with $r \simeq r^E_{HBr}$ and $P \simeq r^E_{Br_2}$. For Ellison's potential-energy surface, Equation (5-33), the local minimum value of $V_L(r,P)$ for $r \simeq r^E_{HBr}$, $P \simeq r^E_{Br_2}$ is located at r = 1.45 Å, P = 2.3 Å.

It will be assumed that the "activated state" for the "repulsive" energy surface exists when r = 1.45 Å, P = 2.3 Å. If Equation (6-5) is to possess a minimum with respect to r at r = 1.45 Å, P = 2.3 Å, then r_E(P = 2.3 Å) must be equal to 1.45 Å. The form for $V_L(r,P)$ in Equation (6-5) does not allow for a local minimum with respect to P at P = 2.3 Å, but according to Figure 6 this minimum was very slight even in the case of Ellison's potential-energy surface. Thus, by this somewhat arbitrary definition of the "activated state" configuration, the "repulsive" poten-

tial-energy function can be written at r = 1.45 Å and P = 2.3 Å as

$$V_L(r = 1.45\,\text{Å}, P = 2.3\,\text{Å}) = \exp(-2.3\epsilon) - D_{HBr} = -41{,}000 \qquad (6\text{-}7)$$

Because D_{HBr} is 62,753 gram $Å^2/sec^2$,

$$\delta = 21{,}753\ \exp(2.3\epsilon) \qquad (6\text{-}8)$$

Another relationship involving δ and ε can be obtained by assuming that at r = 1.45 Å and some large value of P, say P = 4.0 Å, the "repulsive" function given by Equation (6-5) has the same value as that given by the "attractive" potential-energy function, Equation (5-33). Since this value is calculated from Equation (5-33) to be - 61,994 gram $Å^2/sec^2$, then

$$21{,}753\ \exp(-1.7\epsilon) = D_{HBr} - 61{,}994 \qquad (6\text{-}9)$$

and ε = 1.974 $Å^{-1}$. Substituting this value for ε into Equation (6-8) yields δ = 2,103,319 gram $Å^2/sec^2$.

The "repulsive" potential-energy surface can now be written as

$$V_L(r, P) = 2{,}103{,}319\ \exp(-1.974\,P) - D_{HBr} \qquad (6\text{-}10)$$

$$+ D(P)\left\{1 - \exp\left[-a(P)\,(r - r_E(P))\right]\right\}^2$$

The Function D(P). In order to construct a suitable expression for the parametric function D(P), the value D(P) should possess at P = 2.3 Å in order for Equation (6-5) to remain a reasonable approximation to the actual potential-energy surface should be determined. A plot of the actual potential-energy surface versus r at P = 2.3 Å should yield a curve qualitatively similar to that shown in Figure 2. Since experimental evidence (101) points to a low activation energy (about 2.0 kilocalories per mole), point B on Figure 2 should correspond to a value not much greater than $-D_{Br_2}$. From Figure 2 it is seen that D(P = 2.3 Å) should be taken as the vertical distance between points A and B. Because point A corresponds to - 41,000 gram $Å^2/sec^2$ and point B should only be a few thousand gram $Å^2/sec^2$ above $-D_{Br_2}$ (31,898 gram $Å^2/sec^2$), it is feasible to set D(P) equal to 17,000 gram $Å^2/sec^2$ at P = 2.3 Å; that is,

$$D(P = 2.3\ Å) = 17{,}000 \tag{6-11}$$

Furthermore, if the approximate functional behavior of D(P) for Ellison's potential-energy surface is retained, then D(P) will begin at some large value (about D_{HBr}) at P = 0, decrease smoothly to 17,000 gram $Å^2/sec^2$ at P = 2.3 Å, and then increase, approaching D_{HBr} as P approaches infinity. A function which qualitatively describes this behavior is

$$D(P) = D_{HBr}\left[\beta + \gamma \tanh(|P-2.3|)\right] \tag{6-12}$$

The function within the brackets can be called the "switching function" for

D(P) since it describes the shifting of the dissociation parameter D(P) as r_{Br_2} increases. Suplinskas (41) used this terminology to describe a similar function in his study of the reaction K + HBr → KBr + H.

From the requirement that D(P) equal 17,000 gram $Å^2/sec^2$ at P = 2.3 Å and D(P) approaches D_{HBr} as P approaches infinity, $\beta = 0.27090$ and $\gamma = 0.72910$.

The Function a(P). It now remains to formulate a plausible expression for the parametric function a(P). Referring to Table 5, it is seen that a(P) equals 1.828 $Å^{-1}$ when P is zero, increases smoothly to 2.387 $Å^{-1}$ when P = 2.3 Å, and then smoothly decreases to 1.809 $Å^{-1}$ as P approaches infinity. Thus, it is practical to use a "switching function" like that in Equation (6-12) to describe the behavior of a(P) with respect to P:

$$a(P) = G + H \tanh(N|P-2.3|) \qquad (6\text{-}13)$$

Here, G, H, and N are constants which will be determined from the following requirements on a(P):

(1) a(P) is equal to the parameter a in Table 4 for HBr when P is very large; i.e.,

$$a(P \to \infty) = 1.809\ Å^{-1} \qquad (6\text{-}14)$$

(2) For $|P - 2.3| > 1.0$ Å, it is assumed that a(P) for the "repulsive" potential-energy surface will take on values similar to those corresponding to Ellison's potential-energy surface. From Table 2, the average

of a (P = 1.3 Å) and a(P = 3.3 Å) is 1.860 $Å^{-1}$. Taking this value for a(P) in Equation (6-12), one obtains

$$a(P = 1.3, 3.3) = 1.860\ Å^{-1} \tag{6-15}$$

(3) Finally, it should be decided what the desirable value of a(P) would be at P = 2.3 Å. In order that the perturbed Morse oscillator method can yield reaction cross-sections in qualitative agreement with experiment, it is imperative that the function τ of Equation (5-83) be small at P = 2.3 Å when n_f is three. From Equations (4-15) and (4-22), it is evident that ϵ_n(P = 2.3 Å, n_f = 3) will be larger, the larger is a(P = 2.3 Å). To insure that a(P = 2.3 Å) is sufficiently large to yield large reaction cross-sections for n_f = 3, it will be allowed to have a value somewhat larger than that corresponding to Ellison's potential-energy surface; that is, for the "repulsive" potential-energy function, a(P = 2.3 Å) will be 4.00 $Å^{-1}$ instead of 2.387 $Å^{-1}$, as shown in Table 2. Because of the three quantitative requirements for a(P), the constants in Equation (6-13) are easily found to be G = 4.00 $Å^{-1}$, H = 2.191 $Å^{-1}$, and N = 2.221 $Å^{-1}$. Thus,

$$a(P) = 4.00 - 2.191 \tanh(2.221|P-2.3|) \tag{6-16}$$

Numerical Procedure for Reaction Cross-Sections Corresponding to the "Repulsive" Potential-Energy Surface

Now that a suitable "repulsive" potential-energy surface has been formulated, the perturbed Morse oscillator method can be applied to calculate the corresponding reaction cross-sections. Essentially, this involves

repeating the procedure outlined in Chapters IV and V although the second order perturbation treatment described by Equations (4-23) through (4-28) can be eliminated. This simplification results from the direct formulation of the "repulsive" potential-energy surface in the form of Equation (4-3); thus, the term V_p in Equation (4-1) is zero, and the perturbation correction is unnecessary.

The numerical integration of

$$I(\ell_1, 0, \ell_3) = \int_{P=1.8}^{3.0} \int_{r=0.9}^{2.5} dP\, dr\, P^2 r^2 \frac{u_{\ell_1}(k_n P)}{k_n P} j_0(k_i r) \qquad (6\text{-}17)$$

$$\times j_{\ell_3}(\tfrac{1}{2} k_i P)\, Z_{n_i}(P)\, \bar{R}_{n_f}(r;P)\, \bar{U}_f(r,P)$$

was performed in the manner described in Chapter V. Due to the alteration of the potential-energy surface, a few factors in the integrand, i.e., $\bar{R}_{n_f}(r;P)$, $u_{l_1}(k_n P)$, and $\bar{U}_f(r,P)$, differ from those used in the previous calculations. All other numerical aspects of the procedure outlined in Chapter V were adopted without alteration for the computation of the reaction cross-sections corresponding to the "repulsive" potential-energy surface. Thus, the discussion that follows will be limited to the subject of calculating the functions $\bar{R}_{n_f}(r;P)$, $u_{l_1}(k_n P)$, and $\bar{U}_f(r,P)$.

The Function $u_{l_1}(k_n P)$. The solutions to the differential equation

$$\frac{d^2 u_{\ell_1}}{dP^2} + \left\{ \frac{2\mu_f}{\hbar^2} \left[E - \epsilon_n(P) \right] - \frac{\ell_1(\ell_1+1)}{P^2} \right\} u_{\ell_1} = 0 \qquad (6\text{-}18)$$

must be recalculated for the "repulsive" potential-energy surface, which affects $u_{l_1}(k_n P)$ through the function $\epsilon_n(P)$. Since the "repulsive" potential-energy surface was constructed so that $\epsilon_n(P)$ is larger in the region $P \tilde{=} 2.3$ Å than the corresponding function for Ellison's surface, the function

$$\tau = \frac{2\mu_f}{\hbar^2}\left[E - \epsilon_n(P)\right] - \frac{l_i(l_i+1)}{P^2} \qquad (6\text{-}19)$$

is smaller than $P \tilde{=} 2.3$ Å. Thus, for the "repulsive" potential-energy surface, the function $u_{l_1}(k_n P)$ will not oscillate in the region around $P \tilde{=} 2.3$ Å as rapidly as did Ellison's potential-energy surface. For instance, suppose $u_{l_1}(k_n P)$ is plotted versus P for both Ellison's and the "repulsive" potential-energy surface for $E_{tr,i} = 1000$ gram $Å^2/sec^2$, $n_i = 0$, $l_i = 60$, $n_f = 3$, and $l_f = 6$. It can be shown that $u_{l_1}(k_n P)$ has about thirty nodes between $P \tilde{=} 2.0$ and $P \tilde{=} 2.6$ Å for Ellison's potential-energy surface, whereas only five nodes are present over the same region for the "repulsive" potential-energy surface. Thus, the canceling effect that the oscillation of $u_{l_1}(k_n P)$ has on the integration of Equation (6-17) will be less marked for the "repulsive" potential-energy surface than for Ellison's.

Using either Equations (4-55) or (4-57), depending on whether or not the criteria in Equations (4-53) and (4-54) are met, values of the function $u_{l_1}(k_n P)$ were calculated for all the required combinations of initial and final states. As in the case for Ellison's potential-energy surface, this calculation was performed during the main computer program; that is, the functions $u_{l_1}(k_n P)$ were computed during the actual integration

program for $I(l_1,0,l_3)$, whereas the functions $\bar{U}_f(r,P)$ and $\bar{R}_{n_f}(r;P)$ were previously calculated and entered as input data.

Potential-Energy Functions

Values of the potential-energy function $\bar{U}_f(r,P)$ were computed and stored on cards for later use as input data. For convenience, the equations used in this calculation are summarized as follows:

$$V_L(r,P) = U_m(P) + D(P)\left\{1 - \exp\left[-a(P)\,(r - r_E(P))\right]\right\}^2 \tag{6-20}$$

$$U_m(P) = 2,103,319\ \exp(-1.974\ P) - D_{HBr} \tag{6-21}$$

$$D(P) = D_{HBr}\left[0.27090 + 0.72910\ \tanh(|P-2.31|\right. \tag{6-22}$$

$$a(P) = 4.00 - 2.191\ \tanh(2.221\,|P-2.31|) \tag{6-23}$$

$$r_E(P) = 1.45 \tag{6-24}$$

$$\bar{U}_f(r,P) = V_L(r,P) + D_{Br_2} - D_{Br_2}\left\{1 - \exp(P-2.284)\right\}^2 \tag{6-25}$$

Here, the variables P, r, and $r_E(P)$ have the dimensions of Å, the functions $V_L(r,P)$, $U_m(P)$, $D(P)$, and $\bar{U}_f(r,P)$ have the dimensions gram $Å^2/sec^2$, and

a(P) has the dimension Å^{-1}.

Eigenfunctions and Eigenvalues of Perturbed Morse Oscillator

Because the term V_p in Equation (4-1) vanishes for $V_L(r,P)$ as formulated above, the perturbed Morse oscillator eignefunctions and eigenvalues equal $\overline{R}^{o}_{n_f}(r;P)$ and $\epsilon^{o}_{n}(P)$, respectively. From Equations (4-13) through (4-21) values of these functions can easily be computed. For convenience, the above mentioned equations are rewritten in the order that they must be used to obtain $\overline{R}^{o}_{n_f}(r;P)$ and $\epsilon^{o}_{n}(P)$:

$$A(P) = \left[2\mu_{HBr}/\hbar^2\right]^{1/2} / a(P) \tag{6-26}$$

$$\beta = 2\,A(P)\sqrt{D(P)} - 2n_f \tag{6-27}$$

$$X = 2\,A(P)\sqrt{D(P)}\;\exp\left[-a(P)\left(r - r_E(P)\right)\right] \tag{6-28}$$

$$M(n_f,\beta;X) = 1 + \frac{(-n_f)}{\beta}X + \frac{(-n_f)(-n_f+1)}{\beta(\beta+1)}\frac{X^2}{2!} + \cdots \tag{6-29}$$

$$+ \frac{(-n_f)(-n_f+1)(-n_f+2)\cdots(-1)}{\beta(\beta+1)(\beta+2)\cdots(\beta+n_f-1)}\frac{X^{n_f}}{n_f!}$$

$$R^{\circ}_{n_f}(r;P) = \exp(-X/2)\,(X/2)^{A(P)\sqrt{D(P)} - (n_f + 1/2)}\, M(n_f, \beta; X)/r \qquad (6\text{-}30)$$

$$\epsilon^{\circ}_{n}(P) = \frac{2\sqrt{D(P)}}{A(P)}\,(n_f + 1/2) - \frac{(n_f + 1/2)^2}{A^2(P)} + U_m(P) \qquad (6\text{-}31)$$

$$+ B_{HBr}\, \ell_f(\ell_f+1) - \alpha_{HBr}\,(n_f + 1/2)\,\ell_f(\ell_f+1) - T_{HBr}\,\ell_f^2(\ell_f+1)^2$$

The symbol μ_{HBr} denotes the reduced mass for HBr, while the other undefined symbols have the same menaing as in Equations (4-9) through (4-20).

It is more convenient to use the normalized eigenfunctions

$$\bar{R}_{n_f}(r;P) = N_{n_f}(P)\; R^{\circ}_{n_f}(r;P) \qquad (6\text{-}32)$$

where the normalizing constant is

$$N_{n_f}(P) = \left[\int_{0.9}^{2.5} \left(R^{\circ}_{n_f}(r;P)\right)^2 r^2\, dr\right]^{-1/2} \qquad (6\text{-}33)$$

The computed values for $\bar{R}_{n_f}(r;P)$ and $\epsilon_n(P)$ were stored on cards for use as input data with the main program.

Range of Initial and Final Conditions

Values of the reaction cross-sections $\bar{\sigma}(k_i, n_i, l_i; k_n, n_f)$ and

$S(k_i, n_i, l_i)$ were calculated for all the combinations of the initial values:

$$E_{tr,i} = 500, 1000, 1500, 2000 \quad \text{gram } \text{Å}^2/\text{sec}^2 \tag{6-34}$$

$$n_i = 0, 1, 2, 3, 4, 5, 6, 7$$

$$l_i = 30, 60, 90, 120$$

These conditions have a high probability of occurrence at a temperature of 1000°K, and should be representative of most of the collisions occurring between H and Br_2 at that temperature.

Discussion of Results

Using the modification mentioned in the previous section to alter the numerical procedure outlined in Chapter V, values of $S(k_i, n_i, l_i)$ were calculated for the range of initial conditions given in Equation (6-34). Tables 13, 14, 15, and 16 contain $S(k_i, n_i, l_i)$ for $E_{tr,i}$ = 500, 1000, 1500, 2000 gram $\text{Å}^2/\text{sec}^2$, respectively.

To examine the behavior of the reaction cross-sections with respect to the final vibrational state, the cross-sections $S(k_i, n_i, l_i)$ were broken down into their components $\bar{\sigma}(k_i, n_i, l_i; k_n, n_f)$ for several different initial conditions. Tables 17 and 18 show that, for most of the initial conditions, the largest values of $\bar{\sigma}(k_i, n_i, l_i; k_n, n_f)$ correspond to the formation of HBr in the lower vibrational states. How this behavior translates

Table 13. Reaction Cross-Section S Corresponding to $E_{tr,i}$ = 500 gram $Å^2/sec^2$.

n_i	l_i	S, $Å^2$	n_i	l_i	S, $Å^2$
0	30	6.9989	5	30	4.5320
0	60	7.1675	5	60	4.5829
0	90	7.1328	5	90	4.4924
0	120	7.0350	5	120	4.6943
1	30	6.6960	6	30	4.1062
1	60	6.5863	6	60	3.9401
1	90	6.6675	6	90	3.9400
1	120	6.4848	6	120	4.0031
2	30	5.9525	7	30	3.6592
2	60	6.0841	7	60	3.5438
2	90	5.9480	7	90	3.6123
2	120	5.8783	7	120	3.6701
3	30	5.4506			
3	60	5.5875			
3	90	5.4431			
3	120	5.4955			
4	30	5.1856			
4	60	5.0876			
4	90	5.0838			
4	120	4.9094			

Table 14. Reaction Cross-Section S Corresponding to $E_{tr,i}$ = 1000 gram $Å^2/sec^2$.

n_i	l_i	S, $Å^2$	n_i	l_i	S, Å
0	30	7.5671	5	30	4.6865
0	60	7.3824	5	60	4.5987
0	90	7.4420	5	90	4.6216
0	120	7.2333	5	120	4.5933
1	30	6.6789	6	30	4.1459
1	60	6.5210	6	60	4.0919
1	90	6.6892	6	90	4.2573
1	120	6.4122	6	120	4.1994
2	30	5.9123	7	30	3.5288
2	60	5.9666	7	60	3.6528
2	90	5.8944	7	90	3.5411
2	120	6.0211	7	120	3.5078
3	30	5.5512			
3	60	5.5484			
3	90	5.4050			
3	120	5.5962			
4	30	5.1777			
4	60	5.1018			
4	90	5.0461			
4	120	4.9273			

Table 15. Reaction Cross-Section S Corresponding to $E_{tr,i}$ = 1500 gram $Å^2/sec^2$.

n_i	l_i	S, $Å^2$	n_i	l_i	S, $Å^2$
0	30	7.1989	5	30	4.0168
0	60	7.0789	5	60	4.1333
0	90	7.6819	5	90	4.2081
0	120	6.7733	5	120	4.0077
1	30	6.6056	6	30	3.8623
1	60	6.7170	6	60	3.7991
1	90	6.4204	6	90	3.8006
1	120	6.5328	6	120	3.8770
2	30	5.9692	7	30	3.6413
2	60	5.9988	7	60	3.7931
2	90	6.0129	7	90	3.7332
2	120	5.8412	7	120	3.5216
3	30	5.4511			
3	60	5.3999			
3	90	5.4030			
3	120	5.5002			
4	30	4.9183			
4	60	4.8003			
4	90	4.7556			
4	120	4.4212			

Table 16. Reaction Cross-Section S Corresponding to $E_{tr,i}$ = 2000 gram $Å^2/sec^2$.

n_i	l_i	S, $Å^2$	n_i	l_i	S, $Å^2$
0	30	7.3194	5	30	4.7727
0	60	7.4188	5	60	4.7334
0	90	7.2202	5	90	4.6236
0	120	7.3597	5	120	4.6587
1	30	6.5785	6	30	4.2040
1	60	6.7955	6	60	4.1172
1	90	6.5202	6	90	4.1964
1	120	6.4958	6	120	4.2050
2	30	5.9641	7	30	3.5791
2	60	5.8959	7	60	3.8637
2	90	5.8509	7	90	3.8572
2	120	5.9594	7	120	3.4502
3	30	5.4561			
3	60	5.3799			
3	90	5.3958			
3	120	5.4001			
4	30	5.0598			
4	60	5.1738			
4	90	5.0163			
4	120	5.1253			

Table 17. Reaction Cross-Section $\bar{\sigma}$ Corresponding to $E_{tr,i}$ = 1500 gram Å^2/sec^2.

n_i	l_i	n_f	$\bar{\sigma}$, Å^2
0	30	0	1.8709
0	30	1	2.6707
0	30	2	1.8437
0	30	3	0.5959
0	30	4	0.1462
0	30	5	0.0485
0	30	6	0.0230
0	60	0	0.3199
0	60	1	0.6176
0	60	2	3.2168
0	60	3	1.8711
0	60	4	0.7139
0	60	5	0.2236
0	60	6	0.1260
0	90	0	0.3070
0	90	1	0.4330
0	90	2	3.8247
0	90	3	2.1361
0	90	4	0.6611
0	90	5	0.2358
0	90	6	0.0842
0	120	0	0.5468
0	120	1	1.1100
0	120	2	2.5201
0	120	3	1.7048
0	120	4	0.6151
0	120	5	0.1733
0	120	6	0.0554
0	120	7	0.0478
4	30	0	0.0256
4	30	1	0.4606
4	30	2	2.4207
4	30	3	1.3924
4	30	4	0.4646
4	30	5	0.1128
4	30	6	0.0321
4	30	7	0.0095
4	60	0	0.0215
4	60	1	0.4278
4	60	2	2.1171
4	60	3	1.5306
4	60	4	0.5159

Table 17. (Continued)

n_i	l_i	n_f	$\bar{\sigma}$, Å^2
4	60	5	0.1305
4	60	6	0.0449
4	60	7	0.0120
4	90	0	0.0085
4	90	1	0.1208
4	90	2	0.6311
4	90	3	2.1775
4	90	4	1.2428
4	90	5	0.4059
4	90	6	0.1392
4	90	7	0.0298
4	120	0	0.0102
4	120	1	0.2181
4	120	2	0.7370
4	120	3	1.8614
4	120	4	1.1078
4	120	5	0.3507
4	120	6	0.1088
4	120	7	0.0272
7	30	0	0.0267
7	30	1	0.2277
7	30	2	0.7228
7	30	3	1.4266
7	30	4	0.8009
7	30	5	0.3426
7	30	6	0.0773
7	30	7	0.0167
7	60	0	0.0110
7	60	1	0.2015
7	60	2	0.4724
7	60	3	1.5257
7	60	4	1.0953
7	60	5	0.3846
7	60	6	0.0831
7	60	7	0.0195
7	90	0	0.0105
7	90	1	0.1819
7	90	2	0.3814
7	90	3	0.6323
7	90	4	1.6133
7	90	5	0.6755
7	90	6	0.1686
7	90	7	0.0551
7	90	8	0.0146

Table 17. (Continued)

n_i	l_i	n_f	$\bar{\sigma}$, Å^2
7	120	0	0.0034
7	120	1	0.0991
7	120	2	0.2413
7	120	3	0.5634
7	120	4	1.2218
7	120	5	0.9408
7	120	6	0.3405
7	120	7	0.0806
7	120	8	0.0307

Table 18. Reaction Cross-Section $\bar{\sigma}$ Corresponding to $E_{tr,i}$ = 2000 gram Å^2/sec^2.

n_i	l_i	n_f	$\bar{\sigma}$, Å^2
1	30	0	0.3629
1	30	1	0.7314
1	30	2	3.1559
1	30	3	1.7252
1	30	4	0.4729
1	30	5	0.1110
1	30	6	0.0192
1	60	0	0.5221
1	60	1	1.0642
1	60	2	1.4450
1	60	3	1.7450
1	60	4	1.3306
1	60	5	0.5079
1	60	6	0.1397
1	60	7	0.0410
1	90	0	0.3811
1	90	1	0.9877
1	90	2	2.4651
1	90	3	1.7217
1	90	4	0.7576
1	90	5	0.1428
1	90	6	0.0489
1	90	7	0.0153
1	120	0	0.5376
1	120	1	1.1004
1	120	2	2.5316
1	120	3	1.5634
1	120	4	0.5665
1	120	5	0.1442
1	120	6	0.0360
1	120	7	0.0161
4	30	0	0.0127
4	30	1	0.3066
4	30	2	0.8072
4	30	3	2.1249
4	30	4	1.3042
4	30	5	0.4664
4	30	6	0.0301
4	30	7	0.0077
4	60	0	0.0187
4	60	1	0.0872
4	60	2	0.8117

Table 18. (Continued)

n_i	l_i	n_f	$\bar{\sigma}$, Å^2
4	60	3	2.2063
4	60	4	1.4195
4	60	5	0.5494
4	60	6	0.0702
4	60	7	0.0108
4	90	0	0.0079
4	90	1	0.1082
4	90	2	0.6194
4	90	3	2.4575
4	90	4	1.3487
4	90	5	0.3722
4	90	6	0.0823
4	90	7	0.0201
4	120	0	0.0063
4	120	1	0.0971
4	120	2	0.5388
4	120	3	2.4724
4	120	4	1.4661
4	120	5	0.4271
4	120	6	0.0899
4	120	7	0.0276
7	30	0	0.0137
7	30	1	0.1172
7	30	2	0.6212
7	30	3	1.6229
7	30	4	0.9114
7	30	5	0.2173
7	30	6	0.0566
7	30	7	0.0188
7	60	0	0.0098
7	60	1	0.0725
7	60	2	0.4361
7	60	3	1.7086
7	60	4	1.1327
7	60	5	0.3964
7	60	6	0.0868
7	60	7	0.0208
7	90	0	0.0097
7	90	1	0.1528
7	90	2	0.2722
7	90	3	0.5117
7	90	4	1.5887
7	90	5	0.9443

Table 18. (Continued)

n_i	l_i	n_f	$\bar{\sigma}$, Å^2
7	90	6	0.3009
7	90	7	0.0614
7	90	8	0.0155
7	120	0	0.0028
7	120	1	0.0718
7	120	2	0.2032
7	120	3	0.4947
7	120	4	1.3080
7	120	5	0.8943
7	120	6	0.3546
7	120	7	0.0837
7	120	8	0.0371

with respect to the detailed rate constants K must be determined through the use of Equation (5-79).

Dependence of Reaction Cross-Sections $\bar{\sigma}$ on the Final Vibrational State

By calculating the cross-sections $\sigma(k_i, n_i, l_i; k_n, n_f, l_f)$ for all of the possible final states corresponding to the initial conditions and employing Equation (5-77), the reaction cross-sections $\bar{\sigma}(k_i, n_i, l_i; k_n, n_f)$ were determined. The results are reported for (1) all the possible combinations of $E_{tr,i}$ = 1500 gram $Å^2/sec^2$, n_i = 0, 4, 7, and l_i = 30, 60, 90, 120 in Table 17, and (2) all the possible combinations of $E_{tr,i}$ = 2000 gram $Å^2/sec^2$, n_i = 1, 4, 7, and l_i = 30, 60, 90, and 120 in Table 18.

Assuming the initial conditions are described by a Maxwell-Boltzmann distribution for a temperature of 1000°K, $E_{tr,i}$ = 1500 gram $Å^2/sec^2$ corresponds to a relative velocity about midway between the most probable and average relative speeds. The average relative translational energy at 1000°K is $E_{tr,i}$ = 2000 gram $Å^2/sec^2$.

The fraction of Br_2 in the indicated vibrational-rotational states are given by the quantity

$$F_{int}(n_i, l_i) = \frac{(2l_i+1)\, e^{-E_{int}(n_i, l_i)/kT}}{Q_{int}} \; g_{l_i} \qquad (6\text{-}35)$$

where $E_{int}(n_i, l_i)$ are the coupled vibrational-rotational energy levels, g_{l_i} is their degeneracy factor, and Q_{int} is their corresponding partition function (112).

From Tables 17 and 18 it is obvious that most of the H + Br_2 colli-

sions involve those internal states of Br_2 leading to reaction cross-sections which are peaked at the lower vibrational levels of HBr. Since the integrand in Equation (5-79) is proportional to $F_{int}\,\bar{\sigma}$, it is apparent that the larger detailed reaction rate constants will occur for $n_f \leq 4$. Therefore, when Equation (6-20) is used as the potential-energy surface, there exists excellent agreement between the experimental results of Polanyi (10) and the perturbed Morse oscillator calculations.

The Total Reaction Cross-Sections S

For all combinations of the initial conditions given in Equation (6-34), values of $S(k_i, n_i, l_i)$ were obtained by summing the cross-sections $\bar{\sigma}(k_i, n_i, l_i; k_n, n_f)$ over all the possible vibrational states of HBr. Tables 13, 14, 15 and 16 contain the results of this effort for $E_{tr,i}$ = 500, 1000, 1500, 2000 gram $Å^2/sec^2$, respectively.

As in the case for Ellison's potential-energy surface, the reaction cross-sections $S(k_i, n_i, l_i)$ are not strongly dependent on initial conditions. This result is again due to the use of Equation (3-49) for the exact wave function; that is, the wave function χ_f^- does not take into account the distortion of the incoming wave function, Equation (3-27), by the potential $V_L(r,P)$. The slight decrease of S as n_i increases is physically untenable, since increasing initial energy should lead to greater probability of reaction. The function $Z_{n_i}(P)$ has n_i nodes, and apparently the increased oscillation of $Z_{n_i}(P)$ creates a canceling effect in the integral $I(l_1,0,l_3)$. Since the use of χ_f^- does not allow for the distortion of $Z_{n_i}(P)$ in the early stages of the collision, the declining trend of S with increasing n_i cannot be overcome.

The Simple Collision Theory

The magnitude of the reaction cross-sections $S(k_i, n_i, l_i)$ compares favorably with the cross-section required for the simple collision theory of bimolecular reaction rates (113) to produce a frequency factor in agreement with experiment (114). For instance, the simple collision theory yields the following expression for the rate constant of a reaction A + B → C + D:

$$K_t = \left[\frac{8 k_B}{\pi \mu_i}\right]^{1/2} N_a S_{AB} T^{1/2} \exp(-E_{act}/k_B T) N_a \qquad (6\text{-}36)$$

where k_B is Boltzmann's constant equal to 1.38054 gram $Å^2/sec^2$ per degree Kelvin, and N_a is Avogadro's number, or 6.02252×10^{23} $mole^{-1}$. The quantity E_{act}, called the activation energy, is the minimum amount of relative translational energy with which A and B must collide in order for reaction to occur. The symbol S_{AB} denotes the collision cross-section of molecules A and B based on the hard sphere model. Taking a typical value of $S(k_i, n_i, l_i)$ from Tables 13 through 16, say, S = 7.0789 $Å^2$ corresponding to $E_{tr,i}$ = 1500 gram $Å^2/sec^2$, $n_i = 0$, $l_i = 60$, and setting $S_{AB} = S$, one obtains a frequency factor

$$N_a S_{AB} \left[8 k_B/\pi \mu_i\right]^{1/2} T^{1/2} = 6.23 \times 10^{12} T^{1/2} \text{ cc/(mole-sec)} \qquad (6\text{-}37)$$

Equation (6-37) is in excellent agreement with the experimental range of frequency factors $6.52 \times 10^{12} T^{\frac{1}{2}} - 11.34 \times 10^{12} T^{\frac{1}{2}}$ cc/(mole-sec) proposed

by Levy (101), Campbell and Fristrom (114), and Britton and Cole (115).

Because of the weak dependence of $S(k_i, n_i, l_i)$ on the initial conditions, K_t will not be markedly influenced by temperature. The insensitivity to temperature is in semi-qualitative agreement with the results of most experimental studies (102, 103), which attributes this behavior to a low activation energy for $H + Br_2 \rightarrow HBr + Br$. As mentioned in Chapter V, however, the lack of influence of the initial conditions on $S(k_i, n_i, l_i)$ is due primarily to the use of χ_f^- as the exact wave function and only slightly to the low activation energy of the potential $V_L(r,P)$.

Determination of Reaction Rate Constants by the Modern Collision Theory

The end result of the modern collision theory (1, 2) was the derivation of the equations

$$K_t = \pi \sum_{n_i=0}^{\infty} \sum_{l_i=0}^{\infty} \iint (k_i/\mu_i)\, S(k_i, n_i, l_i)\, F_H(\vec{P}_H) \tag{6-38}$$

$$\times F_{Br_2}(n_i, l_i, \vec{P}_{Br_2})\, d^3\vec{P}_H\, d^3\vec{P}_{Br_2}$$

$$\bar{K} = \pi \sum_{n_i=0}^{\infty} \sum_{l_i=0}^{\infty} \iint (k_i/\mu_i)\, \bar{\sigma}(k_i, n_i, l_i; k_n, n_f) \tag{6-39}$$

$$\times F_H(\vec{P}_H)\, F_{Br_2}(n_i, l_i, \vec{P}_{Br_2})\, d^3\vec{P}_H\, d^3\vec{P}_{Br_2}$$

Assuming a Maxwell-Boltzmann distribution for the reactant molecules, the reaction rate constants $\overline{\overline{K}}$ and K_t can be obtained from the reaction cross-sections $\overline{\sigma}(k_i, n_i, l_i; k_n, n_f)$ and $S(k_i, n_i, l_i)$, respectively.

Unfortunately, the limitations of computer time made it impractical to consider initial conditions other than those listed in Equation (6-34). Because of the weak dependence of $\overline{\sigma}$ and S upon initial conditions, however, the reaction rate constants $\overline{\overline{K}}$ and K_t can be evaluated approximately from Equations (6-38) and (6-39) by using the cross-sections corresponding to the average initial translational, vibrational, and rotational energies. At 1000°K, the average molecular translational, vibrational, and rotational energies are 2072, 1090, and 1381 gram $Å^2/sec^2$, respectively. These energies correspond closely to the initial conditions $n_i = 1$, $l_i = 90$, and $E_{tr,i} = 2000$ gram $Å^2/sec^2$, for which the reaction cross-section S is given in Table 16; hence, let S_{aV} denote S(2000, 90).

The temperature at which Polanyi (10) determined the values of $\overline{\overline{K}}(n_f)/\overline{\overline{K}}(n_f = 3)$ for $H + Br_2 \rightarrow HBr + Br$ was about 500°K (based on the rotational temperature). For comparison, therefore, the cross-sections used in Equation (6-39) should correspond to average translational, vibrational, and rotational energies of 1036, 419, and 690 gram $Å^2/sec^2$, respectively. The initial conditions $E_{tr,i} = 1500$ gram $Å^2/sec^2$, $n_i = 0$, and $l_i = 60$, correspond closely to the above values, so the cross-sections $\overline{\sigma}(1000, 0, 60; k_n, n_f)$ of Table 17 will be used for comparison with the data in Table 3 and will be denoted as $\overline{\sigma}_{aV}(n_f)$.

The variables of integration in Equations (6-38) and (6-39) can be converted from the absolute momenta $\vec{p}_H$, $\vec{p}_{Br_2}$ to the momenta of the center-

of-mass and relative motion (1, 3, 22). Conversion to spherical coordinates and integration over all variables except the magnitude p_i of the relative momentum yields (1, 3)

$$\bar{\bar{K}}(n_f) = (4\pi/\mu_i^4)(\mu_i/2\pi k_B T)^{3/2} \sum_{n_i=0}^{\infty} \sum_{l_i=0}^{\infty} F_{int}(n_i, l_i) \tag{6-40}$$

$$\times \int_0^{\infty} exp(-p_i^2/2\mu_i k_B T)\, \bar{\sigma}(k_i, n_i, l_i; k_n, n_f)\, p_i^3\, dp_i$$

$$K_t = (4\pi/\mu_i^4)(\mu_i/2\pi k_B T)^{3/2} \sum_{n_i=0}^{\infty} \sum_{l_i=0}^{\infty} F_{int}(n_i, l_i) \tag{6-41}$$

$$\times \int_0^{\infty} S(k_i, n_i, l_i)\, exp(-p_i^2/2\mu_i k_B T)\, p_i^3\, dp_i$$

In turn, the variable of integration can be converted from p_i to $E_{tr,i}$ to give (1, 3)

$$\bar{\bar{K}}(n_f) = \frac{(2/k_B T)^{3/2}}{(\pi \mu_i)^{1/2}} \sum_{n_i=0}^{\infty} \sum_{l_i=0}^{\infty} F_{int}(n_i, l_i) \tag{6-42}$$

$$\times \int_0^{\infty} \bar{\sigma}(k_i, n_i, l_i; k_n, n_f)\, E\, e^{-E/k_B T}\, dE$$

$$K_t = \frac{(2/k_B T)^{3/2}}{(\pi \mu_i)^{1/2}} \sum_{n_i=0}^{\infty} \sum_{l_i=0}^{\infty} F_{int}(n_i, l_i) \tag{6-43}$$

$$\times \int_0^{\infty} S(k_i, n_i, l_i)\, E\, e^{-E/k_B T}\, dE$$

Here, $E_{tr,i}$ has been replaced by the dummy variable E. Substituting $\bar{\sigma}_{aV}(n_f)$ for $\bar{\sigma}(n_f)$ and S_{aV} for S, and summing over n_i, l_i result in

$$\bar{\bar{K}}(n_f) = \frac{(2/k_B T)^{3/2}}{(\pi \mu_i)^{1/2}}\, \bar{\sigma}_{av}(n_f) \int_0^{\infty} E\, \exp(-E/k_B T)\, dE \tag{6-44}$$

$$K_t = \frac{(2/k_B T)^{3/2}}{(\pi \mu_i)^{1/2}}\, S_{av} \int_0^{\infty} E\, \exp(-E/k_B T)\, dE \tag{6-45}$$

since

$$\sum_{n_i=0}^{\infty} \sum_{l_i=0}^{\infty} F_{int}(n_i, l_i) = 1 \tag{6-46}$$

The integral in Equations (6-44) and (6-45) is easily evaluated as $(k_B T)^2$, so

$$\bar{\bar{K}}(n_f) = (8 k_B T/\pi \mu_i)^{1/2}\, \bar{\sigma}_{av}(n_f) \tag{6-47}$$

$$K_t = (8 k_B T / \pi \mu_i)^{1/2} S_{av} \qquad (6\text{-}48)$$

Equations (6-47) and (6-48) give the rate constants in the units $Å^3$/molecule-sec. If Equation (6-48) is multiplied by $N_a \times 10^{-24}$, the frequency factor of the simple collision theory results in units of cc/mole-sec. Using the value of $S_{aV} = 6.5202\ Å^2$ from Table 16, one obtains

$$K_t = 3.00 \times 10^{14}\ Å^3/\text{molecule-sec} = 1.81 \times 10^{14}\ cc/\text{mole-sec} \qquad (6\text{-}49)$$

at T = 1000°K. Since the range of experimental values quoted from various sources (101, 114, 115) is 1.04×10^{14} - 6.30×10^{14} cc/mole-sec at 1000°K, the agreement between experiment and the admittedly crude calculation above is remarkable.

From Equation (6-47) it is seen that

$$\bar{\bar{K}}(n_f) / \bar{\bar{K}}(n_f = 3) = \bar{\sigma}_{av}(n_f) / \bar{\sigma}_{av}(n_f = 3) \qquad (6\text{-}50)$$

Using the values of $\bar{\sigma}_{aV}(n_f)$ in Table 17, the ratio $\bar{\bar{K}}(n_f)/\bar{\bar{K}}(3)$ can be determined for comparison with Polanyi's experimental results (10). In Table 19, the values of $\bar{\bar{K}}(n_f)/\bar{\bar{K}}(3)$ calculated from Equation (6-50) are compared with the values in Table 3. There is notable qualitative agreement between experiment and the simple calculation represented by Equations (6-47) and (6-50).

Table 19. Theoretical and Experimental Detailed Rate Constants for Formation of HBr in Various Vibrational States; Normalized to the Detailed Rate Constant for the Third Vibrational State.

Vibrational Quantum Number of HBr	Theoretical Detailed Rate Constant	Experimental Detailed Rate Constant
3	1.00	1.00
4	0.38	0.64
5	0.12	0.19
6	0.07	0.05

CHAPTER VII

CONCLUSIONS AND RECOMMENDATIONS

Conclusions

The foregoing investigation has demonstrated the severe complications encountered in the quantum mechanical description of chemical reactions. Even the relatively simple derivation of an expression for the reaction cross-section involved tedious attention to detail. Furthermore, the subsequent calculation of the reaction cross-sections required so much computer time, even on a high-speed computer, that computations were limited to a few representative initial conditions.

It was shown that good agreement between theory and experiment can be obtained if sufficient care is taken in approximating the exact wave function for the collision. Using the perturbed Morse oscillator method to describe the distortion of the HBr bond in the presence of another bromine atom resulted in reaction cross-sections which, when used in a simplified collision theory, gave rate constants that compared favorably with experiment. On the other hand, the dependence of the rate constants was obscured by the seemingly lack of dependence of the reaction cross-sections on initial conditions. This lack of dependence was caused by the expansion of the exact wave function in terms of distorted final wave functions. Even if this difficulty were not present, however, calculation of reaction cross-sections corresponding to all the initial conditions required to use the unsimplified collision theory of reaction rates would consume a prohibitive amount of computer time.

Detailed rate constant calculations by the perturbed Morse oscillator method reinforce the classical mechanical results of Polanyi. That is, "attractive" potential-energy surfaces lead to higher vibrational states for the products, whereas "repulsive" potential-energy surfaces result in less vibration of the product molecule. Since infrared chemiluminescence spectroscopy has demonstrated that the product molecules in the reaction $H + Br_2 \rightarrow HBr + Br$ are formed predominantly in the lower vibrational states, it is concluded that the potential-energy surface for this reaction is "repulsive". Of course, the exact degree of repulsiveness has not been accurately determined. The potential-energy surface which yielded results in good agreement with experiment was, by the definition of Polanyi, about two-thirds "repulsive".

Recommendations

Another method for obtaining the total rate constants K_t of the reaction $H + Br_2 \rightarrow HBr + Br$ is to consider the reverse reaction $HBr + Br \rightarrow Br_2 + H$. Just as in the case of the forward reaction, the exact wave function for the latter process could be conveniently expanded in terms of perturbed Morse oscillator functions of HBr. For the reverse reaction, however, this expansion corresponds to the exact wave function evolving from the initial asymptotic state, or Ψ_i^+, and as such will describe more explicitly the distortion of the initial relative motion. Thus, the effect of the activation energy will not be as obscured as it was when χ_f^- was used to describe the forward reaction. If the resulting rate constant for $HBr + Br \rightarrow H + Br_2$ is denoted by K_t^r, the rate constant K_t^f for the forward reaction can be obtained from

$$K_t^f = K_t^r K_{eq}$$

where K_{eq} is the equilibrium constant for the forward reaction.

Aside from the study of exothermic, bimolecular, reactive collisions, the perturbed Morse oscillator method could be used to study the vibrational excitation of a strongly bound diatomic molecule AB upon collision with an atom C which only slightly distorts the AB bond. That is, expressions for the cross-sections of the inelastic process

$$C + AB \rightarrow C + AB^*$$

where AB^* is a vibrationally excited molecule, can be derived by modifying the perturbed Morse oscillator method to describe direct collisions rather than rearrangement collisions. Calculations based on this treatment should be in better agreement with experiment than calculations which do not take the distortion of the AB bond into account.

APPENDIX A

COLLISION CROSS-SECTIONS

Molecular Species

In order to keep track of the numerous molecular processes occurring in a reacting mixture of gases, one must devise a system for classifying the various types of molecules. One method is to define a molecular species as including all the molecules possessing the same chemical type and the same internal state; i.e., all of the quantum numbers required to specify completely the internal state must be the same. In the case of a diatomic molecule in the ground electronic state, the required quantum numbers would be the vibrational, total rotational, and z-component rotational quantum numbers, and the nuclear spin.

For identification purposes, the chemical type can be labeled by capital letters, A, B, C, D, ..., and the complete set of quantum numbers can be symbolized by one lower case letter such as i, j, k, l, ..., in parenthesis.

Binary Collisions

Before two molecules collide, they approach each other in an essentially straight trajectory. As their separation decreases, their common force field becomes sufficiently strong to cause the trajectory to curve. As the molecules or the products of their reaction depart to a sufficient separation, the trajectory of relative motion once again becomes a straight line. But, the distortion by the mutual force field causes the

direction of relative departure to deviate from the direction of relative approach. The two spherical coordinates, a polar angle and an azimuthal angle in some suitable coordinate system, describing this deviation are called the scattering angles. For the center of mass coordinate system, Figure 9 contains a diagram of the initial and final stages of the scattering process. The two scattering angles Θ and Φ are clearly shown. Notationally, the two scattering angles can be written as Ω.

Two molecules A(t) and B(j) may collide to exchange momenta (elastic collision), in which case they remain A(t) and B(j) molecules. However, one or both of the molecules may undergo a change in internal state; thus, one or both molecules undergo a species change to A(t′) and B(j′), but the chemical type remains the same. On the other hand, the molecules A(t) and B(j) might react chemically with one another to become C(k) and D(l) molecules, respectively. The probability with which these various types of collisions will occur will be a function of the element of solid angle into which the products are scattered. Let $d\Omega$ represent the element of solid angle oriented in the center of mass spherical coordinate system by the angles Θ and Φ and let $N_s(\Theta, \Phi)\, d\Omega$ be the number of B(j) molecules resulting in D(l) molecules being scattered into $d\Omega$ per second. Species C(k) and D(l) may differ from A(t) and B(j) according to whether the collision is elastic, inelastic, or reactive. Obviously,

$$N_s(\Theta, \Phi)\, d\Omega \sim N_a N_b\, d\Omega \tag{A-1}$$

where N_b = B(j) molecules/cm^2-sec converging on the A(i) molecules

N_a = number of A(i) molecules per cm^3.

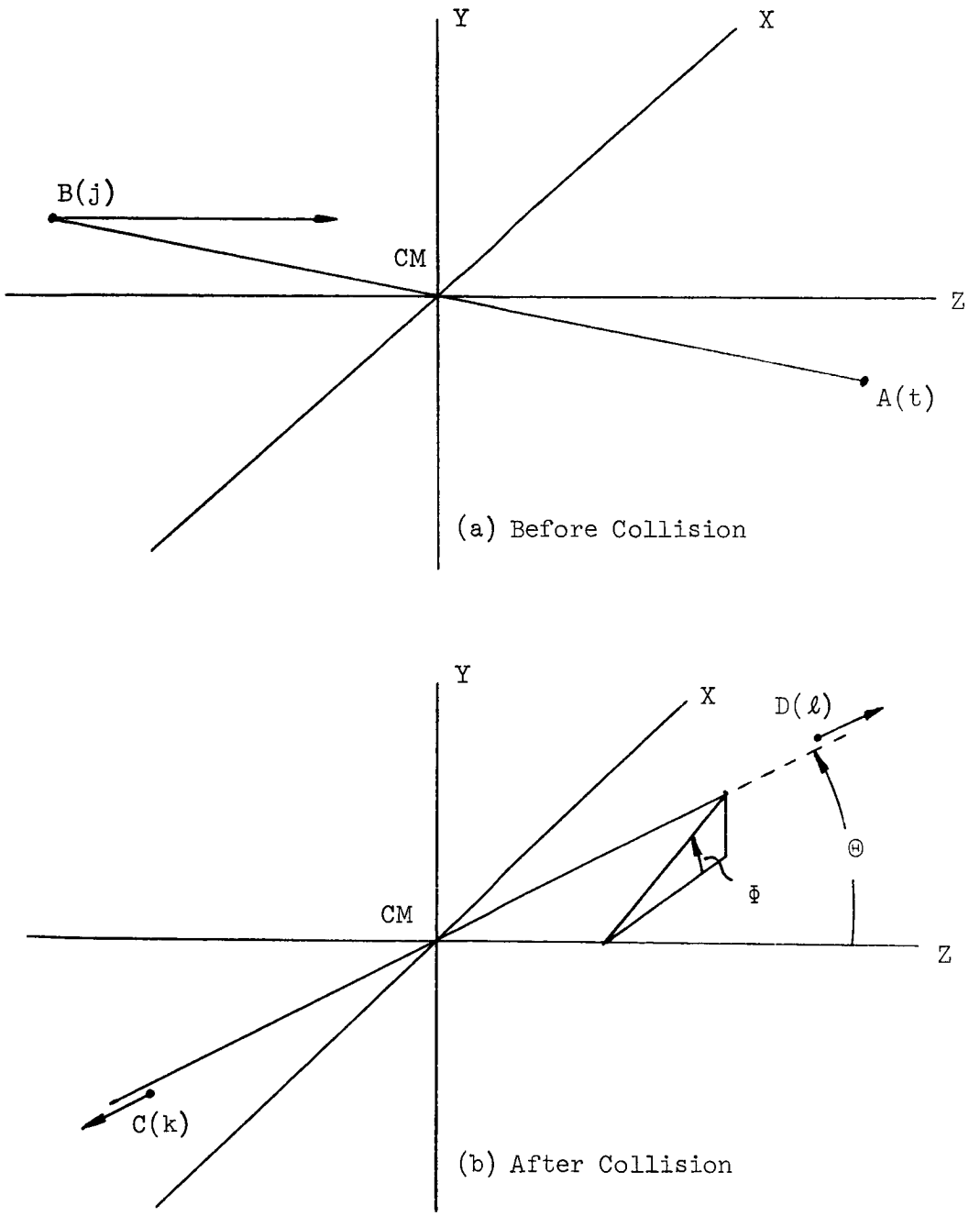

Figure 9. Collision Between Two Molecules with Reaction

Insert a constant of proportionality into this expression so that

$$N_s(\Theta, \Phi)\, d\Omega = \sigma_f^i(\Theta, \Phi) \sin\Theta\, d\Theta\, d\Phi \qquad \text{(A-2)}$$

The quantity $\sigma_f^i(\Theta, \Phi)$ is the differential scattering cross-section for elastic, inelastic, and reactive cross-sections, depending on how C(k) and D(l) differ from A(i) and B(j). The symbols i and f denote the complete sets of initial and final quantum numbers, respectively. From Equation (A-1),

$$\sigma_f^i(\Theta, \Phi)\, d\Omega = \frac{N_s(\Theta, \Phi)\, d\Omega}{N_a N_b} \qquad \text{(A-3)}$$

which has the dimensions of cm^2 per target molecule. Accordingly, $\sigma_f^i(\Theta, \Phi)\, d\Omega$ may be considered to be the area presented by each target molecule A(t) for scattering of the products C(k) and D(l) into the element of solid angle $d\Omega$ when approached by the projectile B(j).

The total differential cross-section, Equation (A-3), can be written as the sum of the particular cross-sections corresponding to elastic, inelastic, and reactive scattering. When theoretical calculations of cross-sections are made, the three types of collisions are usually considered separately.

The total scattering cross-section is defined as

$$\sigma = \int_{\Phi=0}^{2\pi} \int_{\Theta=0}^{\pi} \sigma_f^i(\Theta, \Phi) \sin\Theta \, d\Theta \, d\Phi \qquad \text{(A-4)}$$

Physically, σ represents the area presented by each target molecule for scattering into the total solid angle, 4π steradians. For convergence of the integral in Equation (A-4), σ_f^i must increase less rapidly than $1/\Theta^2$ for decreasing Θ as Θ approaches zero.

In general, both the differential and total collision cross-sections are dependent on the initial relative velocity with which A(t) and B(j) approach each other.

APPENDIX B

CLEBSCH-GORDAN COEFFICIENTS AND ANGULAR MOMENTUM

The discussion that follows closely resembles that of Messiah (116). Relations useful to the development of the main text of the present work, especially Chapters V and VI, are presented without proof. An excellent text by Edmonds (108) treats the subject of angular momentum rigorously.

Notations and Conventions of Angular Momentum

The relations that follow are written in units such that $\hbar = 1$.

Angular Momentum Components

Let the angular momentum operator be represented by $\hat{J}$ and its cartesian coordinates by J_x, J_y, and J_z. Then define the operators

$$J_{\pm} = J_x \pm i J_y \tag{B-1}$$

Commutation Relations

Standard textbooks on quantum mechanics (117) discuss more fully the following relations:

$$[J_x, J_y] = i J_z \tag{B-2}$$

$$[J_y, J_z] = i J_x$$

$$[J_z, J_x] = i J_y$$

$$[J_z, J_\pm] = J_\pm (\pm 1) \tag{B-3}$$

$$[J_+, J_-] = 2 J_z \tag{B-4}$$

where [A, B] = AB - BA is called the commutator of the operators A and B.

Basis Vectors of the Angular Momentum Operators

The following definitions will be useful:

A vector space is spanned by a set of vectors $\{A_i\}$ if any vector in the vector space can be expressed as a linear combination of the set $\{A_i\}$.

The dimension of a vector space is the minimum number of vectors required to span the vector space.

A set of vectors $A_1, A_2, \ldots, A_n$ is linearly independent if the equation

$$c_1 A_1 + c_2 A_2 + \cdots + c_n A_n = \sum_i c_i A_i = 0 \tag{B-5}$$

requires all $c_i = 0$. The set $\{A_i\}$ is linearly dependent if Equation (B-5) can be solved with some $c_i \neq 0$.

A basis of a vector space is some linearly independent set of vectors that spans the vector space; an orthonormal basis of a vector space is some orthonormal set which spans the space.

Spherical Harmonics and Eigenvectors

The spherical harmonics $Y_J^M(\theta, \phi)$, which are simultaneous eigenfunctions of the angular momentum operators $\hat{J}^2$ and J_z, can be considered a

representation of (2J + 1) vectors since M = -J, -J + 1, ..., J - 1, J for fixed J. Using the eigenvector notation of Dirac (118), $Y_J^M(\theta, \phi)$ is written as $|\ J, M\ \rangle$, and

$$\hat{J}^2\ |J,M\rangle = J(J+1)\ |J,M\rangle \tag{B-6}$$

$$J_z\ |J,M\rangle = M\ |J,M\rangle \tag{B-7}$$

$$J_\pm\ |J,M\rangle = \sqrt{J(J+1)-M(M\pm1)}\ \ |J,M\pm1\rangle \tag{B-8}$$

represent the action of $\hat{J}^2$, J_z, and $J_\pm$ on $|\ J, M\ \rangle$.

Dirac (118) defines the eigenket $\langle\ J, M\ |$ such that the orthogonality property of $|\ J, M\ \rangle$ can be expressed as

$$\langle J', M'|\ |J,M\rangle = \langle J', M'|J,M\rangle \tag{B-9}$$

$$= \int_{\varphi=0}^{2\pi}\int_{\theta=0}^{\pi} Y_{J'}^{M'*}(\theta,\phi)\ Y_J^M(\theta,\phi)\ \sin\theta\ d\theta\, d\phi = \delta_{J,J'}\ \ \delta_{M,M'}$$

Coupling of Angular Momentum

Let $\hat{J}_1$ and $\hat{J}_2$ represent the angular momentum operators of the quantum systems 1 and 2, respectively, and let $\hat{J}$ be the angular momentum operator of the total system 1 and 2 combined; then

$$\hat{J} = \hat{j}_1 + \hat{j}_2 \tag{B-10}$$

The tensor product of the $(2j_1 + 1)$ vectors of system 1, $| j_1, m_1 >$, by the $(2j_2 + 1)$ vectors of system 2, $| j_2, m_2 >$, gives the $(2j_1 + 1)(2j_2 + 1)$ simultaneous eigenvectors of j_1^2, j_2^2, J^2, J_z:

$$| j_1 \; j_2 \, , m_1 \; m_2 \rangle \equiv | j_1 , m_1 \rangle \, | j_2 , m_2 \rangle \tag{B-11}$$

from which one can obtain, by a unitary transformation, the $(2j_1 + 1)$ $(2j_2 + 1)$ simultaneous eigenvectors of $\hat{j}_1^2$, $\hat{j}_2^2$, $\hat{J}^2$, J_z, the vectors

$$| j_1 \, j_2 \, J \, M \rangle = \langle j_1 \, j_2 \, m_1 \, m_2 \, | J M \rangle \; | j_1 \, j_2 \, m_1 \, m_2 \rangle \tag{B-12}$$

where $J = | j_1 - j_2 |, \ldots, j_1 + j_2$; $M = -J, \ldots, J$.

The Clebsch-Gordan coefficients

$$\langle j_1 \, j_2 \; m_1 \; m_2 \, | J M \rangle$$

are the coefficients of that unitary transformation (119). The notation for the Clebsch-Gordan coefficients in reference (116) is $C(j_1, j_2, J; m_1, m_2, M)$.

The definition of the eigenvectors in Equations (B-11) and (B-12) is completed by fixing their relative phases as follows:

(i) the $| j_1, m_1 >$, the $| j_2, m_2 >$, and the $| j_1\ j_2\ J\ M >$ obey Equation (B-8).

(ii) $C(j_1, j_2, J; j_1, j_1 - J, J) > 0$ and is real.

Principal Properties of Clebsch-Gordan Coefficients

Reality

The Clebsch-Gordan coefficients are all real

$$C(j_1, j_2, J; m_1, m_2, M) = C^*(j_1, j_2, J; m_1, m_2, M) \quad \text{(B-13)}$$

Selection Rules

The Clebsch-Gordan coefficients vanish unless

$$m_1 + m_2 = M \quad \text{(B-14)}$$

$$|j_1 - j_2| \leq J \leq j_1 + j_2 \quad \text{(B-15)}$$

Permutation Relations

$$C(j_1, j_2, J; m_1, m_2, M) = (-1)^{j_1 + j_2 - J} C(j_2, j_1, J; m_2, m_1, M) \quad \text{(B-16)}$$

$$= (-1)^{j_1 - J + m_2} \sqrt{\frac{2J+1}{2j_1+1}}\, C(J, j_2, j_1; M, -m_2, m_1) \quad \text{(B-17)}$$

$$= (-1)^{j_2 - J - m_1} \sqrt{\frac{2J+1}{2j_2+1}}\, C(j_1, J, j_2; -m_1, M, m_2) \quad \text{(B-18)}$$

$$= (-1)^{j_1 + j_2 - J}\, C(j_1, j_2, J; -m_1, -m_2, -M) \quad \text{(B-19)}$$

Orthogonality Relations

$$\sum_{m_1=-j_1}^{j_1} \sum_{m_2=-j_2}^{j_2} C(j_1, j_2, J; m_1, m_2, M)\, C(j_1, j_2, J'; m_1, m_2, M') = \delta_{J,J'}\, \delta_{M,M'} \quad \text{(B-20)}$$

where $| j_1 - j_2 | \leq J \leq j_1 j_2$, $-J \leq M \leq J$.

$$\sum_{J=j_1-j_2}^{j_1+j_2} \sum_{M=-J}^{J} C(j_1, j_2, J; m_1, m_2, M)\, C(j_1, j_2, J; m_1', m_2', M) \quad \text{(B-21)}$$

$$= \delta_{m_1, m_1'}\, \delta_{m_2, m_2'}$$

where $-j_1 \leq m_1 \leq j_1$ and $-j_2 \leq m_2 \leq j_2$.

Composition Relations for the Spherical Harmonics

$$\int_{\phi=0}^{2\pi}\int_{\theta=0}^{\pi} Y_{j_1}^{m_1}(\theta,\phi)\; Y_{j_2}^{m_2}(\theta,\phi)\; Y_{j_3}^{m_3 *}(\theta,\phi)\; \sin\theta\, d\theta\, d\phi \;= \tag{B-22}$$

$$\left[\frac{(2j_1+1)(2j_2+1)}{4\pi\,(2j_3+1)}\right]^{1/2} C(j_1, j_2, j_3; m_1, m_2, m_3)\, C(j_1, j_2, j_3; 0,0,0)$$

$$Y_{j_1}^{m_1}(\theta,\phi)\; Y_{j_2}^{m_2}(\theta,\phi) = \sum_{L=j_1-j_2}^{j_1+j_2} \sum_{m_L=-L}^{L} \left[\frac{(2j_1+1)(2j_2+1)}{4\pi\,(2L+1)}\right]^{1/2} \tag{B-23}$$

$$\times\, Y_L^{m_L}(\theta,\phi)\, C(j_1, j_2, L; m_1, m_2, m_L)\, C(j_1, j_2, L; 0,0,0)$$

Special Values

When J and M take their maximum value,

$$C(j_1, j_2, j_1+j_2;\; j_1, j_2, j_1+j_2) = 1 \tag{B-24}$$

When either j_1 or j_2 is zero,

$$C(j_1, 0, J;\; m, 0, M) = C(j_1, 0, j_1;\; m_1, 0, m_1) = 1 \tag{B-25}$$

When m_1, m_2, and m_3 all vanish, then

$$C(j_1, j_2, j_3; 0,0,0) = 0 \tag{B-26}$$

if $j_1 + j_2 + j_3$ is odd; if $2p = j_1 + j_2 + j_3$ s even, then

$$C(j_1, j_2, j_3; 0,0,0) = \frac{\sqrt{2j_3+1}}{(-1)^{j_1-j_2}} (-1)^p \sqrt{\Delta(j_1, j_2, j_3)} \tag{B-27}$$

$$\times \frac{p!}{(p-j_1)!\,(p-j_2)!\,(p-j_3)!}$$

where

$$\Delta(a,b,c) = \frac{(a+b-c)!\,(b+c-a)!\,(c+a-b)!}{(a+b+c+1)!} \tag{B-28}$$

APPENDIX C

EFFECT OF INDISTINGUISHABILITY OF BROMINE ATOMS ON REACTION CROSS-SECTIONS

The analysis presented here is to show the effect of indistinguishability of bromine atoms on the calculation of reaction cross-sections for the reaction $H + Br_2 \rightarrow HBr + Br$. The approach used is the same as that of Tang (70), who studied the reaction $D + H_2 \rightarrow DH + H$.

Because the magnetic moment associated with nuclear spin is very small, the coupling between the nuclear spin and other modes of motion is very weak. Thus, a binary collision of the type $A + BC \rightarrow AB + C$, where B and C are identical particles, is not expected to result in any alteration of the nuclear spin of B and C.

In the case of the collision $H + Br_2 \rightarrow HBr + Br$, one bromine atom is labeled as B and the other as C. Also, the relative position vector from the center of mass of AB to C is denoted as $\vec{P}_C$, and the corresponding vector from the center of mass of AC to B is labeled $\vec{P}_B$. The asymptotic form of the wave function (without spin) can be written, in terms of the products, as

$$\Psi(A,B,C) \xrightarrow[P_c \to \infty]{} P_c^{-1} \exp(i k_n P_c) f_n^i(\Theta_c, \Phi_c) Z_n(\vec{r}_{AB}) \qquad \text{(C-1)}$$

or

$$\Psi(A,C,B) \xrightarrow[R_B \to \infty]{} R_B^{-1} \exp(i k_n R_B)\, f_n^{\dagger}(\Theta_B, \Phi_B)\, Z_n(\vec{r}_{AB}) \qquad \text{(C-2)}$$

Since the two bromine isotopes have atomic masses of 79 and 81, they are both fermions (112). Thus, the bromine molecular wave function is antisymmetrical with respect to interchange of B and C, if both B and C have the same mass.

Assume that both bromine atoms have the same mass, and that the total wave function for Br_2 can be approximated as

$$\phi = \phi_{elec}\ \phi_{n.s.}\ \phi_{rot}\ \phi_{vib} \qquad \text{(C-3)}$$

where ϕ_{elec}, $\phi_{n.s.}$, ϕ_{rot}, and ϕ_{vib} are the electronic, nuclear spin, rotational, and vibrational wave functions, respectively. The ground electronic state of Br_2 is symmetrical (112) with respect to inversion of the nuclei, and the vibrational state of any homonuclear molecule is likewise symmetrical. The nuclear spin state for Br_2 can either be symmetrical or antisymmetrical, while the rotational state of any homonuclear molecule is symmetrical for even J states and antisymmetrical for odd J states (112). To preserve the overall antisymmetry of the Br_2 wave function, however, the odd rotational states must correspond to the symmetrical spin states, whereas the even rotational states must coincide with the antisymmetrical spin states.

If the initial state of the bromine molecule is such that the quantum number J is odd, the nuclear spins of the two bromine atoms must be combined in a symmetrical state throughout the collisional process; that

is, the space wave function must remain antisymmetrical with respect to B and C. The antisymmetrical wave function suitable for the description of direct scattering can be written as (70)

$$\Psi(A,B,C) = e^{i\vec{k}_i\cdot\vec{R}_i}\phi_i(\vec{r}_{Br_2}) - \frac{\mu_f}{2\pi\hbar^2}\sum_n \iint \frac{e^{ik_n|\vec{R}-\vec{R}'|}}{|\vec{R}-\vec{R}'|}\phi_n(\vec{r}_{Br_2}) \qquad \text{(C-4)}$$

$$\times \phi_n(\vec{r}_{Br_2})\,\phi_n^*(\vec{r}'_{Br_2})\,U_f(\vec{R}',\vec{r}'_{Br_2})\,\Psi(A,B,C)\,d^3\vec{r}'_{Br_2}\,d^3\vec{R}'$$

where $\phi_n(\vec{r}_{Br_2})$ is the antisymmetrical (including spin) molecular wave function for bromine and n runs through all vibrational and odd rotational states. The total wave function $\Psi(A, B, C)$ can also be written in a form pertaining explicitly to the boundary condition with atom B going to infinity:

$$\Psi(A,B,C) = -\frac{\mu_f}{2\pi\hbar^2}\sum_n \iint \frac{\exp(ik_n|\vec{P}_B-\vec{P}'_B|)}{|\vec{P}_B-\vec{P}'_B|} Z_n(\vec{r}_{AC})\,Z_n^*(\vec{r}'_{AC}) \qquad \text{(C-5)}$$

$$\times \bar{U}_i(\vec{r}'_{AC},\vec{P}'_B)\,\Psi(A,B,C)\,d^3\vec{r}'_{AC}\,d^3\vec{P}'_B$$

where n now runs through all vibrational states and rotational states (even and odd) of HBr. Likewise, for the case of atom C going to infinity,

$$\Psi(A,B,C) = -\frac{\mu_f}{2\pi\hbar^2} \sum_n \iint \frac{\exp(i k_n |\vec{P}_c - \vec{P}_c'|)}{|\vec{P}_c - \vec{P}_c'|} Z_n(\vec{r}_{AB}) Z_n^*(\vec{r}_{AB}') \tag{C-6}$$

$$\bar{u}_i(\vec{r}_{AB}', \vec{P}_c') \; \Psi(A,B,C) \; d^3\vec{r}_{AB}' \; d^3\vec{P}_c'$$

Because the antisymmetry of the wave function Ψ(A, B, C) is lost in Equations (C-5) and (C-6), an antisymmetrical combination of the two must be made to give the total wave function:

$$\Psi(A,B,C) = \left[\frac{e^{i k_n P_c}}{P_c} Z_n(\vec{r}_{AB}) - \frac{e^{i k_n P_B}}{P_B} Z_n(\vec{r}_{AC}) \right] \tag{C-7}$$

$$\left\{ -\frac{1}{\sqrt{2}} \frac{\mu_f}{2\pi\hbar^2} \sum_n \iint \exp(-i k_n P_c') \, Z_n^*(\vec{r}_{AB}') \, \bar{u}_i(\vec{r}_{AB}', \vec{P}_c') \right.$$

$$\left. \times \left[\Psi(A,B,C) - \Psi(A,C,B) \right] \right\} d^3\vec{r}_{AB}' \; d^3\vec{P}_c'$$

The exchange amplitude, the expression inside the braces, can be related to the incident wave function by using Equation (C-4) for Ψ in the integrand of Equation (C-7). Since Ψ of Equation (C-4) is antisymmetrical, the second term in the bracket under the integral sign of Equation (C-7)

just duplicates the first term. As a result, the asymptotic form of Equation (C-7) is

$$\Psi(A,B,C) \xrightarrow[P_c \to \infty]{} \sqrt{2}\; P_c^{-1} \sum_n \exp(i k_n P_c)\, Z_n(\vec{r}_{AB})\, f_n^i(\Theta,\Phi) \qquad \text{(C-8)}$$

with

$$f_n^i(\Theta,\Phi) = -\left(\frac{\mu_f}{2\pi\hbar^2}\right)\iint \exp(-i\vec{k}_n\cdot\vec{P}_c)\, Z_n^*(\vec{r}_{AB}')\, U_i(\vec{r}_{AB}',\vec{P}_c') \qquad \text{(C-9)}$$

$$\times\, \Psi(A,B,C)\, d^3\vec{r}_{AB}'\, d^3\vec{P}'$$

It is apparent that the differential cross-section for any particular state is

$$\sigma_f^i(\Theta,\Phi) = \frac{2k_n}{k_i}\,\frac{\mu_i}{\mu_f}\,\left|f_n^i(\Theta,\Phi)\right|^2 \qquad \text{(C-10)}$$

Using similar arguments, the same result is obtained for bromine molecules initially in even (J even) rotational states. Also, for bromine molecules consisting of both isotopes (atomic masses 79 and 81), the distinguishability of Br^{79} and Br^{81} make the above argument unnecessary. In this case, the differential reaction cross-section for the reaction of H with each of the isotopic species is

$$\sigma_f^i(\Theta, \Phi) = \frac{k_n}{k_i} \frac{\mu_i}{\mu_f} \left| f_n^i(\Theta, \Phi) \right|^2 \qquad \text{(C-11)}$$

The small difference in μ_f for Br^{79} and Br^{81} enables one to closely approximate the differential reaction cross-section for HBr formation by Equation (C-10).

For all cases, therefore, the correct differential cross-section is essentially twice that obtained by concentrating on the reaction of H with one particular atom in Br_2.

BIBLIOGRAPHY*

1. M. A. Ellison and J. O. Hirschfelder, J. Chem. Phys. 30, 1426 (1959).

2. J. Ross and P. Mazur, J. Chem. Phys. 35, 19 (1961).

3. R. D. Present, Kinetic Theory of Gases (McGraw-Hill Book Company, Inc., New York, 1958).

4. S. W. Benson, The Foundations of Chemical Kinetics (McGraw-Hill Book Company, Inc., New York, 1960), p. 155.

5. D. R. Herschbach and J. H. Birely, J. Chem. Phys. 44, 1690 (1966).

6. J. C. Polanyi and S. D. Rosner, J. Chem. Phys. 38, 1028 (1963).

7. D. R. Herschbach, K. R. Wilson, G. H. Kwei, J. A. Norris, R. R. Herm, and J. H. Birely, J. Chem. Phys. 41, 1154 (1964).

8. J. C. Polanyi, J. Quantitative Spectroscopy and Radiative Transfer 3, 471 (1963).

9. F. O. Ellison, J. Am. Chem. Soc. 86, 2115 (1964).

10. J. C. Polanyi, J. R. Airey, P. D. Pacey, Eleventh Symposium (International) on Combustion, Berkeley, California (1966) (to be published).

11. R. N. Pease, Equilibrium and Kinetics of Gas Reactions (Princeton University Press, Princeton, New Jersey, 1942).

12. J. O. Hirschfelder, M. J. Henkel, W. P. Spaulding, Equations for Hydrogen-Bromine Flame Propagation (University of Wisconsin Naval Research Laboratory, Report No. CF-1112, Madison, Wisconsin, 1949).

13. V. N. Kondratiev, Chemical Kinetics of Gas Phase Reactions (Addison-Wesley Publishing Company, Inc., Reading, Massachusetts, 1964).

14. R. M. Fristron and A. A. Westenberg, Flame Structure,(McGraw-Hill Book Company, Inc., New York 1965).

15. R. D. Present, J. Chem. Phys. 31, 747 (1959).

16. K. E. Shuler and E. W. Montroll, Adv. in Chem. Phys. 1, 361 (1958).

17. C. S. Wang Chang and G. E. Uhlenbeck, Transport Phenomena in Polyatomic Molecules, (University of Michigan, Publication CM-681, Ann Arbor, Michigan, 1951).

18. D. Beck, E. F. Green, and J. Ross, J. Chem. Phys. 37, 1028 (1963).

19. M. Ackerman, E. F. Green, A. L. Moursund, and J. Ross, J. Chem. Phys. 41, 1183 (1964).

20. K. J. Laidler and J. C. Polanyi, Prog. in Reaction Kinetics 3, 1 (1965).

21. S. Glasstone, K. J. Laidler, and H. Eyring, The Theory of Rate Processes (McGraw-Hill Book Company, Inc., New York, 1941).

22. M. Karplus, R. N. Porter, and R. D. Sharma, J. Chem. Phys. 43, 3259 (1965).

23. A. Messiah, Quantum Mechanics, (John Wiley & Sons, Inc., New York, 1961), pp. 231-241.

24. N. F. Mott and H. S. W. Massey, The Theory of Atomic Collisions (Oxford University Press, Oxford, England, 1949), pp. 100-109.

25. T. Y. Wu and T. Ohmura, The Quantum Theory of Scattering,(Prentice-Hall, Inc., Englewood Cliffs, New Jersey, 1962), pp. 211-250.

26. K. J. Laidler, Chemical Kinetics,(McGraw-Hill Book Company, Inc., New York, 1965).

27. M. Born and R. Oppenheimer, Ann. Physik.84, 457 (1927).

28. Ref. 13, pp. 124-127.

29. R. G. Parr, Quantum Theory of Molecular Electronic Structure (W. A. Benjamin, Inc., New York, 1963).

30. J. C. Slater, Quantum Theory of Molecules and Solids; Vol. 1, Electronic Structure of Molecules,(McGraw-Hill Book Company, Inc., New York, 1963).

31. C. J. Ballhausen and H. B. Gray, Molecular Orbital Theory (W. A. Benjamin, Inc., New York, 1964).

32. W. T. Simpson, Theories of Electrons in Molecules (Prentice-Hall, Inc., Englewood Cliffs, New Jersey, 1962).

33. L. C. Pauling, The Nature of the Chemical Bond, (Cornell University Press, Ithaca, New York, 1960).

34. R. G. Parr, D. P. Craig, and I. G. Ross, J. Chem. Phys. 18, 1561 (1950).

35. S. F. Boys and I. Shavitt (University of Wisconsin Naval Research Laboratory, Technical Report WIS-AF-13, 1959).

36. Ref. 21, pp. 1-4.

37. R. E. Weston, J. Chem. Phys. 31, 892 (1959).

38. H. Eyring and M. Polanyi, Z. Physik. Chem. B12, 279 (1931).

39. P. M. Morse, Phys. Rev. 34, 57 (1929).

40. S. Sato, J. Chem. Phys. 23, 2465 (1955).

41. F. O. Ellison, J. Am. Chem. Soc. 85, 3540 (1963).

42. W. Moffitt, Proc. Roy. Soc. (London) A210, 245 (1951).

43. F. T. Wall, L. A. Hiller, and J. Mazur, J. Chem. Phys. 29, 255 (1958).

44. F. T. Wall, L. A. Hiller, and J. Mazur, J. Chem. Phys. 35, 1284 (1961).

45. F. T. Wall and R. N. Porter, J. Chem. Phys. 39, 3112 (1963).

46. F. T. Wall and R. N. Porter, J. Chem. Phys. 36, 3256 (1962).

47. M. Karplus, R. N. Porter, and R. D. Sharma, J. Chem. Phys. 40, 2033 (1964).

48. R. N. Porter and M. Karplus, J. Chem. Phys. 40, 1105 (1964).

49. D. L. Bunker and N. C. Blais, J. Chem. Phys. 37, 2713 (1962).

50. D. L. Bunker and N. C. Blais, J. Chem. Phys. 39, 315 (1963).

51. D. L. Bunker and N. C. Blais, J. Chem. Phys. 41, 2377 (1964).

52. S. Datz and E. H. Taylor, J. Chem. Phys. 39, 1896 (1963).

53. M. Karplus and L. M. Raff, J. Chem. Phys. 41, 1267 (1964).

54. M. Karplus and L. M. Raff, J. Chem. Phys. 44, 1212 (1966).

55. D. R. Herschbach, G. H. Kwei, and J. A. Norris, J. Chem. Phys. 34, 1842 (1961).

56. D. R. Herschbach, Dis. Faraday Soc. 33, 149 (1962).

57. J. R. Airey, R. R. Getty, J. C. Polanyi, and D. R. Snelling, J. Chem. Phys. 41, 3255 (1964).

58. H. Beutler and M. Polanyi, Z. Physik. Chem. B1, 3 (1928).

59. M. G. Evans and M. Polanyi, Trans. Faraday Soc. 35, 616 (1939).

60. P. J. Kuntz, E. M. Nemeth, S. D. Rosner, C. E. Young, and J. C. Polanyi, J. Chem. Phys. 44, 1168 (1966).

61. J. O. Hirschfelder, C. F. Curtiss, and R. B. Bird, Molecular Theory of Gases and Liquids,(John Wiley & Sons, New York, 1954).

62. J. C. Polanyi, J. Applied Optics, (Chemical Laser Supplement), January, 1965.

63. S. Golden, J. Chem. Phys. 17, 620 (1949).

64. P. A. M. Dirac, The Principles of Quantum Mechanics, (Oxford University Press, London, 1947), pp. 167-178.

65. S. Golden and A. M. Peiser, J. Chem. Phys. 17, 630 (1949).

66. E. Bauer and T. Y. Wu, J. Chem. Phys. 21, 726 (1953).

67. Ref. 21, pp. 7-9.

68. J. Mazur and R. J. Rubin, J. Chem. Phys. 31, 1395 (1959).

69. E. M. Mortensen and K. S. Pitzer, Chem. Soc. (London), Special Publication Number 16 (1962).

70. K. T. Tang, Ph.D. Thesis, Columbia University, New York, 1965.

71. R. J. Suplinskas, Ph.D. Thesis, Brown University, Providence, Rhode Island, 1965.

72. Ref. 23, p. 179.

73. K. R. Greider, Phys. Rev. 133, B1483, (1964).

74. E. Gerjuoy, Annals of Phys. 5, 58 (1958).

75. B. A. Lippmann, Phys. Rev. 102, 264 (1956).

76. S. T. Epstein, Phys. Rev. 106, 598 (1957).

77. M. Gell-Munn and M. L. Goldberger, Phys. Rev. 91, 398 (1953).

78. Ref. 23, p. 68.

79. H. Goldstein, Classical Mechanics,(Addison-Wesley Publishing Company, Inc., Reading, Massachusetts, 1950).

80. E.T. Whittaker, A Treatise on the Analytical Dynamics of Particles and Rigid Bodies, (Cambridge University Press, Cambridge, England, 1937), p. 339.

81. D. ter Haar, Phys. Rev. 70, 222 (1946).

82. Ref. 23, p. 378.

83. Ref. 23, pp. 836-839.

84. N. F. Mott, Proc. Cambridge Philosophical Soc. 27, 553 (1931).

85. Ref. 24, p. 105.

86. D. R. Bates, H. S. W. Massey, and A. L. Stewart, Proc. Roy. Soc. (London) A216, 437 (1953).

87. H. Eyring, J. Walter, and G. E. Kimball, Quantum Chemistry,(John Wiley & Sons, New York, 1944), pp. 92-99.

88. K. S. Kunz, Numerical Analysis,(McGraw-Hill Book Company, Inc., New York, 1957), p. 204.

89. Ref. 87, pp. 72-75.

90. A. Abramowitz and I. A. Stegun, Handbook of Mathematical Functions, (Dover Publications, New York, 1965), pp. 503-536.

91. G. W. King, Spectroscopy and Molecular Structure, (Holt, Rinehart, and Winston, Inc., 1964), p. 173.

92. G. Herzberg, Spectra of Diatomic Molecules, (D. Van Nostrund Company, Inc., 1950), p. 501.

93. Ref. 87, pp. 95-96.

94. Ref. 24, p. 105.

95. Ref. 25, p. 231.

96. Ref. 25, pp. 4-6.

97. Ref. 23, p. 496.

98. Ref. 25, pp. 1-124.

99. Ref. 25, p. 233.

100. E. A. Mason, R. J. Munn, and F. J. Smith, J. Chem. Phys. 41, 3978 (1964).

101. A. Levy, J. Phys. Chem. 62, 570 (1958).

102. L. Pauling and E. B. Wilson, Jr., Introduction to Quantum Mechanics, (McGraw-Hill Book Company, Inc., New York, 1935).

103. F. O. Ellison, J. Am. Chem. Soc. 85, 3544 (1963).

104. J. M. Hulburt and J. O. Hirschfelder, J. Chem. Phys. 9, 61 (1941).

105. D. Steele, E. R. Lippincott, and J. T. Vanderslice, Rev. Modern Phys. 32, 219 (1960).

106. Ref. 92, pp. 501-520.

107. Ref. 21, pp. 85-152.

108. A. Edmonds, Angular Momentum in Quantum Mechanics, (Princeton University Press, Princeton, New Jersey, 1957).

109. L. I. Schiff, Quantum Mechanics, (McGraw-Hill Book Company, Inc., New York, 1955), p. 236.

110. Ref. 88, p. 452.

111. J. C. Polanyi, Chemistry in Britain, 151 April, 1966.

112. N. Davidson, Statistical Mechanics, (McGraw-Hill Book Company, Inc., New York, 1962), pp. 105-129.

113. R. H. Fowler and E. A. Guggenheim, Statistical Thermodynamics, (Cambridge University Press, Cambridge, England, 1960), p. 505.

114. E. S. Campbell and R. M. Fristrom, Chem. Rev. 58, 173 (1958).

115. D. Britton and R. M. Cole, J. Phys. Chem. 65, 1302 (1961).

116. Ref. 23, pp. 1054-1060.

117. Ref. 23, pp. 507-581.

118. Ref. 64, p. 18.

119. Ref. 23, pp. 286-292.

---

* Abbreviations in this Bibliography follow the form used in Chemical Abstracts (1965).

VITA

James Carl Pirkle, Jr. was born on June 2, 1938 in Atlanta, Georgia. He attended public schools in Pelham, Georgia before entering the Georgia Military College, from which he received his high school diploma in 1956. The same year he entered the Georgia Institute of Technology as a student in chemical engineering, and in June, 1961 received the degree of Bachelor of Chemical Engineering, Cooperative Plan.

He entered the Graduate Division of the Georgia Institute of Technology in September, 1961 and received the M.S. degree in chemical engineering in June, 1962. Immediately thereafter, he joined the staff of the Georgia Tech Engineering Experiment Station where he directed the Salina Water Conversion project from 1962-1963 and the Gaseous Kinetics project from 1963-1965. Simultaneously, he was enrolled in the Ph.D. program of the School of Chemical Engineering and was a General Electric Foundation Fellow from 1963 to 1965.

At present he is on the Senior Staff of the Johns Hopkins University Applied Physics Laboratory. He is a member of Phi Eta Sigma, the Briaerean Society, and Sigma Xi. He is married to the former Helen Lavane Smith of Milledgeville, Georgia and they have two children.